# First-principles based computation of lattice dynamics in substitutionally disordered alloys


**by**

**Biswanath Dutta**


A Thesis
submitted for the degree of

**Doctor of Philosophy**

Thesis Supervisor

**Dr. Subhradip Ghosh**



Department of Physics
Indian Institute of Technology Guwahati
Guwahati 781039, India


August 2011

# First-principles based computation of lattice dynamics in substitutionally disordered alloys

**by**

**Biswanath Dutta**

A Thesis
submitted for the degree of
**Doctor of Philosophy**

Supervisor

**Dr. Subhradip Ghosh**

Department of Physics
Indian Institute of Technology Guwahati
Guwahati 781039, India

August 2011

# *Declaration*

The work in this thesis is based on research carried out at the Department of Physics, Indian Institute of Technology Guwahati, India under the supervision of Dr. Subhradip Ghosh. No part of this thesis has been submitted elsewhere for any other degree or qualification. Works presented in the thesis are all my own unless referenced to the contrary in the text.

Signed: _____

Date: _____

# *Certificate*

It is certified that the work contained in the thesis entitled "*First-principles based computation of lattice dynamics in substitutionally disordered alloys*" by Mr. Biswanath Dutta, a student of the Department of Physics, IIT Guwahati was carried out under my supervision and has not been submitted elsewhere for award of any degree.


Subhradip Ghosh

*Dedicated to my family*

# *Acknowledgements*

It gives me immense pleasure to extend my heartfelt thanks to all those who have helped me during my research work. I would like to express my sincere gratitude to my supervisor Dr. Subhradip Ghosh for his patient guidance. I am thankful to him for giving me some interesting research problems and for his constant support. He has been a wonderful person to work with and has been a great source of inspiration. I was immensely benefitted by the discussions which we used to have in regular intervals.

I take this opportunity to thank my doctoral committee members - Prof. A. Srinivasan, Dr. S. Basu and Dr. G. Das for the immensely useful discussions during the yearly assessments of my research work. I am thankful to all other faculty members of Physics department for being helpful in all regards. My special thanks to Prof. S. Ravi, Prof. Alika Khare and Dr. Charudatt Kadolkar for their timely help and support. I thank all the technical assistants of the department who helped me in various ways during my research period. Its my privilege to thank Dr. Biplab Sanyal, Uppsala University, Sweden for fruitful discussions and useful collaboration. I would like to thank Dr. Munima Sahariah and Dr. Amal Medhi for their valuable suggestions.

I am grateful to CSIR for the financial support.

It is my great pleasure to thank all the research scholars of the department for providing such a friendly atmosphere during my research period. My special thanks to Meera who has been be so kind and supportive. The friendly nature of my batchmates - Aneesh, Arpita and Biswanath Samantaray has made my stay in IIT Guwahati really pleasant. Special thanks to Jaheer, Vindhyawasini and Supriya for entertaining discussions over black-tea sessions. I thank Sumanta and Souvik with whom I have shared many experiences of my research life. I would always treasure the friendship of my childhood friends - Tumpa, Rupu, Dabbu, Ranjit and many more. My heartfelt thanks to Tirthankar and Victor for being wonderful friends of mine. The friendship of Haimanti, Debashree and Aditi will be always cherished. It is my pleasure to thank Sonali and Basanti for being wonderful friends of mine.

I feel privileged to thank all my teachers. I am blessed to get teachers like Swadesh Ranjan Pandit, Bablu Sarkar and Birabrata Das. I would like to thank Dr. Khanindra kumar Sarma and Dr. Om Prakash Sah who inspired me a lot during my younger days. My special thanks

to Prof. Dilip Kumar Choudhury and Dr. Buddhadev Bhattacharjee whose intelligence and dedication towards work have inspired me to pursue research in Physics.

I am grateful to my family for their love, support and encouragement. The brotherly love of Somnath has immensely influenced my life. I owe my life to them. I am thankful to God for giving me such wonderful in-laws. I thank my brother in-law and sister in-law for being so understanding. The selfless love of Diya, Dibya, Jhili and Rick will always be treasured.

Finally, my heartfelt thanks to Poulumi for all her supports during the tough days of PhD. Her unconditional love always motivates me to excel in life. In short, my life would have been incomplete without her.

# *Abstract*

The computation of phonon spectra in disordered alloys in an accurate and reliable way has been a longstanding problem in the area of condensed matter research. Available theoretical tools so far did not have the necessary ingredients to treat the mass, the force-constant and the environmental disorders on an equal footing. In this thesis, we have worked on the development of new first-principles based formalisms to alleviate these problems. Within the framework of first-principles electronic structure formalisms, the disordered alloy is usually modelled by a large supercell, thus making the computation of lattice dynamics prohibitively demanding. In this thesis, we, therefore, have adopted various strategies to model the interatomic force-constants of a disordered alloy based upon the results of computation of dynamical matrices on smaller systems. These are then used in the computation of configuration-averaged quantities by the recently developed Itinerant Coherent Potential Approximation (ICPA), an analytic, self-consistent, translationally invariant formalism which treats the three kinds of disorder relevant for lattice dynamics on equal footing. Thus, we arrive at formalisms which seamlessly integrate the first-principles electronic structure based methodologies with the methods for configuration-averaging with reliable accuracy. Major part of the thesis deals with a modeling strategy based on transferable force constant (TFC) model which suggests that 'force constant vs bond length' relationship for a given chemical bond, which can be obtained from a small number of first-principles calculations, is transferable across different structures. We combine it with the ICPA to propose DFPT-TFC-ICPA, a new first-principles based tool, which is used extensively in this thesis to calculate the complete phonon spectra and associated quantities for a wide variety of alloys which involve magnetic type-II alloys ($Fe_xPd_{1-x}$) and alloys with significant mass and size differences among the constituents ($Cu_xPd_{1-x}$, $Cu_xAu_{1-x}$ and $Ni_xPt_{1-x}$). Our motivations are different in each of these systems. While in $Fe_xPd_{1-x}$, the role of force constant disorder among various pairs of species on the phonon spectra is discussed in detail, the focus in $Cu_{0.715}Pd_{0.285}$ and $Cu_{0.75}Au_{0.25}$ has been a thorough investigation of the influence of size mismatch of end-point components on the phonon dispersions. In $Ni_xPt_{1-x}$ alloys, the origin of the experimentally observed anomalous features in the phonon branches is investigated by computing the lattice dynamics for the alloy system at various compositions. Substantial discrepancy between our calculated results and those obtained by the experiments, in case of $Ni_{0.25}Pt_{0.75}$, however, propelled us to find an alternative modeling strategy which has the ability to treat environmental disorder (*e.g.*,

short-range order) in a better way. An improved modeling scheme is thereafter realized by adopting the 'special quasirandom structure' (SQS) to model the random environment in a disordered alloy. We demonstrate this new formalism, which is a combination of SQS and ICPA, by computing the phonon spectra of $Ni_{0.5}Pt_{0.5}$. The better agreement of our results with the experiments over previous models of disorder suggests that the SQS+ICPA formalism can serve as a tractable first-principles based computational tool to address the issues in a real random alloy in a better way as the effects of different environments are incorporated in the construction of the SQS. Overall, the results presented in the thesis show that both the TFC-ICPA and the SQS-ICPA formalisms upon integration with first-principles electronic structure methods have provided necessary solutions to the challenging problem of a proper microscopic understanding of the lattice dynamical behaviour in disordered alloys.

# Contents

**Acknowledgements** **xi**

**Abstract** **xiii**

**List of figures** **xix**

**1 Introduction** **1**
- 1.1 Role of Lattice Vibrations . . . 2
- 1.2 Experimental Techniques . . . 5
  - 1.2.1 Neutron scattering cross-sections . . . 5
- 1.3 Theoretical Developments . . . 7
  - 1.3.1 Basic Approximations . . . 8
    - 1.3.1.1 The Harmonic Approximation . . . 8
    - 1.3.1.2 The Adiabatic Approximation . . . 9
  - 1.3.2 Models of Lattice Vibration . . . 10
    - 1.3.2.1 Einstein Model . . . 11
    - 1.3.2.2 Debye Model . . . 11
    - 1.3.2.3 Born-von Karman Model . . . 12
    - 1.3.2.4 Ab-*initio* Methods . . . 13
- 1.4 Lattice dynamics of Alloys . . . 14
  - 1.4.1 The mass effect . . . 15
  - 1.4.2 The size mismatch effect . . . 15
  - 1.4.3 The charge transfer effect . . . 16
  - 1.4.4 The short-range order effect . . . 17
- 1.5 Outline of the thesis . . . 17

**2 Methods of configuration averaging for phonon excitations in random alloys** **21**
- 2.1 Introduction . . . 21
- 2.2 Virtual crystal approximation (VCA) . . . 24
- 2.3 Average t-matrix approximation (ATA) . . . 24
- 2.4 Coherent potential approximation (CPA) . . . 25
- 2.5 Generalizations of the CPA . . . 26

2.6 Itinerant coherent potential approximation (ICPA) . . . 28
2.6.1 The Augmented Space Formalism . . . 29
2.6.2 Multiple-scattering picture . . . 33
2.7 Summary . . . 41

**3 First-principles based modeling of inter-atomic force constants 43**
3.1 Introduction . . . 43
3.2 Density functional theory (DFT) . . . 44
3.3 Density functional perturbation theory (DFPT) . . . 47
3.4 Modeling the inter-atomic force constants . . . 50
3.4.1 Application: $Pd_xFe_{1-x}$ ($x = 0.96, 0.9$) . . . 51
3.4.1.1 Computational details . . . 52
3.4.1.2 Results . . . 53
3.4.2 Limitations of the modeling strategy . . . 62
3.5 Transferable force-constant (TFC) model . . . 63
3.6 Summary . . . 65

**4 Applications of DFPT-TFC-ICPA method for binary alloys 67**
4.1 Introduction . . . 67
4.2 Computational Details . . . 72
4.3 Results and Discussion . . . 73
4.3.1 $Pd_xFe_{1-x}$ for $x = 0.96$, 0.9, 0.5 and 0.28 . . . 73
4.3.1.1 $Pd_{0.96}Fe_{0.04}$, $Pd_{0.9}Fe_{0.1}$ and $Pd_{0.28}Fe_{0.72}$ . . . 73
4.3.1.2 $Pd_{0.5}Fe_{0.5}$ . . . 78
4.3.2 $Cu_{0.715}Pd_{0.285}$ and $Cu_{0.75}Au_{0.25}$ . . . 82
4.3.2.1 $Cu_{0.715}Pd_{0.285}$ . . . 83
4.3.2.2 $Cu_{0.75}Au_{0.25}$ . . . 89
4.3.3 $Ni_xPt_{1-x}$ for $x = 0.95$, 0.70, 0.50 and 0.25 . . . 98
4.3.3.1 $Ni_{0.95}Pt_{0.05}$ . . . 98
4.3.3.2 $Ni_{0.70}Pt_{0.30}$ . . . 102
4.3.3.3 $Ni_{0.50}Pt_{0.50}$ . . . 105
4.3.3.4 $Ni_{0.25}Pt_{0.75}$ . . . 108
4.4 Summary . . . 110

**5 Incorporation of the local environment effects 113**
5.1 Introduction . . . 113
5.2 Methodology . . . 114
5.2.1 Structural model . . . 115
5.2.2 Averaging procedure for force-constants . . . 115
5.3 Example: $Ni_{0.5}Pt_{0.5}$ . . . 118
5.4 Summary . . . 123

**6 Conclusions** **125**

**Bibliography** **129**

**Publications** **139**

**Vita** **141**

# List of Figures


1.1 Substitutional alloy . . . . . 14
1.2 Interstitial alloy . . . . . 15

2.1 Multiple scattering picture in the CPA and the ICPA . . . . . 34
2.2 Schematic representation of the ICPA formalism . . . . . 41

3.1 Phonon dispersion curves for $Pd_{0.9}Fe_{0.1}$ calculated in the ICPA with the force constants obtained from model potential . . . . . 54
3.2 Phonon dispersion curves for FCC Fe computed at the experimental lattice constant of $Pd_{0.90}Fe_{0.1}$ . . . . . 55
3.3 Phonon dispersion curves for $Pd_{0.96}Fe_{0.04}$ calculated in the ICPA with the concentration-averaged Fe-Pd force constants . . . . . 56
3.4 Phonon dispersion curves for $Pd_{0.9}Fe_{0.1}$ calculated in the ICPA with the concentration-averaged Fe-Pd force constants . . . . . 57
3.5 Partial and total structure factors for $Pd_{0.96}Fe_{0.04}$ and $Pd_{0.9}Fe_{0.1}$ calculated using the concentration-averaged Fe-Pd force constants . . . . . 57
3.6 Phonon dispersion curves for $Pd_{0.96}Fe_{0.04}$ calculated in the ICPA with 20% reduced Fe-Pd force constants . . . . . 59
3.7 Phonon dispersion curves for $Pd_{0.9}Fe_{0.1}$ calculated in the ICPA with 20% reduced Fe-Pd force constants . . . . . 60
3.8 Partial and total structure factors for $Pd_{0.96}Fe_{0.04}$ calculated with 20% reduced Fe-Pd force constants . . . . . 61
3.9 Partial and total structure factors for $Pd_{0.9}Fe_{0.1}$ calculated with 20% reduced Fe-Pd force constants . . . . . 61
3.10 Schematic representation of the DFPT-TFC-ICPA method . . . . . 64

4.1 Nearest neighbor stretching and bending force constants for $Pd_xFe_{1-x}$ as a function of bond length . . . . . 74
4.2 Phonon dispersion curves for $Pd_{0.96}Fe_{0.04}$ calculated in the ICPA with the force constants obtained using 'bond stiffness vs bond length' method . . . . 76
4.3 Phonon dispersion curves for $Pd_{0.9}Fe_{0.1}$ calculated in the ICPA with the force constants obtained using 'bond stiffness vs bond length' method . . . . . 77
4.4 Phonon dispersion curves for $Pd_{0.28}Fe_{0.72}$ calculated in the ICPA with the force constants obtained using 'bond stiffness vs bond length' method . . . . 78

4.5 Phonon dispersion curves for $Pd_{0.50}Fe_{0.50}$ calculated in the ICPA with the force constants obtained at the $L1_0$ bond length using 'bond stiffness vs bond length' method. . . . . 79
4.6 Partial and total structure factors for $Pd_{0.50}Fe_{0.50}$ calculated using the force constants extracted at the disordered alloy bond length . . . . . 80
4.7 Partial and total structure factors for $Pd_{0.50}Fe_{0.50}$ calculated using the force constants extracted at the $L1_0$ bond lengths . . . . . 81
4.8 Nearest neighbor stretching and bending force constants for $Cu_xPd_{1-x}$ as a function of bond length . . . . . 84
4.9 Phonon dispersion curves for $Cu_{0.715}Pd_{0.285}$ calculated in the ICPA with the force constants extracted at the alloy bond length (top panel) and at the relaxed bond lengths (bottom panel) . . . . . 85
4.10 Partial and total structure factors for $Cu_{0.715}Pd_{0.285}$ calculated using force constants extracted at the alloy bond length . . . . . 86
4.11 Partial and total structure factors for $Cu_{0.715}Pd_{0.285}$ calculated using force constants extracted at the relaxed bond lengths . . . . . 87
4.12 Nearest neighbor stretching and bending force constants for $Cu_xAu_{1-x}$ as a function of bond length . . . . . 88
4.13 Phonon dispersion curves for $Cu_{0.75}Au_{0.25}$ calculated in the ICPA with the force constants extracted at the alloy bond length. . . . . 89
4.14 Partial and total structure factors for $Cu_{0.75}Au_{0.25}$ calculated using force constants extracted at the alloy bond length . . . . . 91
4.15 Phonon dispersion curves for $Cu_{0.75}Au_{0.25}$ calculated in the ICPA with the force constants extracted at the new relaxed bond lengths . . . . . 92
4.16 Partial and total structure factors for $Cu_{0.75}Au_{0.25}$ calculated using force constants extracted at the relaxed bond lengths . . . . . 93
4.17 Phonon dispersion curves for $Cu_{0.75}Au_{0.25}$ calculated in the VCA with the force constants obtained by fitting experimental frequencies to the Born-von Karman model . . . . . 94
4.18 Phonon dispersion curves for $Cu_{0.75}Au_{0.25}$ calculated in the CPA with the force constants obtained by fitting experimental frequencies to the Born-von Karman model . . . . . 95
4.19 Disorder-induced widths and the vibrational densities of states for $Cu_{0.75}Au_{0.25}$ and $Cu_{0.715}Pd_{0.285}$ . . . . . 96
4.20 Nearest neighbor stretching and bending force constants for $Ni_xPt_{1-x}$ as a function of $x$, the Ni concentration . . . . . 99
4.21 Phonon dispersion curves for $Ni_xPt_{1-x}$ calculated in the ICPA with the force constants extracted at the alloy bond length . . . . . 100
4.22 Partial and total structure factors for $Ni_{0.95}Pt_{0.05}$ calculated by the DFPT-TFC-ICPA method . . . . . 101
4.23 Disorder-induced widths in $Ni_xPt_{1-x}$ calculated by the DFPT-TFC-ICPA method 102

4.24 Vibrational densities of states for $Ni_{0.70}Pt_{0.30}$ calculated by the DFPT-TFC-ICPA method . . . . . 103
4.25 Partial and total structure factors for $Ni_{0.70}Pt_{0.30}$ calculated by the DFPT-TFC-ICPA method . . . . . 104
4.26 Partial and total structure factors for $Ni_{0.50}Pt_{0.50}$ calculated by the DFPT-TFC-ICPA method . . . . . 106
4.27 Vibrational densities of states for $Ni_{0.25}Pt_{0.75}$ calculated by the DFPT-TFC-ICPA method . . . . . 108
4.28 Partial and total structure factors for $Ni_{0.25}Pt_{0.75}$ calculated by the DFPT-TFC-ICPA method . . . . . 109

5.1 Dispersion of bond distances computed by the SQS . . . . . 118
5.2 Phonon dispersion curves for $Ni_{0.5}Pt_{0.5}$ alloy computed by the SQS-ICPA, the CPA and the empirical-ICPA methods . . . . . 121

# Chapter 1

# Introduction

In classical mechanics, it is well known that a system of particles in stable equilibrium, when disturbed, performs vibrations, such that every particle remains in the neighborhood of its equilibrium position [1]. For the description of the vibrational motions, a set of co-ordinates $\{r_i\}$ can be introduced which are linear functions of the displacements of the particles and vary independently of one another, each as a sinusoidal function of time $A_i Sin(2\pi\nu_i t + \delta_t)$ (the frequency $\nu_i$ is determined by the nature of forces, whereas, $A_i$ and $\delta_i$ are arbitrary constants). Such coordinates are known as the normal coordinates of the system and the corresponding motions as the normal modes. The system, from this viewpoint, is simply a collection of independent harmonic oscillators, each oscillating with a frequency $\nu_i$. If we impose the quantum-mechanical commutation rules on the canonical momenta, the quantum harmonic-oscillator energy spectrum is obtained. These elementary units of lattice excitations are known as phonons. The phonons are bosons and represent perhaps the simplest elementary excitation in a solid. They are represented by wave-vector $\vec{q}$ and angular frequency $\omega_s$ for vibrational polarization $s$. The energy of the phonon mode associated with polarization $s$ is $\hbar\omega_s$ and the corresponding momenta is $\hbar\vec{q}$. The study of lattice vibrations in a solid is essentially concerned with finding out the vibrational modes $\omega_s$ as a function of wave-vector $\vec{q}$.

The importance of the study of phonon excitations in modern day materials research stems from the fact that many a materials properties can only be understood upon consideration of lattice dynamics [2]. The '*static lattice model*' which does not allow the atoms on a lattice to move from their equilibrium positions, although can explain a large number of materials

properties such as chemical and mechanical properties, structural properties, optical properties, electronic and magnetic properties, electronic structure *etc.*, it, however, has serious limitations. Such oversimplified model of immobile ions fails to explain thermal (e.g. heat capacity, thermal expansion) and transport (e.g. thermal conductivity) properties, phenomena related to the electron-phonon coupling such as the resistivity in metals and the superconductivity and the interaction of various types of radiations with the solid [3]. The *static lattice model* is also inadequate in understanding the mechanism behind phase transitions in solids. These inadequacies of the static lattice model points to the importance of lattice vibrations in understanding materials properties. In the next sub-section, we present a brief review on the role of lattice vibrations in state-of-the-art materials research.

## 1.1 Role of Lattice Vibrations

Over the last few decades, the area of lattice vibrations has received considerable interest because of their role in governing several important material properties [4]. In the beginning, the one particular area which grabbed all the attention was the specific heat behavior at low temperatures. Specific heat $C_v$ is an important thermodynamic quantity which refers to the material's ability to absorb heat energy at constant volume. The static model of lattice failed to give a proper mathematical description of this quantity in solids at low temperatures where the observed specific heat varies as $T^3$ for both metals and insulators. The qualitative deviation form the observed behavior at low temperatures occurs due to limitations in the underlying assumptions of the model which assumes that all contributions to the specific heat come from the electronic degrees of freedom alone. This leads to a linear temperature dependence of specific heat for metals, whereas, for insulators the dependence becomes exponential. The observed $T^3$-dependence can only be explained by introducing the motion of the lattice into the theory in a quantum-mechanical way.

The knowledge of the lattice vibrational contribution also becomes crucial in the calculation of several other thermal properties of solids which are determined by the appropriate thermodynamic potential relevant to the given sample. In an ensemble where the sample volume and temperature are independent variables, the relevant potential is the Helmholtz free energy, $F = E - TS$. To understand the effect of lattice vibrations, the free energy, in general,

can be decomposed into a configurational contribution $\mathbf{F_{config}}$ and a vibrational contribution $\mathbf{F_{vib}}$ so that:

$$F^{\alpha} = E^{\alpha}_{config} - TS^{\alpha}_{config} + E^{\alpha}_{vib} - TS^{\alpha}_{vib} \tag{1.1}$$

where, $\mathbf{F}^{\alpha}$ is the free energy of a phase $\alpha$ with energetic contribution **E** and an entropic contribution **S**. Here, the key quantity which needs to be calculated in order to have access to the thermal properties is the vibrational free energy $\mathbf{F_{vib}}$. This can be demonstrated very efficiently for insulators in which electronic excitations are of negligible importance at temperatures below $\frac{E_g}{k_B}$. Due to negligibly small probability of electronic excitations over the band gap $E_g$, there is nothing left in a rigid lattice insulator except vibrational excitations that could account for the pronounced thermal expansions typically observed in experiments. From microscopic point of view, this phenomenon can be attributed to the increase in the average bond distances between the atoms due to an enhancement in vibrational amplitude with increase in temperature. The *quasiharmonic approximation* in this regard provides a very useful and efficient formalism to calculate thermal properties of materials taking into account the vibrational effects. Within this approximation [5], the effects of anharmonicity at temperatures far from the melting point is incorporated through the volume dependence of the phonon spectra. The important quantities which are usually calculated in the quasiharmonic approximation include equilibrium lattice parameters, elastic constants, specific heat and thermal expansion coefficients, as a function of the temperature [6, 7].

The relative stability of various phases of a material is also governed by lattice vibrational behavior. Induced by either temperature or pressure, phase transitions are often driven by a lattice instability. In the temperature-induced phase transitions, the vibrational entropy $S^{\alpha}_{vib}$ which is a measure of the average stiffness of a material, plays the pivotal role in stabilizing a particular phase over the other. A phase with a larger vibrational entropy is stabilized relative to other phases, since a larger vibrational entropy results in a lower free energy, as is seen in Eq. (1.1). Evidence of such vibrational entropy driven stabilization of a particular phase at elevated temperatures exists for a wide variety of material systems which include elemental materials (Li, Ti, Hf, La, Sc) as well as alloys (Cu-Au)[8–10]. Contrary to this, anharmonicity does not necessarily play an important role in pressure-induced phase transitions [11, 12]. One or more harmonic frequencies may become soft as a consequence of the changes in volume and atomic positions caused by applied pressure. It is, therefore, important to identify the

soft phonon modes as these modes are responsible for observed phase transitions. Melting is another temperature driven phenomenon which can not be explained by the static lattice model. In this process, the ions leave their normal equilibrium positions and wander great distances through the resulting liquid. At sufficiently high temperatures, the increased atomic vibrations lead to softening of the inter-atomic forces which is known to be the underlying cause of the melting of solids. Therefore, an adequate theory of melting process must take into account the increasing amplitude of lattice vibrations with increasing temperature.

The transport properties also need accurate treatment of lattice vibrations. While in metals, both free electrons and phonons contribute to the transport properties, all aspects of transport in insulators can only be understood only when the vibrations of the lattice are taken into account [3]. In a perfectly periodic potential, electrons suffer no collisions which would lead to infinite thermal and electrical conductivity in metals. The observed finite values for both the conductivity can only be explained by considering scattering of electrons from lattice vibrations. On the other hand, in insulators, there are too few electrons in partially filled bands to conduct appreciable amounts of heat; the thermal conductivity is predominantly due to the lattice degrees of freedom. Another well investigated phenomenon where phonons play a major role is *superconductivity*. It is understood from the BCS theory of superconductivity [13–15] that electrons in the low temperature couple by means of phonons to produce cooper pairs which move without resistance through the crystal lattice. If the lattice were rigorously static, there would have been no superconductors. It has also been found that lattice vibrations can interact with light to produce what is known as Brillouin scattering [16] which is used in laser spectroscopy. Velocity of sound in the medium is another important property which can be explained by lattice vibrations. In the low wave vector limit where the wave length becomes very large, the medium behaves as continuum and hence the phonon dispersion relation becomes similar to that of sound waves from which the sound velocity can easily be computed.

In the next two sub-sections, we briefly describe the experimental techniques and the theoretical models which are relevant for the study of lattice vibrations in solids.

## 1.2 Experimental Techniques

The experimental literature on the investigation of lattice vibrations rely mainly on inelastic neutron scattering technique [17–22]. The strength of neutrons is that they are well suited to the study of both static and dynamic properties of matter and therefore, they represent a valuable probe of condensed matter. Neutrons interact with the nuclei by two different mechanisms [23, 24]; first process involves nuclear scattering by strong but short-ranged nuclear forces, while the second one is magnetic scattering by the magnetic moments of the atoms inside a crystal. In this thesis, however, we are mostly concerned with nuclear scattering processes.

The principal aspect of neutron scattering which makes it suitable for probing phonon modes is the wavelength of thermal neutrons which is of the same order as the inter-atomic distances in solids. Thermal neutrons correspond to a energy of 0.025 eV and have a wavelength $\lambda$ = 1.798 $\AA$ which matches well with the lattice parameters of crystals and thus, the wave vector has about the same order of magnitude as the width of the Brillouin zone. Not only the wave length, the energy and momenta of thermal neutrons also match well with those of phonons. In contrast, frequencies of electromagnetic radiation in the infrared or visible region, though, can be used to measure phonon frequencies, but owing to their larger wavelengths, measurements are restricted to phonon wave vectors close to the center of the Brillouin zone. Besides, the modes accessible by Raman scattering and infrared spectroscopy are limited by selection rules. X-ray photons, on the other hand, can interact with phonons throughout the Brillouin zone, but their frequencies are much higher compared to the phonon frequencies (by a factor of $10^6$) so that the relative energy exchange between x-ray and lattice is negligible making it too difficult to measure phonon frequencies.

### 1.2.1 Neutron scattering cross-sections

Consider a general inelastic scattering process where an incident neutron of wave vector $\mathbf{k}_i$ is scattered by the sample into a final state of wave vector $\mathbf{k}_f$ with the creation of a phonon of wave vector $\mathbf{Q} = \mathbf{k}_i$ - $\mathbf{k}_f$ and energy $\hbar\omega = \mathrm{E}_i$ - $\mathrm{E}_f = \frac{\hbar^2}{2m}(\mathbf{k}_i^2 - \mathbf{k}_f^2)$, where m denotes the mass of the neutron. For nuclear scattering, the interaction potential $V(\mathbf{r})$ between the neutrons and the scattering atom is conventionally described by the Fermi pseudopotential as:

$$V(\mathbf{r}) = \frac{2\pi\hbar^2}{m} b\delta(\mathbf{r}), \tag{1.2}$$

where $b$ is the scattering length. It is worth mentioning at this point that the neutron scattering processes can be classified into two different categories: coherent and incoherent scattering. In the coherent scattering process, the neutron waves scattered from each scattering center preserve the coherency of the wave and hence, they can produce interference effects. On the other hand, in the incoherent case, any macroscopic interference is being prevented by the randomness in the phase and the scattering intensity is effectively a sum of scattering intensities from each nucleus. The calculation of phonon dispersion curves along special directions utilize coherent scattering process, whereas, the incoherent scattering is suitable for the determination of phonon densities of states. The differential cross-sections for these two categories of scattering processes are given by:

$$\left(\frac{\partial^2\sigma}{\partial\Omega\partial E}\right)_{coh}(\mathbf{Q},\omega) = \frac{\sigma_{coh}}{4\pi}\frac{k_f}{k_i}\frac{1}{2\pi\hbar}\sum_{l,l'}\int_{-\infty}^{\infty}\langle exp(-i\mathbf{Q}.\mathbf{R}_{l'}(0))exp(i\mathbf{Q}.\mathbf{R}_l(t))\rangle exp(-i\omega t)dt \tag{1.3}$$

$$\left(\frac{\partial^2\sigma}{\partial\Omega\partial E}\right)_{inc}(\mathbf{Q},\omega) = \frac{\sigma_{inc}}{4\pi}\frac{k_f}{k_i}\frac{1}{2\pi\hbar}\sum_{l}\int_{-\infty}^{\infty}\langle exp(-i\mathbf{Q}.\mathbf{R}_l(0))exp(i\mathbf{Q}.\mathbf{R}_l(t))\rangle exp(-i\omega t)dt \tag{1.4}$$

where, $\sigma_{coh}$ and $\sigma_{inc}$ are the total coherent and incoherent scattering cross-sections and $\mathbf{R}_l$ denote nuclear positions in cell $l$. The bracket $\langle\rangle$ denotes thermal average and the quantity within bracket represents a space-time correlation function. In case of coherent scattering, the correlation function is considered between different atoms at different times, whereas in the incoherent case, each atom is treated separately and the correlation function is for one atom at different times.

The neutron scattering cross-sections, in a more general way can be expressed in terms of scattering function $S(\mathbf{Q},\omega)$:

$$S(\mathbf{Q},\omega) = \frac{1}{2\pi\hbar}\int_{-\infty}^{\infty} e^{-i\omega t}dt \int G(\mathbf{r},t)e^{i\mathbf{Q}.\mathbf{r}}d^3r \tag{1.5}$$

where, $G(\mathbf{r},t)$ is the pair-(or self-)correlation function (also called the van Hove correlation function [25]) which contains all the information on the system available from neutron scattering experiment and can be expressed in the following way-

Pair-correlation function

$$G(\mathbf{r},t) = \left(\frac{1}{2\pi}\right)^3 \int d\mathbf{Q} e^{-i\mathbf{Q}.\mathbf{r}} \sum_{l,l'} \langle exp(-i\mathbf{Q}.\mathbf{R}_{l'}(0)) exp(i\mathbf{Q}.\mathbf{R}_l(t)) \rangle \tag{1.6}$$

Self-correlation function

$$G(\mathbf{r},t) = \left(\frac{1}{2\pi}\right)^3 \int d\mathbf{Q} e^{-i\mathbf{Q}.\mathbf{r}} \sum_{l} \langle exp(-i\mathbf{Q}.\mathbf{R}_{l}(0)) exp(i\mathbf{Q}.\mathbf{R}_l(t)) \rangle \tag{1.7}$$

In coherent scattering, $G(\mathbf{r},t)$ corresponds to the pair-correlation functions, whereas, in incoherent scattering it is limited to the self-correlations.The relation between scattering function $S(\mathbf{Q},\omega)$ and the cross-sections for coherent and incoherent scattering processes are:

$$\left(\frac{\partial^2\sigma}{\partial\Omega\partial E}\right)_{coh} = \frac{\sigma_{coh}}{4\pi}\frac{k_f}{k_i} S_{coh}(\mathbf{Q},\omega) \tag{1.8}$$

$$\left(\frac{\partial^2\sigma}{\partial\Omega\partial E}\right)_{inc} = \frac{\sigma_{inc}}{4\pi}\frac{k_f}{k_i} S_{inc}(\mathbf{Q},\omega) \tag{1.9}$$

## 1.3 Theoretical Developments

The theoretical study of lattice vibrations in crystalline solids often involves some fundamental assumptions to simplify the complexity associated with real systems. We present here a brief review on the basic approximations which are essential to understand the lattice dynamical behavior in solids followed by the fundamental models for calculation of vibrational properties in solids.

### 1.3.1 Basic Approximations

In what follows, we present two basic approximations widely incorporated in the state-of-the-art calculation of lattice dynamics in solids.

#### 1.3.1.1 The Harmonic Approximation

The theory of harmonic approximation [1, 3] is based upon a simple assumption which states that the displacement of each ion from its equilibrium position is small compared to the inter-ionic spacing. Introduced for mathematical convenience, the harmonic equations of motion have exact solutions which can lead to precise quantitative results, often in excellent agreement with observed solid properties at least at relatively low temperatures. Here, we state the salient features of this approximation very briefly.

Consider a system consisting of N atoms. Let $M_s$ be the mass of atom $s$, $R_{ls}$ is the position of the $s_{th}$ atom in the $l_{th}$ lattice cell and $u_s(R_l)=R_{ls}$ - $R^0_{ls}$ is its displacement away from its equilibrium positions. In the harmonic approximation, the classical equations of motion are:

$$M_s\ddot{u}_{\alpha s}(R_l) = -\sum_{l's'\beta} C_{\alpha s,\beta s'}(R_l - R_{l'})u_{\beta s'}(R_{l'}) \tag{1.10}$$

where $u_{\alpha s}$ is the $\alpha_{th}$ component in Cartesian coordinates of $u_s$ and

$$C_{\alpha s,\beta s'}(R_l - R_{l'}) = \frac{\partial^2 E}{\partial u_{\alpha s}(R_l)\partial u_{\beta s'}(R_{l'})}\,|_{u_s=0} \tag{1.11}$$

The 3×3 matrix $C_{\alpha s,\beta s'}$ is the inter-atomic force constant matrix which is defined as the force exerted in the $\alpha$-direction on the atom $s$ when the atom $s'$ is displaced a unit distance in the $\beta$-direction.

Due to translational invariance of the lattice, the solution of the infinite set of coupled Eqs. (1.8) are *normal modes* characterized by a vector **q** in reciprocal space and having the form:

$$u_s(R_l, t) = \frac{1}{\sqrt{M_s}} v_s(\mathbf{q})\mathbf{e}^{\mathbf{iqR_l - i\omega t}} \tag{1.12}$$

The equations of motions become:

$$\omega^2 v_{\alpha s}(\mathbf{q}) = \sum_{\beta \mathbf{s}'} \mathbf{D}_{\alpha \mathbf{s},\beta \mathbf{s}'}(\mathbf{q}) \mathbf{v}_{\beta \mathbf{s}'}(\mathbf{q}) \tag{1.13}$$

where $D(\mathbf{q})$ is the *dynamical matrix* which is a $3N_{at} \times 3N_{at}$ hermitian matrix with $N_{at}$ is the number of atoms per unit cell and can be defined as:

$$D_{\alpha s,\beta s'}(\mathbf{q}) = \frac{\mathbf{1}}{\sqrt{M_s M_{s'}}} \sum_{\mathbf{l}} \mathbf{C}_{\alpha \mathbf{s},\beta \mathbf{s}'}(\mathbf{R_l}) \mathbf{e}^{-\mathbf{iqR_l}} \tag{1.14}$$

Therefore, the complete description of the harmonic properties of a crystal can be obtained from the knowledge of the inter-atomic force constants defined in Eqs. (1.9) or (1.12).

#### 1.3.1.2 The Adiabatic Approximation

The adiabatic approximation or commonly known as the Born Oppenheimer approximation [26] is a widely used approximation in solid state physics which decouples the "fast" electronic degrees of freedom from the "slow" ionic ones by virtue of their large mass differences. It assumes that the electronic response to an atomic displacement is instantaneous as compared to the ionic response, thereby, making it possible to separate the electronic and the ionic subsystems. The typical ionic mass $m_i$ is $\sim 10^5$ times bigger than the mass of an electron $m_e$ and the typical kinetic energy of an electron of an electron $E_{ke}$ is $\sim 10^3$ times bigger than the typical ionic kinetic energy $E_{ki}$, implying that the ratio between the typical velocity of an electron $v_e$ and that of an ion $v_i$ becomes $(v_e/v_i) = \sqrt{E_{ke} m_i / E_{ki} m_e} \sim 10^4$. Thus the electrons, being much lighter than the ions, can move in a solid much faster than the nuclei and the electronic configuration can be considered as completely relaxed in its ground state at each position the ions assume during their motion. This implies that during study of the electronic degrees of freedom the ions can be considered at rest and therefore, the total wavefunction of the system can (approximately) be written as the product of a function describing the ions and another for the electrons depending only parametrically upon the ionic positions:

$$\Psi(\mathbf{R}, \mathbf{r}) = \mathbf{\Phi}(\mathbf{R}) \psi_{\mathbf{R}}(\mathbf{r}) \tag{1.15}$$

where $\mathbf{R} = \{\mathbf{R_I}\}$ is the set of all nuclear coordinates and $\mathbf{r} = \{\mathbf{r_i}\}$ is the same quantity for all the electrons in the system. Within this approximation, the ionic wavefunction $\Phi(\mathbf{R})$ is the solution of the Schrodinger equation:

$$\left(-\sum_I \frac{\hbar^2}{2M_I}\frac{\partial^2}{\partial \mathbf{R_I^2}} + E(\mathbf{R})\right)\Phi(\mathbf{R}) = \varepsilon\mathbf{\Phi}(\mathbf{R}) \tag{1.16}$$

where $M_I$ is the mass of the $I^{th}$ nucleus and $E(\mathbf{R})$ is the so called Born-Oppenheimer potential energy surface corresponding to the ground state energy of the electronic system when the nuclei are fixed in the configuration $\mathbf{R}$. The potential energy surface can be computed solving the Schrodinger problem for the electrons:

$$\left(-\sum_i \frac{\hbar^2}{2m}\frac{\partial^2}{\partial \mathbf{r_i^2}} + \frac{e^2}{2}\sum_{i\neq j}\frac{1}{\mid r_i - r_j \mid} - \sum_{iI}\frac{Z_I e^2}{\mid r_i - R_I \mid} + \frac{e^2}{2}\sum_{I\neq J}\frac{Z_I Z_J}{\mid R_I - R_J \mid}\right)\psi^{\alpha}_{\mathbf{R}}(\mathbf{r}) = \mathbf{E}_{\alpha}(\mathbf{R})\psi^{\alpha}_{\mathbf{R}}(\mathbf{r}) \tag{1.17}$$

where $Z_I$ is the charge of the $I^{th}$ nucleus, $-e$ and $m$ are the electronic charge and mass and $\alpha$ is an index for the electronic state.

This approximation which completely neglects the *non adiabatic* terms, is extremely helpful in simplifying many complex situations. For example, in most real materials (e.g., covalent and metallic systems), the ionic motion is inextricably coupled to the motion of the valence electrons. The adiabatic approximation which allows the separation of the electronic and the ionic degrees of freedom provides a very useful simplification to deal with such tricky problems.

### 1.3.2 Models of Lattice Vibration

Here, we illustrate some of the very fundamental theoretical models which have been developed over the years to describe lattice vibrations in a crystal. We present the underlying assumptions and the associated limitations for various approaches.

#### 1.3.2.1 Einstein Model

In this model [27], the atoms in a crystal are treated as independent quantum harmonic oscillators with no correlation between the motion of different atoms. This leads to atomic vibrations which remain entirely unaffected by the motion of the neighbors. The model also makes the simplifying assumption that all the atoms vibrate with the same fundamental frequency, i.e.,

$$\omega(\mathbf{q}) = \omega_{\mathbf{E}} \tag{1.18}$$

The Einstein model has achieved reasonable success; its results are in good agreement with the experiments over most of the temperature range. The theory accounts satisfactorily for the breakdown of equipartition of energy at low temperatures and predicts correctly the specific heat value to be zero at $T = 0$ K. However, the decay of specific heat with decreasing temperature is faster than what is seen in experiments. The observed specific heat at very low temperatures approaches zero as $T^3$ rather than exponentially as predicted by the model. This basic deficiency of the Einstein model is a result of the over simplified assumption that the oscillators do not interact. If the atoms do not interact with one another, sound waves would not propagate through solids.

#### 1.3.2.2 Debye Model

An improved model [28] with correlated atomic motion was brought about by Debye in 1912 to deal with the low temperature discrepancy in Einstein's model. The proposed model known as the elastic isotropic continuum model was the most simplistic view of a solid in which the atomic crystal structure was smeared out and treated as a continuous elastic medium. Within this approximation, the phonon problem is solved in the acoustic limit with the dispersion relations for the three acoustic branches are assumed to be the same and represented by

$$\omega(\mathbf{q}) = \mathbf{v_s q}, \tag{1.19}$$

where $v_s$ is mean sound velocity.

Based on such a simple approximation of continuous medium, the model is surprisingly effective to capture the essential physics behind many important features, including the $T^3$-dependence of specific heat at low temperatures. In spite of its manifold successes, the model, however, becomes inadequate at higher temperatures. The assumption of ignoring the discreteness of the lattice is expected to hold well at low temperatures as modes of only low frequency or long wavelength for which the consequences of discreteness are irrelevant, are involved there. But at high temperature, when the wavelength is short enough to be comparable to inter-atomic spacing, the calculation of the vibrational properties requires a knowledge of the crystal structure and the Debye approximation certainly breaks down. An important consequence of this failure is that the model of Debye can not be used to calculate the phase diagrams correctly. While computing the vibrational free energy differences between different compounds, the high frequency portion of the phonon densities of states plays a significant role which Debye model describes incorrectly. Among other deficiencies, the optical modes which become relevant in polyatomic solids are completely ignored within this model. Also from the theoretical point of view, the model is unrealistic due to the existence of singularities in the density of states.

#### 1.3.2.3 Born-von Karman Model

Around the same time as Debye worked out his theory of specific heats, Max Born and Theodore von Karman proposed another model [29, 30] in which the atomic structures of solids entered explicitly. Within this model which considers interactions of an atom with its neighbors, the restoring force on an atom is determined not by the displacement of the atom from its equilibrium position, but by its displacement relative to its neighbors. This was initially proposed to model the inter-atomic forces between nearest neighbors with a central and non-central component. Later, the model was modified to incorporate the interactions between higher neighbors. The effective crystal potential energy which was proposed for the second order term $V_2$ is given by

$$V_2 = \frac{1}{2}\sum_{lb}^{p}\sum_{l'b'}^{p}\sum_{i}^{3}\sum_{j}^{3}\Phi_{ij}(\mathbf{lb};\mathbf{l'b'})\mathbf{u_i}(\mathbf{lb})\mathbf{u_j}(\mathbf{l'b'}), \tag{1.20}$$

where $p$ is the total number of atoms in the lattice crystal structure and $\Phi_{ij}$ are the force constants between atoms **lb** and $\mathbf{l'b'}$. These inter-atomic force constants are considered as parameters which are fitted to the experimental data for the phonon modes. The corresponding vibrational frequencies $\omega(\mathbf{q})$ are then derived from the eigenvalues of the dynamical matrix **D**.

#### 1.3.2.4 Ab-*initio* Methods

Although the Born-von Karman model provides a vast improvement over the previously available models, it, however, has certain limitations which need to be addressed. For the computation of lattice dynamics in a completely random alloy, the model assumes an average lattice and neglects any fluctuations due to the presence of specie with different chemical properties. Therefore, this formalism never provides a correct picture of the complex nature of inter-atomic forces in a substitutionally disordered alloy. Moreover, the force constants are considered as fitting parameters for the experimentally obtained normal mode frequencies, possibly leading to several sets of force constants which may describe the frequencies equally well. Such deficiencies are completely done away within the *first-principles* electronic structure methods which provide an accurate and parameterless calculation of microscopic electron response to lattice vibrations. The first such microscopic theory of lattice dynamics was formulated in terms of dielectric matrices by Martin *et al.* in 1970 [31]. However, the constraint that the electron-ion interaction must be described by a local potential had limited its utility [32, 33] for the study of vibrational properties. Modern day calculations mainly rely on two approaches which include the direct method [34–36] and the linear response method [37, 38]. While the heavy computational cost associated with the direct method has limited its applicability to zone-center and selected zone-boundary phonon modes in relatively simple materials, the latter approach in contrast is most efficient for the calculation of full phonon dispersion curves and the vibrational density of states. A brief account of the linear response approach will be presented in Chapter 3.

## 1.4 Lattice dynamics of Alloys

Metals are rarely used in their pure forms as almost all pure metals are too soft and ductile for any practical applications. Therefore, in most of the cases, one deals with a metallic alloy which can be defined as a mixture of two or more chemical elements, one of which at least is a metal. The alloying element can be distributed over the crystal lattice sites of the host element and yield a solid solution or it can form different phases showing up as particles in a matrix. In the present discussion we restrict ourselves to solid solutions only which are formed through homogeneous mixture of two or more kinds of atoms in the solid state. In a solid solution, the range of concentration of the alloying element relative to the host element may vary which makes it distinctly different from a chemical compound in which this concentration is fixed. There are in general two different types of alloys which are distinguished based on the position of occupancy of the alloying element. If the atoms of the parent metal are replaced in the crystal lattice by the atoms of the alloying agent then we get what is known as *substitutional alloy* (see Fig. 1.1). Alternatively, if the alloying atoms do not substitute the host metal atoms, but rather enter in the interstices between the host atoms then the alloy is called *interstitial alloy* (see Fig. 1.2).

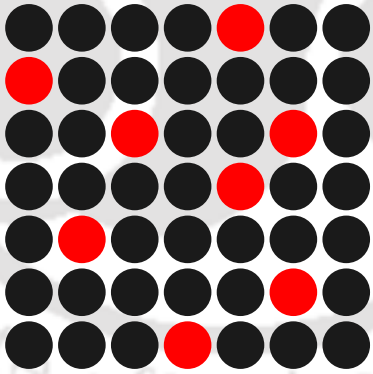

FIGURE 1.1: Substitutional alloy where some of the host element atoms are replaced by atoms of the alloying element of similar size.

The vibrational properties of an alloy are dependent upon quite a number of factors which are mostly related to the elemental properties of the constituent atoms. Next,we discuss some of these issues very briefly.

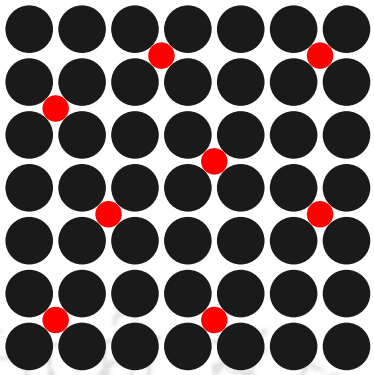

FIGURE 1.2: Interstitial alloy where some of the interstices (holes) in the host element structure are occupied by smaller atoms of the alloying element.

### 1.4.1 The mass effect

Novel features in the phonon spectra can be expected if the alloy constituents have large mass ratio. Localized phonon modes are present for a system with sufficiently light impurities in a matrix of heavy atoms. Being associated with the vibrations of the lighter atoms, these modes are localized with a frequency which is above the host phonon band. Conversely, for a system with light host atoms having heavy impurities, resonance modes corresponding to the vibrations of the heavy atoms with rather low frequencies arise that are within the continuous host phonon band. Experimental measurements have shown both resonant and localized modes for a number of alloys. For example, resonance modes are observed in Cr-W, Ni-Pd, Y-Tb and and Mo-Re alloys [39–43] in the low concentration limit of the heavy element, whereas, in the case of low concentration of the lighter element localized modes are observed in Cu-Al, Nb-Ta, Ge-Si and Rb-K [44–46] alloys. The theoretical calculations are also consistent with the experimental findings for most of these alloys [42, 47–49].

### 1.4.2 The size mismatch effect

The size mismatch of the end-point components of an alloy has been found to have pronounced effect on the vibrational properties of the alloy. When atoms of different sizes are constrained to coexist on a lattice, an atom of larger (smaller) size can experience compressive (tensile) stress depending upon whether it is surrounded with atoms of smaller (larger) sizes. While the presence of larger atoms in the neighborhood reduces the amplitude of lattice

vibrations resulting in a locally stiffer region; the smaller atoms sitting on the neighboring lattice sites creates extra space which results in a locally softer region. The first evidence of this phenomenon has been found in embedded atom method (EAM) [50] based calculations on the disordered state of $Cu_3Au$ compound [51] where the presence of highly compressed pairs of Au atoms lowers the vibrational entropy of the disordered state. A similar effect has been observed in $Ni_3Al$ [52], where very compressed pairs of Al atoms are present in the disordered state. First-principles calculations on $Pd_3V$ [53] have established the role of local lattice relaxation, an even more intriguing size-related effect. In the disordered state of the system, the atoms undergo significant relaxations away from their ideal lattice sites. This leads to incompatible equilibrium lengths for the three types of chemical bonds which needs to be addressed to explain the vibrational entropy changes in the disordered state.

### 1.4.3 The charge transfer effect

As the name suggests, charge transfer in metallic alloys arises from spillover of mobile electrons from one constituent metal to the other. This effect, in general, involves filling or emptying of individual bands as well as their hybridization. There have been numerous studies over the years [54–56] to understand the origin of charge transfer in metallic alloys. These investigations have pointed out that the *electronegativity* of an atom which refers to the power to attract electrons towards itself plays a major role in determining the flow of electrons. As the less electronegative element loses valence electrons to the more electronegative element, a greater difference between the electronegativities of the two bonded species will, therefore, result in a greater charge transfer, in general. The Fermi energy ($E_F$) of the bonded elements is also relevant in the context of charge transfer. It has been noticed that the charge flows from an element with higher value of $E_F$ to an element with lower value of $E_F$. The greater the difference between the Fermi energies of the two elements, the greater is the charge transfer magnitude.

The charge transfer modifies the electronic configuration of the impurity and its neighboring host ions significantly which is subsequently reflected in the inter-atomic interactions between different chemical species in a random alloy. Thus, the calculation of the impurity potential and its interactions with the host ions in metallic alloys must be performed in a self-consistent way taking into account the charge transfer effects. In a recent study on aluminium

transition-metal (TM) systems [57], pronounced composition dependence of the calculated force constants has been observed. This phenomenon, considered to be a consequence of charge transfer effects associated with the bonding in these systems had to be taken care of to yield accurate and reliable results.

### 1.4.4 The short-range order effect

To deal with disordered materials, the most useful approach is to assume that the atoms of the various species are distributed randomly over the sites of the underlying lattice. However, in different physical situations, the atomic arrangement is not random, but may exhibit some degree of short-range order (SRO), i.e., the excess probability of finding certain pairs of atoms relative to random statistics. Depending upon whether the atoms of a given kind tend to surround themselves preferentially with atoms of the same kind or of a different kind, the atomic arrangement is called clustering or ordering. This ordering (or clustering) tendency influences the local chemical environment which eventually determines the inter-atomic interactions between various species in a random alloy. Therefore, the presence of SRO may alter the vibrational entropy differences among various phases of a compound and hence their relative stability. There exists numerous investigations both on the experimental and the theoretical front which signify the presence of short range order and their simultaneous effect on various alloy properties. While the experimental measurements have reveled the existence of short range ordering on a number of Cu- and Ni-based alloys [58–64], the theoretical calculations have also provided ample evidence of short range ordering in metal alloys such as Cu-Au, Cu-Zn and Ni-Au [65–67].

## 1.5 Outline of the thesis

Study of lattice vibrations in solids offers interesting perspectives regarding materials properties and behavior. This is even more intriguing in substitutionally disordered alloys as the presence of three different kinds of disorder: the mass, the force-constant and the environment results in novel features in the phonon spectra. In order to understand the lattice dynamical properties in this class of materials, a thorough microscopic understanding of the

roles played by the presence of each of these three types of disorder, are, therefore, necessary. The modeling of these three types of disorder, often inter-wined with one another, is a challenging problem. Although the advent of first-principles electronic structure formalisms have made possible the calculations of phonon spectra in systems with perfect periodicity, a tractable methodology to incorporate the random environment in a disordered alloy is yet to be found. The intractability arises due to the fact that within the framework of state-of-the-art first-principles methodologies, random environment in a disordered alloy is simulated by constructing prohibitively large artificial periodic structures. Such a limitation aggravates the challenge posed by the problem of investigating lattice dynamics in these systems.

In this thesis, we have worked on the development of new first-principles based formalisms to compute the lattice dynamics in substitutionally disordered alloys which can incorporate the effects of disorder in mass, force constant and environment on equal footing. We have validated our approaches by computing the phonon dispersion spectra and elastic properties for a variety of alloys which involve magnetic type-II alloy ($Fe_xPd_{1-x}$) and alloys with significant mass and size differences among the constituents ($Cu_xAu_{1-x}$ and $Ni_xPt_{1-x}$).

Chapter 2 discusses various methods for performing the configuration averaging, a key part in computation of elementary excitations in substitutionally disordered alloys. While several schemes have been proposed to perform the all important configuration averaging in disordered systems, most of them do not fulfill all the requirements to study the phonon excitations where off-diagonal disorder plays a significant role. Notable among them are the virtual crystal approximation (VCA) and the average t-matrix approximation (ATA). The VCA models the disordered sample as consisting of sites with a constant average potential and thus, fails to account for strong on-site disorder. The ATA, though modifies this shortcoming, but, fails to include the effect of scattering from the medium in a self-consistent way. The coherent potential approximation (CPA) provides a significant improvement over these two by constructing the scattering medium in a self-consistent way. But, its success is limited because of its single-site nature. This is more so in case of phonon excitations, due to the fact that the multi-site correlations are a must in treatment of phonons.

The recently developed itinerant coherent potential approximation (ICPA) takes care of the shortcomings and provides a successful, self-consistent, analytic method to perform the configuration averaging in substitutionally disordered alloys. Since this method handles the

multi-site correlations appropriately, the reliable computation of phonon spectra becomes possible. In this thesis, we use this method for computation of the configuration-averaging of necessary quantities.

Chapter 3 introduces the ideas of first-principles based modeling of inter-atomic interactions in substitutionally disordered alloys. Although the ICPA is able to illustrate the importance of the force-constant disorder in the context of phonon spectra in disordered alloys, its accuracy is heavily dependent upon the reliability of the inter-atomic force constants. The most trustworthy source available in this regard are the first-principles electronic structure methods, but these methods are difficult to employ for our systems of interest, the reasons for which have been mentioned earlier. In this thesis, we work on different hybrid approaches to model the inter-atomic force-constants in random alloys. The first such attempt is based upon the results of *ab initio* calculations and the intuitive argument about dependence of force constants on bond lengths. This strategy improves upon previous theoretical results on $Pd_xFe_{1-x}$ alloys and provides reasonably good agreement with experiments. The crude approximations used in this approach, however, restricts its applicability to alloys with arbitrary concentrations. Further improvements are realized by adopting the transferable force-constant (TFC) model of Ceder and co-workers which suggests that the "force constant versus bond length" relationship is transferable across different compositions for a given alloy. The novel feature of this approach is that the inter-atomic force-constants for a given specie pair can be calculated with modest computational cost and at any arbitrary composition. By adopting the TFC model, we formulate a new approach to compute lattice dynamics in substitutionally disordered alloys which is a combination of first-principles density functional perturbation theory (DFPT), the TFC model for accurate computation of force-constants in random alloys and the ICPA method for configuration averaging in disordered environment.

Chapter 4 discusses the application of the DFPT-TFC-ICPA approach for a number of binary alloys at arbitrary compositions. A thorough analysis of the phonon spectrum in $Pd_xFe_{1-x}$ is presented over the entire concentration range. As compared to our previous approach, the DFPT-TFC-ICPA method provides force-constants which represent the inter-atomic interactions in these alloys more realistically and therefore, an overall improvement in the phonon dispersion curves is observed. This is followed by application of our method to size-mismatched binary alloys $Cu_{0.715}Pd_{0.285}$ and $Cu_{0.75}Au_{0.25}$, where the effects of size mismatch of the end-point components on the lattice dynamics are investigated. We demonstrate that the local lattice relaxations play a very crucial role in determining the lattice dynamical

properties of these alloys. On incorporation of bond-length fluctuations, excellent agreement with the experimental results is achieved for $Cu_{0.715}Pd_{0.285}$, whereas, some discrepancies are observed for $Cu_{0.75}Au_{0.25}$ which are attributed to the limitations in the experiments. We close this chapter by presenting results for another size-mismatched alloy $Ni_xPt_{1-x}$ for which the agreement between our results and that of the experiments is reasonably good except for the case of $Ni_{0.25}Pt_{0.75}$ where we see a qualitative difference between the two in the phonon dispersion curves. Ambiguous nature of experimental results and the non-incorporation of short-range order in our calculations are the possible explanations for this discrepancy. In a nutshell, this chapter demonstrates that the DFPT-TFC-ICPA method has the required accuracy and reliability regarding computation of vibrational properties of disordered alloys.

Chapter 5 focuses on construction of better structural models for substitutional disorder so that the methodology can be made completely parameter free and the environmental disorder can be treated in a better way. To this end, we model the disordered alloy by constructing special quasi-random structure (SQS) which is an artificial periodic structure where the atoms occupy the lattice sites in a way that closely mimic the pair-correlation functions of the real alloy with a given composition. Such an accurate modeling of the environmental disorder paves the way for a reliable description of phonon spectra in alloys with short-range order where the force-constants between a pair of specie is dominated by a particular configuration of the nearest neighbor environment around an atom. We demonstrate the novelties of this new formalism which is a combination of reliable force-constants calculated by the SQS method and the ICPA as a self-consistent analytic method for configuration averaging, by computing the phonon dispersion spectra of $Ni_{0.50}Pt_{0.50}$ alloy. The agreement of our results with the experiments is much better than previous models of disorder suggesting that the proposed formalism represents the inter-atomic interactions among various pairs of chemical species in a disordered environment of an alloy better.

Chapter 6 concludes with a summary of the main results of the thesis. The importance of these results alongwith the possible extensions are discussed thereafter.

# Chapter 2

# Methods of configuration averaging for phonon excitations in random alloys

## 2.1 Introduction

The Hamiltonian for lattice vibrations in disordered systems is given in a site representation as-

$$H = \sum_{l,\alpha} \frac{{p_\alpha^l}^2}{2m_\alpha^l(s_l)} + \frac{1}{2} \sum_{\alpha,\alpha',l,l'} \Phi_{\alpha\alpha'}^{ll'}(s_l, s_{l'}) u_\alpha^l u_{\alpha'}^{l'} \tag{2.1}$$

where, $p$ and $u$ are momentum and displacement operators respectively, $l$ specifies the unit cell at $\mathbf{R}(l)$, $\alpha$ specifies one of the $3\nu$ Cartesian coordinates of the $\nu$ atoms in the cell, $m$ is mass of an atom and $\{s_l\}$ is the set of occupation numbers associated with the site $\{l\}$. Since in this thesis we consider only the binary alloys $A_{C_A}B_{C_B}$, the occupation number $s_l = 1$ if $l$ is occupied by $A$ and $s_l = 0$, otherwise. The feature which makes the theory of phonon excitations difficult is the inseparability of diagonal and off-diagonal disorder. The reason for this is that the force-constant sum rule, i.e. the force constants between a site $i$ and its neighbors $j$ obey the relation $\mathbf{\Phi}_{ii} = -\sum_{j\neq i} \mathbf{\Phi}_{ij}$, must be rigorously satisfied even if the system is disordered. In other words, a single defect at one site in the system perturbs even the diagonal Hamiltonian on its neighbors, thereby imposing environmental disorder on the force-constants. Hence,

any theory must include diagonal, off-diagonal, and *environmental* disorder as well in order to produce reliable results for phonons.

Solving the eigenvalue problem with the Hamiltonian (2.1) could be quite an involved job. However, to make a connection to the experimentally measurable physical quantities, it is sufficient to have a knowledge of the configuration-averaged Green's function of the alloy. For example, the partial Green's functions $\ll G^s(\omega) \gg$ can be related to the incoherent scattering structure factor which is directly measured in the experiments,

$$\ll S_{incoh}\left(\vec{Q},\omega\right) \gg = \sum_s b_s^2 \vec{Q} \cdot \mathcal{I}m \ll G^s(\omega) \gg \cdot \vec{Q}, \tag{2.2}$$

where $b_s$ is the incoherent scattering length for atoms of type $s$, $Q$ is the phonon wavenumber and <<>> denotes configuration averaging. Similarly, a knowledge of the configuration-averaged spectral function $<< G_\lambda^{ss'}(\vec{q}, w^2) >>$ associated with the species pair $s, s'$ enables one to calculate the coherent-scattering structure factors which are also measured directly in the neutron-scattering experiments and are given by,

$$\ll S_\lambda(\vec{q},\omega) \gg_{coh} = \sum_{ss'} d_s d_{s'} \frac{1}{\pi} \mathcal{I}m \ll G_\lambda^{ss'}\left(\vec{q},\omega^2\right) \gg \tag{2.3}$$

where, $\lambda$ is the normal-mode branch index and $d_s$ is the coherent scattering length for the species $s$. The phonon frequencies and the disorder-induced widths are obtained respectively from the peaks and from the widths of these coherent scattering structure factors.

Also, the total vibrational density of states can be obtained from the imaginary part of the configuration-averaged mass-weighted Green's function as follows,

$$\nu(\omega) = \frac{1}{3\pi N} \mathcal{I}m\{Tr \ll \mathbf{m}.\mathbf{G}(\omega^2) \gg\} \tag{2.4}$$

where $\mathbf{m}$ is the mass matrix, and $N$ is the number of sites. The partial density of states for atoms of type $s$ is defined as

$$\nu(\omega)_s = \frac{m_s}{3\pi N} \mathcal{I}m\{Tr \ll G(\omega^2)^{ss} \gg_{ii}\} \tag{2.5}$$

Here, the focus is particularly on the configuration-averaged displacement-displacement (one-phonon) Green's function [68] which can be defined as-

$$\ll G_{\alpha\alpha'}(l,l';t) \gg = \ll u_{\alpha}(l,t), u_{\alpha'}\left(l',0\right) \gg \tag{2.6}$$

Using the Hamiltonian in Eq. 2.1, one can write the equation of motion of this Green's function in frequency domain as-

$$m^{l}_{\alpha}(s_l)\omega^2 G^{ll'}_{\alpha\alpha'}(s_l, s_{l'};\omega) = \delta_{\alpha\alpha'}\delta^{ll'} + \sum_{\alpha'',l''} \Phi^{ll''}_{\alpha\alpha''}(s_l, s_{l''}) G^{l''l'}_{\alpha''\alpha'}(s_{l''}, s_{l'};\omega) \tag{2.7}$$

or, in matrix form

$$\mathbf{G}\left(\{s_l\},\omega^2\right) = \left[\omega^2 \mathbf{m}(\{s_l\}) - \mathbf{\Phi}(\{s_l\})\right]^{-1} \tag{2.8}$$

The configuration averaged Green's function, therefore, is,

$$\ll \mathbf{G}\left(\omega^2\right) \gg = \ll \left[\mathbf{m}\omega^2 - \mathbf{\Phi}\right]^{-1} \gg . \tag{2.9}$$

It is $\ll \mathbf{G} \gg$ which carries all the dynamical informations of interest, and the essential difficulty of the theory of phonons in random systems arises from taking the configuration average of the inverse of the matrix $\mathbf{m}\omega^2 - \mathbf{\Phi}$. For any real system, the large number of atoms ($N$ is of the order of Avogadro's number) and the associated configurations of these atoms makes the evaluation of configuration averaged quantities an impossible task. Thus, several approximations have been adopted over the years to make the configuration averaging a tractable problem. The fundamental equation which allows great simplification of the problem is the Dyson's equation which states that the configuration averaged Green's function $\ll \mathbf{G}\left(\omega^2\right) \gg$ can be obtained by simply calculating the self-energy $\mathbf{\Sigma}\left(\omega^2\right)$. The equation can be defined as-

$$\ll \mathbf{G}\left(\omega^2\right) \gg = \left[\mathbf{G}_0^{-1}\left(\omega^2\right) - \mathbf{\Sigma}\left(\omega^2\right)\right]^{-1} . \tag{2.10}$$

where, $\mathbf{G}_0\left(\omega^2\right) = \left(\overline{\mathbf{m}}\omega^2 - \overline{\mathbf{\Phi}}\right)^{-1}$ is the unperturbed Green's function and $\overline{\mathbf{m}}$ and $\overline{\mathbf{\Phi}}$ are the configuration-averaged mass and force-constant operators respectively. The corresponding self-energy $\mathbf{\Sigma}\left(\omega^2\right)$ in Eq. 2.10 includes the effect of scattering due to fluctutaions in the medium. In substitutionally disordered alloys due to associated complexities, the calculation of $\mathbf{\Sigma}\left(\omega^2\right)$ is a tedious job which is usually taken care off with the help of approximate methods involving various simplifying assumptions. Next, we discuss some of these methods very briefly.

## 2.2 Virtual crystal approximation (VCA)

This is conceptually the simplest approach [69] to deal with the problem of configuration averaging in disordered binary alloys having any arbitrary composition. Within this approximation, an alloy of type $A_xB_y$ is modeled as a periodic virtual solid with the same mass $M^{alloy} = \langle M \rangle = xM_A + yM_B$ and the same force constant $\overline{\mathbf{\Phi}} = c_{AA}^2\mathbf{\Phi}_{AA} + c_{BB}^2\mathbf{\Phi}_{BB} + 2c_Ac_B\mathbf{\Phi}_{AB}$ associated with the alloy. The resulting Green function then becomes reminiscent of the Green function of a pure system with the corresponding self-energy $\Sigma$ being real, energy independent and has no dependence on the wave vector $\vec{k}$. It has been fairly successful in explaining the properties of weak scattering alloys in which the wavefunctions are extended over many lattice spacings and each particle sees nearly the same average perturbation. However, a real $\Sigma_{VCA}$ (self-energy of the VCA medium) results in a pure system like infinite lifetime of the $\vec{k}$-states which is certainly in contradiction to the expectation that in a disordered system, the states should be decaying as a result of scattering off the impurities. So, the method is not appropriate for systems with strong disorders. Further, VCA fails to reproduce the split-band behavior observed in many real systems.

## 2.3 Average t-matrix approximation (ATA)

This is the next level of approximation [70] which provides a much improved description of the disordered systems over that of the VCA. Within this approximation, the scattering off a site depends solely on the occupation of the site with the effect of disorder in the local environment being neglected. For small concentrations when the multisite correlation effects

are not so significant, one may neglect the inter-site scattering. The ATA is based on the scattering matrix or the t-matrix which involves only scattering off the same site. The Green function is expressed in terms of the configuration averaged t-matrix which is evaluated within the single site approximation. In contrast to VCA, ATA yields impurity bands and states with finite life times. Its main limitation is its inability to reproduce correctly the band edges of the alloy density of states. This is due to the use of VCA unperturbed Green function as a starting point. As a consequence, the self-energy has the analytic structure of the host lattice Green function and a simple pole. The pole produces the impurity bands but cannot move the unperturbed band-edges from the values in the host (VCA) material. Another serious shortcoming of the ATA is that the self-energy is not determined self-consistently.

## 2.4 Coherent potential approximation (CPA)

This is the most widely used approximation in the context of configuration averaging which was introduced simultaneously by Soven [71] in connection with disordered electronic systems and by Taylor [72] in connection with the lattice dynamics of mass disordered alloys. It belongs to the class of mean field theories analogous to the Weiss molecular field theory of magnetism in which the properties of entire material are determined from the behavior at a localized region, usually taken to be a single site (cell) in the material. The approximation considers a homogeneously disordered medium with only independent scatterings of diagonal sites being involved in the formalism. For a system with homogeneous disorder, the configuration average of any physical quantity over all configurations is independent of position (site) in the lattice. One may, then, consider any single site in a specific configuration and replace the surrounding material by a translationally invariant medium, constructed to reflect the ensemble average over all configurations. In the CPA, this medium is chosen in a self-consistent way. One assumes that averages over the occupation of a site embedded in the effective medium should yield quantities indistinguishable from those associated with a site of the medium itself. Because a translationally invariant medium produces no scattering of a wave, it is assumed that the scattering off a real atom embedded in a CPA medium, averaged over the possible configurations of a single site, should produce the corresponding Green function of the medium itself. This self-consistency condition yields an effective Hamiltonian describing the medium, called the **coherent potential Hamiltonian**.

Here, we choose a binary alloy to describe the essential features of this formalism, which can be generalized rather easily to multicomponent alloys. Consider an alloy of a finite concentration, $C$, of atoms of type $B$ embedded in a host material of type A. The mass matrix of the alloy within the CPA formalism is given by,

$$M_{ij} = M_0(1 - \epsilon_i)\delta_{ij}, \tag{2.11}$$

where, $\epsilon_i$ is the *fractional mass defect* which becomes zero at host atom sites and takes the value $\epsilon_\alpha$ at sites occupied by atoms of type $\alpha$. Hence, $M_0 \equiv M_A$ and $\epsilon_i = 0$ at $A$ sites and $\epsilon_i \equiv \epsilon_B$ at B sites. Due to the consideration of only diagonal disorder, the force constants between various pairs of species in this method are treated only in an average way, identical to the VCA formalism. The corresponding self-energy then becomes-

$$\Sigma\left(\omega^2\right) = \frac{CM_A\epsilon\omega^2}{1 - (1 - C)M_A\epsilon\omega^2\bar{G}_{00}/(1 + \Sigma\bar{G}_{00})}, \tag{2.12}$$

where, $\bar{G}_{00}$ denotes the Green function of the effective medium. Once $\Sigma$ has been determined, $\bar{G}$ can be evaluated as,

$$\bar{G}\left(\omega^2\right) = (M_A\omega^2 - \Sigma - \phi)^{-1} \tag{2.13}$$

## 2.5 Generalizations of the CPA

Despite its success, particularly in the electronic problem, the CPA is a single-site, mean-field approximation and could deal with only diagonal (or mass, in the case of phonons) disorder. The phonon problem is specifically difficult because, in it, diagonal and off-diagonal disorders are impossible to separate. Consequently, we do not expect the CPA to give an adequate description of the phonon problem. This was evident from a number of calculations [73–77], which indicated large discrepancies between the CPA and the experimental results. In the electron problem too, whenever there was offdiagonal disorder, as in the case of alloys with large size difference between its constituents leading to local lattice distortions [78] or

environmental disorder as in the case of alloys with short-range order [79, 80], the CPA was found to be inadequate.

The hunt for adequate extensions of the CPA was quite rigorous during the 1970s and 1980s [81–87]. However, only in certain very special cases, such as the *separable* [82] or the *additive* [83, 84] limits of off-diagonal and environmental disorder, were there successes. Among the cluster generalizations, the *Embedded cluster method (ECM)* was put forward in 1977 [88] where a cluster of real atoms is embedded in an effective medium usually obtained in the CPA. For a given analytic effective medium, the ECM yields analytic, well defined and physically meaningful results but the main disadvantage of the method is that it is non self-consistent and therefore does not yield a new effective medium or improved momentum spectral weight-functions. The effects of scattering from clusters of atoms can be easily included by means of a technique called the *Molecular coherent potential approximation (MCPA)* [89]. It accomplishes the self-consistent incorporation of local environment fluctuations into the effective medium self-energy and yields density of states related to specific cluster configurations. But, it has got some serious drawbacks. Firstly, it is computationally very cumbersome and secondly, it yields a super-lattice effective medium which violates the single site translational invariance of the given lattice. Eventually, three approaches emerged as the most successful. Two of them are based on the augmented-space theorem of Mookerjee [90]: the itinerant coherent-potential approximation (ICPA) of Ghosh *et al.* [91] and the augmented-space recursion (ASR) of Saha *et al.* [92] and Alam *et al.* [93]. The former is an extension of the ideas of Mills and Ratanavaraksa [94] and Kaplan and Gray [95, 96] and the latter combines the augmented-space technique with the recursion method of Haydock *et al.* [97]. The third is a very different and rather striking approach developed by Rowlands *et al.* [98] and Biava *et al.* [99] (the nonlocal CPA or NL-CPA) using the idea of coarse graining in reciprocal space originally proposed by Jarell and Krishnamurthy [100].

In this thesis, we concentrate on the ICPA formalism for the calculation of vibrational properties of disordered binary alloys. In the next section, we briefly describe the salient features of the ICPA.

## 2.6 Itinerant coherent potential approximation (ICPA)

Among the cluster generalizations of the CPA, the recursion method [97] is one of the few formalisms which met with some success for real alloy systems. The method has the ability to handle large clusters and can treat all kinds of disorder on equal footing. However, the approach suffers from the drawback that it is neither self-consistent nor translationally invariant when used alone. Nevertheless, a self-consistent generalization of the CPA to include two-cite scattering using a recursion method [97] in conjunction with the augmented space formalism (ASF) [90, 95, 96] was provided by Yussouf and Mookerjee [101]. The ICPA on the other hand is based on the ideas of travelling cluster approximation (TCA) [94]. Introduced by Mills and Ratanavaraksa, TCA is an extension of the CPA, derived using diagrammatic methods, which provides a successful self-consistent multisite scattering theory, albeit, with the restriction to treating diagonal disorder only. The approximation, however, suffers from several drawbacks which include computational inefficiency and the lack of guidance about the selection of appropriate diagrams. It was later re-derived using the operator methods of the augmented space formalism [90, 95, 96] by Diehl and Leath [102]. The virtues of TCA and ASF were then combined for the first time by Diehl and Leath [103] to describe a theory for phonons with disordered force constants. This approximation, however, is very similar in structure to the additive limit of CPA. Similar ideas based on the TCA and the ASF were used by Kaplan, Leath, Gray and Diehl (KLGD) [104] to develop an improved theory for elementary excitations. Using the diagram symmetry rule of Mills and Ratanavaraksa [94] and the translational symmetry of the augmented space operators [90, 95, 96], they presented a self-consistent multiple scattering theory which include diagonal, off-diagonal and environmental disorder and multisite effects. Such a theory allows one to work with a small number of atoms instead of treating large clusters as is done in recursion. However, they illustrated their method only with one-dimensional models. A tractable generalization of the KLGD method [104] for a single-site scattering of phonons in three-dimensional lattices is provided by Ghosh *et al.* [91]. This formalism known as the ICPA, is an analytic, self-consistent, mean-field based cluster generalization of the single site CPA which considers diagonal, off-diagonal and environmental disorder on equal footing. In addition, the operators in the augmented space are translationally invariant so that the state-of-the-art methods for periodic systems can easily be employed for substitutionally disordered alloys which makes the approach a computationally feasible one.

In the next sub-sections, we describe in brief the ICPA formalism. We first describe the Augmented space formalism [90, 95, 96] and show how the ideas can be implemented within the multiple scattering picture, resulting in an analytic, self-consistent theory for phonon excitations.

### 2.6.1 The Augmented Space Formalism

In the augmented space formalism, the excitations are considered to be moving in periodic potentials in the presence of a 'field' which specifies the disorder. The Hamiltonian, which is expanded to include the disorder field, then by itself completely describes the disordered system. Since the information on random configurations is already incorporated into the Hamiltonian, the configuration averaging is not a further process as in the mean-field approaches, but simply an evaluation of matrix elements. The idea of introducing a 'disorder field' to describe the random fluctuations in the system by extending the Hilbert space to include the disorder field and by representing the Hamiltonian in this new space constitutes the core of the augmented-space formalism. The extended Hilbert space which captures the random fluctuations is called the 'augmented space'.

Here, we work only with a binary alloy $A_{c_A}B_{c_B}$. We assume that each lattice site is randomly occupied by an A atom or by a B atom. The masses are random,

$$m_{ij}^{\alpha\beta} = m_i \delta_{\alpha\beta}\delta_{ij}, \tag{2.14}$$

with $m_i$ randomly taking on the value $m^\Gamma$ if species $\Gamma$ = A, B is on site $i$. The force-constants take on the values $\left(\phi_{ij}^{\alpha\beta}\right)^{\Gamma\Delta}$ if species $\Gamma$ is on site $i$ and species $\Delta$ is on site $j$. $\alpha$ and $\beta$ specify the Cartesian directions.

As shown in Eq. 2.9, the determination of $\ll \mathbf{G} \gg$ requires calculation of the average of the matrix $\mathbf{m}\omega^2 - \mathbf{\Phi}$ which is a tedious job. The augmented-space technique [90, 95] greatly facilitates this averaging. The masses $\mathbf{m}$, force-constants $\mathbf{\Phi}$, and Greens function $\mathbf{G}$ are defined in the dynamical Hilbert space $\Psi$ in which the Hamiltonian of the system operates. For a binary alloy, $\Psi$ is augmented by the space $\Theta$ of all possible atomic configurations of the system. The resulting augmented space $\Omega$ is

$$\Omega = \Psi \otimes \Theta$$

In $\Omega$ or $\Theta$ operators are represented by symbols with superposed carets. In the *configuration representation* within $\Theta$, the state of site $i$ is specified by the single-site state $|A_i\rangle$ if A is on $i$ and by $|B_i\rangle$ if B is on $i$. With respect to these states, the occupation operators $\hat{\eta}_i'^{\Gamma}$, $\Gamma$ = A, B,

$$\begin{aligned} \hat{\eta}_i'^{A}|A_i\rangle &= |A_i\rangle, \quad \hat{\eta}_i'^{A}|B_i\rangle = 0, \\ \hat{\eta}_i'^{B}|B_i\rangle &= |B_i\rangle, \quad \hat{\eta}_i'^{B}|A_i\rangle = 0 \end{aligned} \tag{2.15}$$

are represented by the matrices

$$\hat{\eta}_i'^{A} = \begin{pmatrix} 1 & 0 \\ 0 & 0 \end{pmatrix}, \hat{\eta}_i'^{B} = \begin{pmatrix} 0 & 0 \\ 0 & 1 \end{pmatrix} = \hat{\mathbf{I}}_i - \hat{\eta}_i'^{A}. \tag{2.16}$$

The configuration of the entire system is specified by the direct product of all single-site states $\prod_i |\Gamma_i\rangle$, $\Gamma$ = A, B. The mass operator for site $i$ is given by,

$$\hat{\mathbf{m}}_i' = m^A \hat{\eta}_i'^{A} + m^B \hat{\eta}_i'^{B}. \tag{2.17}$$

Similarly the force-constants for sites $i$ and $j$ are given by

$$\hat{\mathbf{\Phi}}_{ij}' = \phi_{ij}^{AA} \hat{\eta}_i'^{A} \hat{\eta}_j'^{A} + \phi_{ij}^{AB} \hat{\eta}_i'^{A} \hat{\eta}_j'^{B} + \phi_{ij}^{BA} \hat{\eta}_i'^{B} \hat{\eta}_j'^{A} + \phi_{ij}^{BB} \hat{\eta}_i'^{B} \hat{\eta}_j'^{B} \tag{2.18}$$

with the Cartesian indices understood.

Consider now a rotated representation for site $i$ in which the basis vectors for its configuration space are given by

$$\begin{aligned} |0_i\rangle &= \sqrt{c_A}|A_i\rangle + \sqrt{c_B}|B_i\rangle, \\ |1_i\rangle &= \sqrt{c_B}|A_i\rangle - \sqrt{c_A}|B_i\rangle. \end{aligned} \tag{2.19}$$

Here, $|0_i\rangle$ is the site-average state (or the virtual-crystal state) and $|1_i\rangle$ describes a fluctuation away from the average state on site $i$. In this representation, the configuration average of any operator $\hat{\mathbf{A}}$ in $\Theta$ can be carried out simply by taking the expectation value of $\hat{\mathbf{A}}$ with the state

$$|f\rangle = \prod_i |0_i\rangle, \tag{2.20}$$

whereas,

$$|f_i\rangle = |1_i\rangle \prod_{j\neq i} |0_j\rangle. \tag{2.21}$$

describes a state in which there is a fluctuation or a defect in the average state $|f\rangle$ only on site $i$. In this *fluctuation representation* the occupation operators $\hat{\eta}_i'^A$ and $\hat{\eta}_i'^B$ are transformed to

$$\begin{aligned} \hat{\eta}_i^A &= \begin{pmatrix} c_A & \sqrt{c_A c_B} \\ \sqrt{c_A c_B} & c_B \end{pmatrix} \\ \hat{\eta}_i^B &= \begin{pmatrix} c_B & -\sqrt{c_A c_B} \\ -\sqrt{c_A c_B} & c_A \end{pmatrix}. \end{aligned} \tag{2.22}$$

In transforming from the configuration representation to the fluctuation representation, $\hat{\mathbf{m}}'$ goes to $\hat{\mathbf{m}}$ and $\hat{\mathbf{\Phi}}'$ to $\hat{\mathbf{\Phi}}$, as given by Eqs. 2.17 and 2.18, respectively, with the $\hat{\eta}'^{\Gamma}$ of Eq. 2.16 replaced by the $\hat{\eta}^{\Gamma}$ of Eq. 2.22. Thus the dynamical operators $\hat{\mathbf{m}}$ and $\hat{\mathbf{\Phi}}$ are not diagonal with respect to the number of fluctuations or defects in the fluctuation representation and can create them, destroy them, or, in the case of $\phi_{ij}$, cause them to travel, or 'itinerate'. We refer

to the movement of defects induced by the off-diagonal elements of the $\hat{\eta}_i^\Gamma$ as the *itineration of fluctuations* to distinguish it from the *propagation* of phonons. However, these operators are translationally invariant; the randomness in configuration is thus captured by translationally invariant operators in the configuration space $\Theta$. The $\hat{\eta}^\Gamma$ operators constitute the disorder field referred to above.

Any operator $\hat{\mathbf{A}}$ in this augmented space can be represented in block form,

$$\hat{\mathbf{A}} = \begin{pmatrix} \bar{\mathbf{A}} & \mathbf{A}' \\ \mathbf{A}'^{\dagger} & \tilde{\mathbf{A}} \end{pmatrix}, \tag{2.23}$$

where the bold notation $\mathbf{A}$ implies a matrix in the site and Cartesian indices. The four elements of the block matrix are given by

$$\begin{aligned} \bar{\mathbf{A}} &= \mathbf{P}\hat{\mathbf{A}}\mathbf{P}, \\ \mathbf{A}' &= \mathbf{P}\hat{\mathbf{A}}\,(\mathbf{1}-\mathbf{P}), \\ \mathbf{A}'^{\dagger} &= (\mathbf{1}-\mathbf{P})\,\hat{\mathbf{A}}\mathbf{P}, \\ \tilde{\mathbf{A}} &= (\mathbf{1}-\mathbf{P})\,\hat{\mathbf{A}}\,(\mathbf{1}-\mathbf{P}), \end{aligned} \tag{2.24}$$

where $\mathbf{P}$, the projection operator onto the virtual-crystal state, is given by $\mathbf{P} = |f\rangle\langle f|$ . Thus, we see that $\bar{\mathbf{A}}$ is the configuration average of the quantity $\hat{\mathbf{A}}$ while $\mathbf{A}'$, $\mathbf{A}'^{\dagger}$ generate the coupling between the average and the fluctuation states and $\tilde{\mathbf{A}}$ is that part of $\mathbf{A}$ entirely within the space of fluctuation states.

With the restriction of treating explicitly only single fluctuation states $|f_l\rangle$ in the fluctuation space $\Theta - |f\rangle\langle f|$, states in $\Omega$ can be specified by $|i\,f\rangle$ or $|i\,f_l\rangle$ where $i$ is the site index of the dynamical variable in $\Psi$, position or momentum, with the Cartesian index understood. For the site indices of the corresponding matrix elements we shall often use the compact notation

$$\begin{aligned}
\langle if|\hat{\mathbf{A}}|jf\rangle &= \bar{A}_{ij}, \\
\langle if_l|\hat{\mathbf{A}}|jf_{l'}\rangle &= \tilde{A}_{ij}^{(l)(l')}, \\
\langle if|\hat{\mathbf{A}}|jf_l\rangle &= A_{ij}^{\prime(l)}, \\
\langle if_l|\hat{\mathbf{A}}|jf\rangle &= A_{ij}^{\prime\dagger(l)},
\end{aligned} \tag{2.25}$$

where $l$ and $l'$ denote the locations of the concentration fluctuation or defect. The parentheses around $l$ indicate that it is neither a site nor a Cartesian direction index, but indicates instead the position of a *fluctuation* in the lattice.

### 2.6.2 Multiple-scattering picture

A phonon propagating in a random alloy undergoes irreducible multiple scattering [105] both repeatedly off a single fluctuation and successively off fluctuations on the different sites it encounters in the process. The CPA takes into account the former but not the latter. To illustrate how the treatment of this process of multiple scattering by fluctuations differs between the CPA and our formalism we employ a cartoon diagram (Fig. 2.1). The top panel, a two-dimensional cross-section, illustrates the multiple-scattering process included in the CPA. There, the filled circle is a single 'fluctuation site' immersed in an average medium denoted by open circles. The arrow on the left is the direction of phonon propagation. When the phonon meets the fluctuation site, it undergoes irreducible multiple scattering at that site. In the CPA (diagonal disorder), the irreducible scattering by the defect site is confined to the defect site. The circle around the fluctuation site indicates the region of influence of the perturbation. None of the springs are affected by the presence of this defect since the force-constants are the same everywhere. One does an averaging over all the possible occupations of the single site.

The lower three panels in Fig. 2.1 illustrate scattering sites in the ICPA. The difference from the CPA is that the region of influence is not only the site of fluctuation but also its neighboring environment around the fluctuation site. The figure shows an example (dotted contour) where the environment includes nearest neighbors only (The calculations could be extended to further neighbors as well). When the phonon interacts with the fluctuation site in

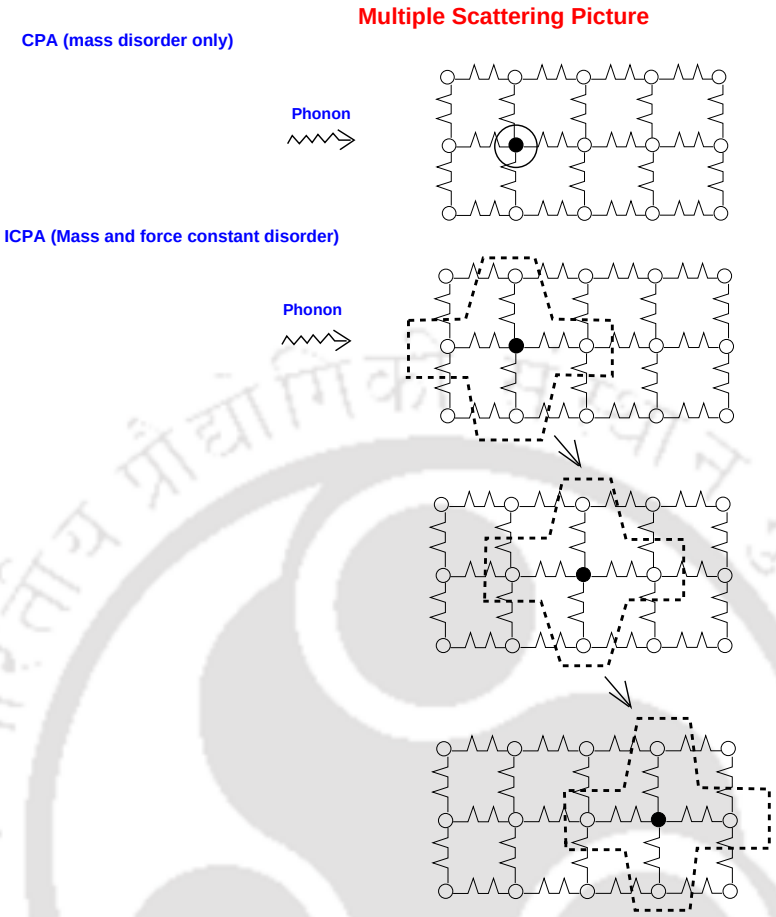


FIGURE 2.1: Multiple scattering picture in the CPA (top) and with the ICPA (bottom). The filled circle is the site of the fluctuation, and the contours around it indicate its area of influence. The arrows with the ICPA indicate the *itineration* of the fluctuation to neighboring sites. The details are given in the text. The diagram is reproduced from [91].

the top panel of the three, it scatters also from all of its neighbors since their spring constants also undergo changes (denoted by the thick spring lines in contrast to the thin ones for the average medium). The whole cluster of atoms undergoes fluctuations in force-constants as the location of the fluctuation site changes. One has to keep in mind that the force-constant between the fluctuation site and its neighbor on the right, say, depends on the occupation of both sites, as is true for the next neighboring site on its right as well. So, one is led to include the irreducible scatterings by the fluctuation on all neighboring sites, which then requires inclusion of scattering by the fluctuations on its neighbors etc., until the irreducible scatterings extend throughout the entire sample. A simple example of this process is indicated in the middle and bottom panels. Indeed, Mills and Ratanavararaksha [94] have shown that once there are non-diagonal terms in the scattering, the self-energy *must* include these migrations (itinerations) of

the scatterer throughout the sample in order to attain unitarity and thereby guarantee that the average Green's function will be properly analytic or Herglotz. The self-consistent scattering and the resulting coherent potential about a single defect thus *itinerates* from defect to defect throughout the sample, making it an *itinerant coherent potential*. The scattering could have started from any site in the sample so that the result is also fully translationally invariant.

The self-energy $\mathbf{\Sigma}\left(\omega^2\right)$ is calculated in the multiple scattering framework which is defined by

$$\ll \mathbf{G}\left(\omega^2\right) \gg = [\mathbf{G}_{vca}^{-1}\left(\omega^2\right) - \mathbf{\Sigma}\left(\omega^2\right)]^{-1}, \tag{2.26}$$

where $\mathbf{G}_{vca}$ is the unperturbed Green's function,

$$\mathbf{G}_{vca} = \left(\overline{\mathbf{m}}\omega^2 - \overline{\mathbf{\Phi}}\right)^{-1}, \tag{2.27}$$

and $\overline{\mathbf{m}}$ and $\overline{\mathbf{\Phi}}$ are the configuration-averaged mass and force-constant operators respectively.

The most important task here is to calculate the self-energy $\mathbf{\Sigma}\left(\omega^2\right)$. Using the 2×2 block representation of augmented-space operators of Eq. 2.23, one can evaluate $\overline{\mathbf{G}}$ which becomes

$$\begin{aligned}
\overline{\mathbf{G}} &= [\left(\overline{\mathbf{m}}\omega^2 - \overline{\mathbf{\Phi}}\right) - \mathbf{K}'\left(\widetilde{\mathbf{m}}\omega^2 - \widetilde{\mathbf{\Phi}}\right)^{-1}\mathbf{K}'^{\dagger}]^{-1} \\
&= [\mathbf{G}_{vca}^{-1} - \mathbf{K}'\{\mathbf{G}_{vca}^{-1} - [\left(\overline{\mathbf{m}}\omega^2 - \overline{\mathbf{\Phi}}\right) - \left(\widetilde{\mathbf{m}}\omega^2 - \widetilde{\mathbf{\Phi}}\right)]\}^{-1}\mathbf{K}'^{\dagger}]^{-1} \\
&= [\mathbf{G}_{vca}^{-1} - \mathbf{K}'\mathbf{F}\mathbf{K}'^{\dagger}]^{-1}
\end{aligned} \tag{2.28}$$

Therefore, the self-energy is given by

$$\mathbf{\Sigma} = \mathbf{K}'.\mathbf{F}.\mathbf{K}'^{\dagger} \tag{2.29}$$

where

$$\mathbf{F} = \widetilde{\mathbf{K}}^{-1} = \{\mathbf{G}_{vca}^{-1}\tilde{\mathbf{I}} - \widetilde{\mathbf{V}}\}^{-1} \tag{2.30}$$

and where

$$\widetilde{\mathbf{V}} = \left(\bar{m}\tilde{\mathbf{I}} - \widetilde{\mathbf{m}}\right)\omega^2 - \left(\bar{\phi}\tilde{\mathbf{I}} - \tilde{\mathbf{\Phi}}\right) \tag{2.31}$$

The quantity $\widetilde{\mathbf{V}}$ denotes all perturbations to the average medium, and $\mathbf{F}$ contains the itineration of the fluctuation in the average medium.

Up to this point, the scattering formalism is exact. The ICPA is now introduced by restricting the states within the configuration space $\Theta - |f\rangle\langle f|$ to the single-fluctuation states, the notation for which is given by Eq. 2.25. Making the site and Cartesian indices explicit, the self-energy $\mathbf{\Sigma}$ in Eq. 2.29 under this restriction can be written as,

$$\Sigma_{ij}^{\alpha\beta} = \sum K'^{(m)}_{\alpha i,\delta k} F^{(m)(n)}_{\delta k,\gamma l} K'^{\dagger(n)}_{\gamma l,\beta j} \tag{2.32}$$

The summations are over the repeated indices and the *fluctuation itinerator* $\mathbf{F}$ is given by a Dyson equation,

$$\mathbf{F}^{(i)(j)} = \mathbf{G}_{vca}[\delta_{(i)(j)} + \sum_{l} \widetilde{\mathbf{V}}^{(i)(l)}\mathbf{F}^{(l)(j)}], \tag{2.33}$$

where only the site index of the fluctuation is shown. The quantities in Eq. 2.32 are translationally invariant as follows:

$$\begin{aligned} K_{ik}^{(m)} &= K_{i-m,k-m}^{(0)}, \\ F_{kl}^{(m)(n)} &= F_{k-m,l-m}^{(0)(n-m)} \end{aligned} \tag{2.34}$$

The single fluctuation in Eq. 2.32 can be considered to have been 'created' by $\mathbf{K}'^{(n)}$ at site $n$, itinerated to site $m$ by $\mathbf{F}^{(n)(m)}$ and 'destroyed' by $\mathbf{K}'^{\dagger(m)}$ at site $m$. The $\mathbf{K}$, $\mathbf{K}'^{\dagger}$ and $\mathbf{F}$

matrices have elements which are non-zero only for site indices within the environment of the appropriate defects i.e. the indices $i$ and $k$ ($l$ and $j$) must be within the neighborhood perturbed by the defect at $m(n)$. The terms with more than one fluctuation (defect) present at a time correspond to coherent pair and 'defect cluster' scattering and are neglected in the single-site scattering considered here. All of these operators act in the augmented space. The Eqs. 2.29 - 2.33 define an itinerant single-site multiple scattering theory.

The restriction in Eq. 2.32 to states of $\Theta - |f\rangle\langle f|$ containing only a single fluctuation is a very severe approximation. Multiple-fluctuation states are of course present in $\mathbf{F}$ and contribute to $\mathbf{\Sigma}$. In the spirit of the CPA, these are included approximately by introducing self-consistency. As in the CPA [68, 104], self-consistency is achieved here replacing $\mathbf{G}_{vca}$ in $\mathbf{F}$ in Eq. 2.33 by a conditional propagator $\mathbf{G}^{(i)}$, identical to $\overline{\mathbf{G}} = \ll \mathbf{G} \gg$ except that all irreducible scatterings beginning or ending on site $i$ are omitted, so that $\mathbf{F}$ would then be given by

$$\mathbf{F}^{(i)(j)} = \mathbf{G}^{(i)}[\delta_{(i)(j)} + \sum_{l} \widetilde{\mathbf{V}}^{(i)(l)}\mathbf{F}^{(l)(j)}] \tag{2.35}$$

In parallel with Eq. 2.26, $\mathbf{G}^{(i)}$ contains a conditional self-energy $\mathbf{\Sigma}^{(i)}$ which is similar to Eq. 2.32, except that it includes only those scatterings that neither start nor end on $i$,

$$\mathbf{G}^{(i)} = [(\mathbf{G}_{vca})^{-1} - \mathbf{\Sigma}^{(i)}]^{-1} \tag{2.36}$$

$$\mathbf{\Sigma}^{(i)} = \sum_{l,m\neq i} \mathbf{K}'^{(l)}\mathbf{F}^{(l)(m)}\mathbf{K}'^{\dagger(m)} \tag{2.37}$$

The ICPA formalism allows $\mathbf{K}'$, $\mathbf{K}'^{\dagger}$ and $\widetilde{\mathbf{V}}$ to include force-constant disorder as well and therefore defect itineration in Eqs. 2.35 - 2.37. Unlike the usual CPA where only a single fluctuation at a site is considered, multiple fluctuations coming from multiple scattering is present in the itinerator $\mathbf{F}$ and therefore contribute to the self-energy $\mathbf{\Sigma}$. In the context of phonon excitations, this enables one to use the formalism to accommodate force constant disorder along with mass disorder.

It now remains to solve these equations, making use of the translational symmetry of the augmented-space operators. This is accomplished by Fourier transforms on the fluctuation-site labels,

$$A(\vec{q})_{mn} = N^{-1} \sum_{l,l'} A^{(l)(l')}_{l+m,l'+n} e^{-i\vec{q}\cdot\vec{R}_{ll'}}, \tag{2.38}$$

and

$$A^{(l)(l')}_{l+m,l'+n} = N^{-1} \sum_{\vec{q}} A(\vec{q})_{mn}\, e^{i\vec{q}\cdot\vec{R}_{ll'}}, \tag{2.39}$$

where $\vec{R}_{ll'}$ is the lattice vector connecting the fluctuation sites $l$ and $l'$, $m$ and $n$ are neighbors of $l$ and $l'$, respectively, and the $\vec{q}$ sum is over the Brillouin zone.

It is also possible to effect Fourier transforms on the site indices themselves. That of the self-energy is

$$\Sigma(\vec{q}) = N^{-1} \sum_{mn} \Sigma_{mn} e^{-i\vec{q}\cdot\vec{R}_{mn}} \tag{2.40}$$

From Eqs. 2.29, 2.34 and 2.38, it follows that

$$\Sigma(\vec{q}) = \sum_{l,m,n,p} K^{(0)}_{lm} F(\vec{q})_{mn} K'^{\dagger(0)}_{np} e^{-i\vec{q}\cdot\vec{R}_{lp}} \tag{2.41}$$

In this notation, Eq. 2.35 becomes

$$F(\vec{q})_{mn} = G^{(0)}_{mn} + \sum_{rp} G^{(0)}_{mr} \widetilde{V}(\vec{q})_{rp} F(\vec{q})_{pn} \tag{2.42}$$

which can be written in matrix notation as

$$\mathbf{F}(\vec{q}) = [\mathbf{G}^{(0)^{-1}} - \widetilde{\mathbf{V}}(\vec{q})]^{-1} \tag{2.43}$$

In order to evaluate $\mathbf{G}^{(0)}$, Eq. 2.36 can be rewritten as,

$$\mathbf{G}^{(0)} = [(\mathbf{G}_{vca})^{-1} - \mathbf{\Sigma}^{(0)}]^{-1} = [\ll \mathbf{G} \gg^{-1} + \widetilde{\mathbf{\Sigma}}^{(0)}]^{-1}, \tag{2.44}$$

where, $\widetilde{\mathbf{\Sigma}}^{(0)} = \left(\mathbf{\Sigma} - \mathbf{\Sigma}^{(0)}\right)$. The conditional self-energy $\widetilde{\mathbf{\Sigma}}^{(0)}$ contains *only* those scatterings which either start or end with a perturbation caused by a fluctuation at site 0. Thus, to evaluate the self-consistent propagator $\mathbf{G}^{(0)}$, we need to know $\ll \mathbf{G} \gg$. But $\ll \mathbf{G} \gg$ is obtained from Eq. 2.26, which becomes

$$\begin{aligned} \ll G(\vec{q}) \gg &= [G_{vca}(\vec{q})^{-1} - \Sigma(\vec{q})]^{-1}, \\ \ll G_{ij} \gg &= N^{-1} \sum_{\vec{q}} \ll G(\vec{q}) \gg e^{-i\vec{q}\cdot\vec{R}_{ij}}. \end{aligned} \tag{2.45}$$

After reaching self-consistency by the procedure described below, these expressions are used to calculate densities of states and spectral functions.

The conditional self-energy $\widetilde{\mathbf{\Sigma}}^{(0)}$ can be broken up into two contributions:

(i) Scattering that starts from a defect at site 0 and ends at site $j$.

(ii) Scattering that starts at $j$ but ends at 0.

This decomposition results in

$$\widetilde{\mathbf{\Sigma}}^{(0)} = \sum_{j} [\mathbf{K}'^{(0)}\mathbf{F}^{(0)(j)}\mathbf{K}'^{\dagger(j)} + \mathbf{K}'^{(j)}\mathbf{F}^{(j)(0)}\mathbf{K}'^{\dagger(0)}] - \mathbf{K}'^{(0)}\mathbf{F}^{(0)(0)}\mathbf{K}'^{\dagger(0)} \tag{2.46}$$

The last term is subtracted to avoid overcounting when $j$=0.

In a block notation similar to that of Eq. 2.23, we have

$$\widetilde{\mathbf{\Sigma}}^{(0)} = \begin{pmatrix} \mathbf{\Sigma}_1 & \mathbf{\Sigma}_3 \\ \mathbf{\Sigma}_3^{\dagger} & 0 \end{pmatrix}, \tag{2.47}$$

$$\mathbf{G}^{(0)} = \begin{pmatrix} \mathbf{G}_1^{(0)} & \mathbf{G}_3^{(0)} \\ \mathbf{G}_3^{\dagger(0)} & \mathbf{G}_2^{(0)} \end{pmatrix}, \tag{2.48}$$

$$\ll \mathbf{G} \gg = \begin{pmatrix} \mathbf{G}_1 & \mathbf{G}_3 \\ \mathbf{G}_3^{\dagger} & \mathbf{G}_2 \end{pmatrix}. \tag{2.49}$$

where, for a general operator $\hat{\mathbf{A}}$, $\mathbf{A}_1$ begins and ends with scattering about site 0, $\mathbf{A}_2$ neither begins nor ends with scattering about site 0 and $\mathbf{A}_3(\mathbf{A}_3^{\dagger})$ begins (ends) with scattering at the site 0 and ends (begins) with scattering about a site different from 0. The term $\mathbf{\Sigma}_2$ is 0 since $\widetilde{\mathbf{\Sigma}}^{(0)}$ must begin or end at the site 0. From Eq. 2.44 , we have

$$\mathbf{G}^{(0)} = \ll \mathbf{G} \gg \left(\mathbf{I} + \widetilde{\mathbf{\Sigma}}^{(0)} \ll \mathbf{G} \gg\right)^{-1}, \tag{2.50}$$

which leads to

$$\mathbf{G}_1^{(0)} = \bar{\mathbf{X}}[\mathbf{I} + \left(\mathbf{\Sigma}_1 - \mathbf{\Sigma}_3\mathbf{G}_2\mathbf{\Sigma}_3^{\dagger}\right)\bar{\mathbf{X}} + \mathbf{\Sigma}_3\mathbf{G}_3^{\dagger}]^{-1}, \tag{2.51}$$

where,

$$\bar{\mathbf{X}} = \left(\mathbf{I} + \mathbf{G}_3\mathbf{\Sigma}_3^{\dagger}\right)^{-1}\mathbf{G}_1. \tag{2.52}$$

In order to evaluate these expressions, we need to calculate four terms: $\mathbf{G}_1$, $\mathbf{\Sigma}_1$, $\mathbf{G}_3\mathbf{\Sigma}_3^{\dagger}$ and $\mathbf{\Sigma}_3\mathbf{G}_2\mathbf{\Sigma}_3^{\dagger}$. The second term $\mathbf{\Sigma}_1$ is just a finite sum of finite matrices and can be evaluated directly, but the last two terms involve sums which range over all sites in the solid and must be evaluated by Fourier transforms. An interesting point to note is that the quantities $G_3\Sigma_3^{\dagger}$ and $\Sigma_3 G_2\Sigma_3^{\dagger}$ represent the scattering and itineration of the disturbance including the effect of the off-diagonal and environmental disorder. In case of diagonal-disorder only, they vanish giving $\mathbf{G}_1^{(0)} = \mathbf{G}_1\,(\mathbf{I} + \mathbf{\Sigma}_1)^{-1}$, which is the CPA self-consistent propagator, and the self-consistent set of equations reduces to the CPA equations.

In Fig 2.2, the scheme of the calculations in the ICPA formalism is represented by a cartoon diagram. Here, the iterations are done till self-consistency is achieved for each $\vec{q}$-point in the Brillouin zone. In the process of achieving self-consistency, one calculates $\ll G \gg$ in both real-space and in $\vec{q}$-space; each is needed to obtain densities of states and spectral densities respectively.

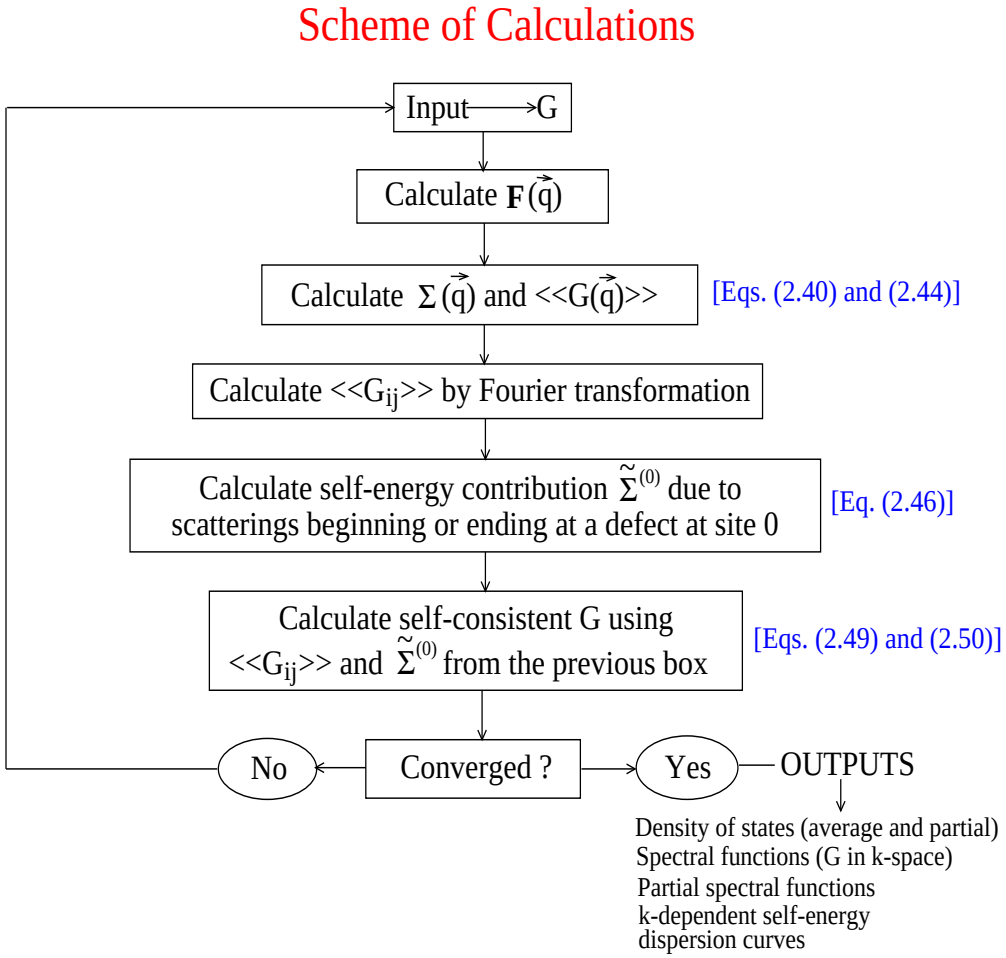


FIGURE 2.2: Scheme of the calculations in the ICPA formalism.

## 2.7 Summary

In this chapter, we have discussed various methods to perform the configuration averaging in disordered alloy environment. It turns out that most of the methods, discussed here, are not suitable for the study vibrational excitations. While VCA does not consider any kind of

fluctuations in the medium, the scheme of calculation within the ATA is not self-consistent. CPA, being a single-site theory, fails to incorporate off-diagonal and environmental disorder which is essential for the study of phonons. The recently developed ICPA provides a successful, self-consistent, analytic method to perform the configuration averaging in substitutionally disordered alloys. We have demonstrated how this multiple-scattering based formalism captures the effects of off-diagonal and environmental disorder. The use of augmented-space to keep track of the configurations of the system has made the formalism simple yet powerful. The Hamiltonian defined in this space contains information about all possible atomic configurations of the system so that the configuration averaging is not a separate process anymore. The augmented space theorem then reduces the problem of configuration averaging to the evaluation of only a single matrix element. Moreover, the underlying translational invariance of the operators in the augmented space allows one to use state-of-the-art methods for ordered systems in case of substitutionally disordered systems as well which makes it a numerically tractable approach. This formalism also enables one to make direct comparison with neutron scattering experiments.

# Chapter 3

# First-principles based modeling of inter-atomic force constants

## 3.1 Introduction

The 'Itinerant Coherent Potential Approximation' (ICPA) has been able to illustrate the importance of the force-constant disorder with regard to the phonon spectra in disordered alloys [91, 106, 107]. However, the key input that needs to be fed into this Green's function based method for performing configuration averaging of physical quantities are the inter-atomic force constants between various pairs of specie. Due to the random chemical environment around each atom in a substitutionally disordered alloy, the force constants corresponding to A-A, B-B, and A-B pairs in a $A_xB_{1-x}$ alloy are different from those in the ordered alloy and in no way resembles the force constants in a completely ordered environment. In order to have significant accuracy in calculated phonon properties one should, therefore, have accurate information on force constants corresponding to various pairs of chemical species. The quest, thus, is to look for a reliable source of inter-atomic force constants in random alloys. The most trustworthy source available in this regard are the first-principles electronic structure methods. However, state of the art *ab initio* calculations always assume some degree of translational symmetry in disordered systems. For calculations of properties in disordered alloys through first-principles techniques, one has to construct either a large supercell or as is done

in conventional alloy theory, a cluster expansion [108] has to be fitted to the ground state energies of a large number of ordered states. While the calculation for a given ordered structure is a relatively routine task with modern first-principles electronic structure codes, this procedure has to be repeated for many configurations in order to properly fit a cluster expansion which makes the whole procedure computationally demanding. Similar is the case for the supercell technique. For calculation of phonon excitations, the computational cost rises even further. Thus, in spite of having a suitable self-consistent, analytical technique to perform the required averaging over various configurations in the disordered systems, the calculations of phonon spectrum in random alloys were rather limited because of these practical difficulties.

In this chapter, we present a new approach to calculate the inter-atomic force constants in random alloys. The formalism is a combination of an *ab initio* method which computes inter-atomic interactions based upon the detailed electronic structures and the intuitive argument about dependence of stretching and bending force constants on bond lengths. In combination with the ICPA, which does the desired averaging over various configurations in the disordered alloy, addressing both mass as well as force constant disorder, we employ our approach to investigate the interrelations between the inter-atomic force constants and the lattice dynamics of $Pd_{0.96}Fe_{0.04}$ and $Pd_{0.9}Fe_{0.1}$ [109]. We present results on phonon frequencies and elastic constants for these two alloys. Significant insight about the inter-atomic interactions between various pairs of chemical specie is obtained in the course of our investigations.

In the next two sections, we discuss the Density functional theory (DFT) [110, 111] and the Density functional perturbation theory (DFPT) [112], which we use for *ab initio* calculations of inter-atomic force constants. The modeling strategy to calculate force constants in random alloys and the corresponding results on phonon frequencies obtained by the ICPA method are discussed in the following section which also illustrates limitations of the present approach. At the very end, we put forward the formulation of a more appropriate modeling strategy which does away with the limitations of the present approach.

## 3.2 Density functional theory (DFT)

Density functional theory is the backbone of the state-of-the-art calculation of electronic structure in condensed matter. The main highlight of this approach is the mapping of a many-body

electronic problem onto a non-interacting one. The formulation of the DFT originated in a famous article written by P. Hohenberg and W. Kohn in 1964 [110]. They established two theorems which constitute the theoretical foundation of DFT:

**Theorem I:** For any system of interacting particles in an external potential $V_{ext}(\mathbf{r})$, the potential $V_{ext}(\mathbf{r})$ is determined uniquely, except for a constant, by the ground state particle density $n_0(\mathbf{r})$.

**Theorem II:** A universal functional for the energy $E(n)$ in terms of the density $n(r)$ can be defined, valid for any external potential $V_{ext}(\mathbf{r})$. For any particular $V_{ext}(\mathbf{r})$, the exact ground state energy of the system is the global minimum value of this functional and the density $n(\mathbf{r})$ that minimizes the functional is the exact ground state density $n_0(\mathbf{r})$.

The meaning of the first theorem is that the ground state density $n_0(\mathbf{r})$ completely determines all the properties of a given many body system. It allows an enormous conceptual simplification of the quantum mechanical problem of searching for the ground state properties of a system of interacting electrons, because it replaces the traditional description based on wave functions (which depend on $3N$ independent variables, $N$ being the number of electrons) with a much more tractable description in terms of the single body charge density, which depends on only three variables. Hohenberg and Kohn also demonstrated that there exists a universal functional $F[n(\mathbf{r})]$ of the electron charge density such that total energy functional becomes

$$E[n(\mathbf{r})] = F[n(\mathbf{r})] + \int V_{ext}(\mathbf{r})n(\mathbf{r})d\mathbf{r} \tag{3.1}$$

where $F[n(\mathbf{r})]$ contains the kinetic energy and the mutual Coulomb interaction of the electrons and $V_{ext}(\mathbf{r})$ represents the external potential acting on the electrons. The minimization of this functional with the condition that the total number of particles, $N$, is preserved:

$$\int n(\mathbf{r})d\mathbf{r} = N, \tag{3.2}$$

directly gives the ground state energy and charge density, from which all the other physical properties can be extracted.

However, a major difficulty in the direct application of this remarkably simple result is that the form of the functional, $F[n]$ is unknown. In order to solve the problem, Kohn and Sham [111] introduced a further development to transform DFT into a practically useful tool. The Hohenberg and Kohn theorems hold independently of the precise form of the electron-electron interaction. In particular, when the strength of the electron-electron interaction vanishes, $F\,[n]$ defines the ground state kinetic energy of a system of non-interacting electrons as a functional of its ground state charge density distribution $T_0\,[n]$. This fact was used by Kohn and Sham (1965) to map the problem of a system of interacting electrons onto an equivalent non-interacting problem. To this end, the unknown functional $F\,[n]$ is cast in the form

$$F\,[n] = T_0\,[n] + \frac{e^2}{2}\int \frac{n\,(\mathbf{r})\,n\left(\mathbf{r}^{'}\right)}{|\mathbf{r}-\mathbf{r}^{'}|}d\mathbf{r}d\mathbf{r}^{'} + E_{xc}\,[n] \tag{3.3}$$

where the second term is the classical electrostatic self-interaction of the electron charge density distribution and the so called *exchange-correlation energy* $E_{xc}$ is defined by Eq. (3.3). Variation of the energy functional with respect to $n\,(\mathbf{r})$ with the constraint that the number of electrons be kept fixed leads formally to the same equation as would hold for a system of non-interacting electrons subject to an effective potential, also called the self-consistent field (SCF) potential, whose form is,

$$V_{SCF}\,(\mathbf{r}) = V\,(\mathbf{r}) + e^2\int \frac{n\left(\mathbf{r}^{'}\right)}{|\mathbf{r}-\mathbf{r}^{'}|}d\mathbf{r}^{'} + v_{xc}\,(\mathbf{r})\,, \tag{3.4}$$

where

$$v_{xc}\,(\mathbf{r}) \equiv \frac{\delta E_{xc}}{\delta n\,(\mathbf{r})} \tag{3.5}$$

is the functional derivative of the exchange-correlation energy, also called the *exchange-correlation potential*.

The power of this trick is that, if one knew the effective potential $V_{SCF}\,(\mathbf{r})$, the problem for non-interacting electrons could be trivially solved without knowing the form of the non-interacting kinetic energy functional $T_0$. To this end, one should simply solve the one-electron Schrodinger equation:

$$\left(-\frac{\hbar^2}{2m}\frac{\partial^2}{\partial \mathbf{r}^2} + V_{SCF}(\mathbf{r})\right)\psi_n(\mathbf{r}) = \epsilon_n \psi_n(\mathbf{r}) \tag{3.6}$$

The ground state charge density distribution and non-interacting kinetic energy functional would then be given in terms of the *auxiliary Kohn-Sham orbitals*, $\psi_n(\mathbf{r})$:

$$n(\mathbf{r}) = 2\sum_{n=1}^{N/2} |\psi_n(\mathbf{r})|^2 \tag{3.7}$$

$$T_0[n] = -2\frac{\hbar^2}{2m}\sum_{n=1}^{N/2}\int \psi_n^*(\mathbf{r})\frac{\partial^2\psi_n(\mathbf{r})}{\partial \mathbf{r}^2}d\mathbf{r}, \tag{3.8}$$

where $N$ is the number of electrons and the system is supposed to be nonmagnetic so that each of the $N/2$ lowest lying orbital states accommodates two electrons of opposite spin.

The ground state energy given by Es. (3.1) and (3.3) can be equivalently expressed in terms of the Kohn-Sham eigenvalues

$$E[n] = 2\sum_{n=1}^{N/2}\epsilon_n - \frac{e^2}{2}\int\frac{n(\mathbf{r})\,n\left(\mathbf{r}'\right)}{|\mathbf{r}-\mathbf{r}'|}d\mathbf{r}d\mathbf{r}' + E_{xc}[n] - \int n(\mathbf{r})\,v_{xc}(\mathbf{r})\,d\mathbf{r} \tag{3.9}$$

Eq. (3.6) has the form of a non linear Schrodinger equation whose potential depends on its own eigenfunctions through the electron charge density distribution. Once an explicit form for the exchange-correlation energy is available, this equation can be solved in a self-consistent way using a variety of methods.

## 3.3 Density functional perturbation theory (DFPT)

Density functional perturbation theory (DFPT) [112] is a density functional theory (DFT) [110, 111] based linear response method to obtain the electronic and lattice dynamical properties in condensed matter systems. The inter-atomic force constants required to calculate the phonon frequencies are derived via the linear response of the electronic subsystems. The

Hellmann-Feynman theorem [113, 114] is used to calculate the elements of the force constant matrices

$$C_{\mathbf{R}_I\mathbf{R}_J} = \frac{-\partial \mathbf{F}_I}{\partial \mathbf{R}_J} = \int \frac{\partial n_{\mathbf{R}}(\mathbf{r})}{\partial \mathbf{R}_J} \frac{\partial V_{\mathbf{R}}(\mathbf{r})}{\partial \mathbf{R}_I} d\mathbf{r} + \int n_{\mathbf{R}}(\mathbf{r}) \frac{\partial^2 V_{\mathbf{R}}(\mathbf{r})}{\partial \mathbf{R}_I \partial \mathbf{R}_J} + \frac{\partial^2 E_N(\mathbf{R})}{\partial \mathbf{R}_I \partial \mathbf{R}_J} \tag{3.10}$$

$\mathbf{R}_I, \mathbf{R}_J$ are the ionic positions, $\mathbf{F}_I$ is the Hellmann-Feynman force on the $I$-th nucleus, $n_{\mathbf{R}}(\mathbf{r})$ is the ground state electronic charge density corresponding to the nuclear configuration $\mathbf{R}$, $V_{\mathbf{R}}(\mathbf{r})$ is the electron-nucleus interaction and $E_N$ is the ion-ion interaction energy. From Eq 3.10, it is clear that the inter-atomic force constants are determined from the ground state charge density and from its linear response to a distortion in the ionic configuration. In the DFPT, these quantities are calculated within the DFT framework with a workload of the same order as that required for a standard ground state total energy calculations.

The theory can be applied to any order, but the main ideas can be seen in the lowest order linear response. In order to simplify the notation and make the argument more general, we assume that the external potential acting on the electrons is a differentiable function of a set of parameters, $\lambda \equiv \{\lambda_i\}$ ($\lambda_i \equiv \mathbf{R}_I$ in the case of lattice dynamics). According to the Hellmann-Feynman theorem, the first and second derivatives of the ground state energy read

$$\frac{\partial E}{\partial \lambda_i} = \int \frac{\partial V_\lambda(\mathbf{r})}{\partial \lambda_i} n_\lambda(\mathbf{r}) d\mathbf{r} \tag{3.11}$$

$$\frac{\partial^2 E}{\partial \lambda_i \partial \lambda_j} = \int \frac{\partial^2 V_\lambda(\mathbf{r})}{\partial \lambda_i \partial \lambda_j} n_\lambda(\mathbf{r}) d\mathbf{r} + \int \frac{\partial n_\lambda(\mathbf{r})}{\partial \lambda_i} \frac{\partial V_\lambda(\mathbf{r})}{\partial \lambda_j} d\mathbf{r} \tag{3.12}$$

The electron density response, $\partial n_\lambda(\mathbf{r})/\partial \lambda_i$, appearing in Eq. 3.12 can be evaluated by linearizing Eqs. 3.7, 3.6 and 3.4 with respect to wave function, density and potential variations. Linearization of Eq. 3.7 leads to

$$\Delta n(\mathbf{r}) = 4 \ \mathrm{Re} \sum_{n=1}^{N/2} \psi_n^*(\mathbf{r}) \Delta \psi_n(\mathbf{r}) \tag{3.13}$$

where the finite difference operator $\Delta^\lambda$ is defined as

$$\Delta^\lambda F = \sum_i \frac{\partial F_\lambda}{\partial \lambda_i} \Delta\lambda_i \tag{3.14}$$

The superscript $\lambda$ has been omitted in Eq. 3.13 as well as in any subsequent formulas where such an omission does not give rise to ambiguities. Since the external potential (both unperturbed and perturbed) is real, each Kohn-Sham eigenfunction and its complex conjugate are degenerate. As a consequence, the imaginary part of the sum appearing in Eq. 3.13 vanishes, so that the prescription to keep only the real part can be dropped.

The variation of the Kohn-Sham orbitals, $\Delta\psi_n(\mathbf{r})$ is obtained by standard first order perturbation theory [115]:

$$(H_{SCF} - \epsilon_n)\,|\Delta\psi_n\rangle = -\,(\Delta V_{SCF} - \Delta\epsilon_n)\,|\psi_n\rangle, \tag{3.15}$$

where,

$$H_{SCF} = -\frac{\hbar^2}{2m}\frac{\partial^2}{\partial \mathbf{r}^2} + V_{SCF}(\mathbf{r}) \tag{3.16}$$

is the unperturbed Kohn-Sham Hamiltonian,

$$\Delta V_{SCF}(\mathbf{r}) = \Delta V(\mathbf{r}) + e^2 \int \frac{\Delta n(\mathbf{r}')}{|\mathbf{r} - \mathbf{r}'|} d\mathbf{r}' + \left.\frac{dv_{xc}(n)}{dn}\right|_{n=n(\mathbf{r})} \Delta n(\mathbf{r}) \tag{3.17}$$

is the first order correction to the self consistent-potential and $\Delta\epsilon_n = \langle\psi_n|\Delta V_{SCF}|\psi_n\rangle$ is the first order variation of the Kohn-Sham eigenvalue, $\epsilon_n$.

Eqs. 3.13-3.17 form a set of self-consistent equations for the perturbed system completely analogous to the Kohn-Sham equations in the unperturbed case (Eqs. 3.4, 3.6 and 3.7) with the Kohn-Sham eigenvalue equation, Eq. 3.6, being replaced by the solution of a linear system, Eq. 3.15. As $\Delta V_{SCF}(\mathbf{r})$ is a linear functional of $\Delta n(\mathbf{r})$, which in turn depends linearly on the $\Delta\psi$'s, the whole self-consistent calculation can be cast in terms of a generalized linear problem. It might appear that there is a problem since the left-hand side of Eq. 3.15 is singular

because the linear operator appearing therein has a null eigenvalue. However, the response of the system to an external perturbation only depends on the component of the perturbation that couples the manifold occupied states with the empty states. The projection onto the empty-state manifold of the first order correction to occupied orbitals can be obtained from Eq 3.15 by replacing its right-hand side with $-P_c \Delta V_{SCF} |\psi_n\rangle$, where $P_c$ is the projector onto the empty-state manifold, and by adding to the linear operator on its left-hand side $H_{SCF} - \epsilon_n$, a multiple of the projector onto the occupied-state manifold, $P_v$, so as to make it non-singular:

$$(H_{SCF} - \alpha P_v - \epsilon_n) |\Delta\psi_n\rangle = -P_c \Delta V_{SCF} |\psi_n\rangle \tag{3.18}$$

The basic algorithm for DFPT consists of solving the set of linear equations 3.18 for $\Delta\psi_n$ and expression 3.17 for $\Delta V_{SCF}$ in terms of of $\Delta n$, which is given by 3.13. Since $\Delta n$ is a function of the set of occupied $\Delta\psi_n$, this forms a self-consistent set of equations which can be solved by any efficient iterative method.

In the next section, we present an approach to model the inter-atomic force constants in random alloys by making use of the results obtained from first-principles DFPT calculations.

## 3.4 Modeling the inter-atomic force constants

The lack of *ab initio* method for computing the inter-atomic force constants in a random alloy environment has made the problem rather tricky. Previously, a few attempts were made to obtain force constants for random alloys from *ab initio* calculations on a single ordered structure having the same symmetry as that of the alloy [91, 106]. Although the calculations are less expensive computationally, the results obtained were far from reality. An alternative approach was provided by Cedar and coworkers [116–118]. In this approach, they found that the relevant force constants are strongly correlated with the bond lengths between a given pair of atoms. Taking cue from their observation that the force constants are dependent upon the bond distances, we here model the inter-atomic force constants for a random binary alloy $A_xB_{1-x}$ in the following way: The A-A and B-B force constants are computed from *ab initio* calculations on elemental A and B with the same Crystal structure and at the same lattice constant as that of the random alloy. With this modeling strategy, the environment around each atom in

the original random alloy and the bond distances can be well represented by the calculations. Modeling the A-B interactions is, however, tricky. Here, we consider the A-B force constants to be simple concentration averages of the A-A and the B-B force constants. In order to test the validity of our modeling strategy, we have chosen $Pd_xFe_{1-x}$ ($x$ = 0.96 and 0.90) alloys. The reason behind this is twofold: first, the size difference between Fe and Pd atoms are not appreciable. Therefore, there wouldn't be significant dispersion of bond distances of Fe-Fe and Pd-Pd pairs and as a result our scheme is ideally suited for these alloy systems. Second, previous theoretical results on phonon frequencies based on a model potential method are available for these systems [119–121]. Since the force constants generated from the model potentials were obtained at the alloy lattice constants, a direct comparison could be effected between our results and those obtained from the model potential calculations.

In the next sub-section, we test the validity of this approach. The proposed modeling scheme is combined with the ICPA method to calculate phonon dispersion curves and elastic constants in $Pd_xFe_{1-x}$ ($x$ = 0.96 and 0.90) alloys. Our observations and further developments are discussed in detail.

### 3.4.1 Application: $Pd_xFe_{1-x}$ ($x = 0.96, 0.9$)

An understanding of the behavior of various inter-atomic force constants in a random environment is a necessity to analyze the phonon spectra and related properties. This necessity is probably more in the case of the so called Type-II alloys where the constituents making up the alloy, themselves crystallize in different structures in their elemental phases while a single unique lattice is formed upon alloying. Examples of such systems are iron-nickel, iron-platinum and iron-palladium. In disordered phases of these alloys, a unique FCC solid solution is formed whereas iron stabilizes in BCC phase at room temperature. It is a well known fact that FCC iron is unstable until one attains very high temperature [122]; the force constants in FCC iron at low temperatures are, therefore, expected to be soft. It would, therefore, be interesting to investigate the changes in the inter-atomic force constants associated with iron atoms, if any, and their impact on the phonon spectra in the disordered phases of a Type-II alloy. We have chosen $Pd_xFe_{1-x}$ alloy for such investigation as a systematic study on the behavior of the inter-atomic force constants and their role on the features of the phonon

dispersion relations, have not been done for this alloy. Neutron scattering experimental results on phonon frequencies and elastic constants are available for x=0.96 and 0.9 [123] in this alloy. The only theoretical results available on these systems are based on a pair-potential method [119], later modified to include three body interactions [120, 121]. In this approach, the model potential is generated from the dissociation energy of a pair of atoms, the distance between them and by fitting to the elastic constants. The three-body term is later evaluated by fitting the total interaction energy of an atom in a particular crystal structure to the total cohesive energy of the element. The inter-atomic force constants are then obtained from the spatial derivatives of these potentials. In case of $Pd_{0.96}Fe_{0.04}$ and $Pd_{0.9}Fe_{0.1}$ the phonon spectrum obtained from the pair-potential only model showed significant deviation with experiments and the elastic constants were off by about 25% on an average. Inclusion of the three-body term improved the phonon frequencies for $Pd_{0.9}Fe_{0.1}$ but no results on the elastic constants were presented. However, in the model potential approach, the role of the electronic structure of the elements forming the alloy were altogether neglected. Since the inter-atomic interactions were dependent solely upon a given crystal structure and not on the electronic structure, the nearest neighbor Fe-Fe and Pd-Pd inter-atomic force constants came out to be of same orders of magnitudes (since the nearest neighbor force constants in a FCC structure are order of magnitude higher than the distant neighbors, we focus on these only). This result is completely counter-intuitive because Fe-Fe force constants are expected to be softer than that of the Pd-Pd ones for the reason mentioned above. The inter-atomic force constants as obtained by the model potential approach, therefore, seems not to represent the actual microscopic picture.

#### 3.4.1.1 Computational details

First-principles Quantum-Espresso code [124], based upon a Plane wave- Pseudopotential implementation of the DFPT, has been used to compute the Fe-Fe and Pd-Pd force constants at the alloy lattice parameters, 7.31 a.u. for $Pd_{90}Fe_{10}$ and 7.339 a.u. for $Pd_{96}Fe_4$. Ultrasoft pseudopotentials [125] with nonlinear core corrections [126] were used. Perdew-Zunger parametrization of the local density approximation (LDA) [127] was used for the exchange-correlation part of the potential. Computation of the Fe-Fe force constants was also done with the PBE-96 GGA [128] exchange-correlation functional for the sake of comparison as there are serious doubts regarding the reliability of LDA results for iron. Plane waves with energies up to 55 Ry are used in order to describe electron wave functions and Fourier components of

the augmented charge density with cutoff energy up to 650 Ry are taken into account. The Brillouin-zone integrations are carried out with Methfessel-Paxton smearing [129] using a 12X12x12 **k**-point mesh. The value of the smearing parameter is 0.02 Ry. These parameters are found to yield phonon frequencies converged to within 5 percent.

After achieving the desired level of convergence for the electronic structure, the force constants are conveniently computed in reciprocal space on a finite **q**-point grid and Fourier transformation is employed to obtain the real space force constants. The number of unique real-spaced force constants and their accuracy depend upon the density of the **q**-point grids: the closer the **q**-points are spaced, the more accurate the force constants are. In this work, we have used a 4x4x4 **q**-point mesh.

The ICPA calculations were done on 400 energy points. The disorder in the force constants were considered for nearest neighboring shell only. A small imaginary frequency part of -0.05 was used in the Green's functions. The Brillouin-zone integration was done over 356 **q**-points in the irreducible Brillouin zone. The simplest linear-mixing scheme was used to accelerate the convergence. The number of iterations ranged from 5 to 15 for all the calculations.

#### 3.4.1.2 Results

In the calculations of phonon spectrum using the model pair-potentials, the system was considered to be a mean-crystal like where the mass was considered to be a concentration average of Fe and Pd masses and the force constant disorder was substantially weak. The weak force-constant disorder resulted from the fact that the Fe-Fe and the Pd-Pd force constants were of nearly the same magnitude and the Fe-Pd force constants were concentration averages of the above two. The Fe and Pd masses have a ratio ~ 1:2; therefore, the mass disorder in the alloy should be significant apart from the force constant disorder. Clearly, a mean crystal model like the one followed in References [119] and [120] would not work properly. To demonstrate this, we have done ICPA calculations with these set of force constants [119, 120] and with the masses of the constituents being kept equal to the concentration averaged mass. The results for $Pd_{0.9}Fe_{0.1}$ are presented in Fig. 3.1. The dispersion curves deviate substantially from the experimental results. The disagreement is greater as one goes towards the zone boundary. The agreement is near perfect for the longer wavelengths. The reason behind such discrepancies can be understood as follows: in the longer wavelength limit, self averaging of both mass and

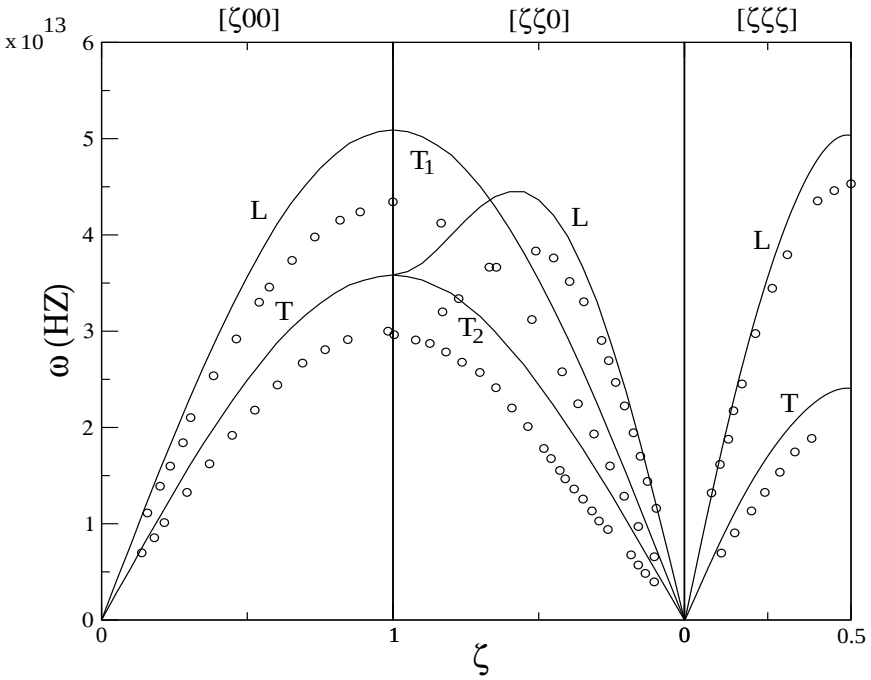


FIGURE 3.1: Dispersion curves (frequency $\omega$ vs reduced wave vector $\zeta$); $\zeta = \frac{|\vec{q}|}{|\vec{q}_{max}|}, \vec{q}$ the phonon wave-vector; for $Pd_{0.9}Fe_{0.1}$ calculated in the ICPA (solid lines) with the force constants obtained from model potential. The circles are the experimental data.

force constants over a single wavelength reduces the ICPA to that of a mean crystal model like the virtual crystal approximation (VCA), making near perfect agreement with the experiments in our case; in the shorter wavelength regime where frequencies are higher, the mass and the force constant disorders play a more significant role. In the mean crystal like model generated by the model potential, all three inter-atomic force constants are pure Pd-like and the mass is an average one which is lower than that of the Pd mass. The phonon frequencies obtained, therefore, are overestimated as the mean crystal is like that of pure Pd with a reduced mass due to neglect of mass and force constant fluctuations.

In order to address the microscopic picture of inter-atomic interactions more realistically, we first focus on the lattice dynamics of FCC Fe at the lattice constants of the alloys considered. The dispersion curves of pure Fe calculated by the *ab initio* DFPT at the alloy lattice constant of $Pd_{0.9}Fe_{0.1}$ are presented in Fig. 3.2. The results with both the LDA exchange-correlation and with the GGA exchange-correlation are presented for the sake of comparison because the LDA is known to fail in reproducing the correct magnetic ground state of BCC iron [130]. The results show that FCC Fe is dynamically unstable at the given lattice constant. This qualitative feature is identical for both exchange-correlation functionals. Quantitatively,

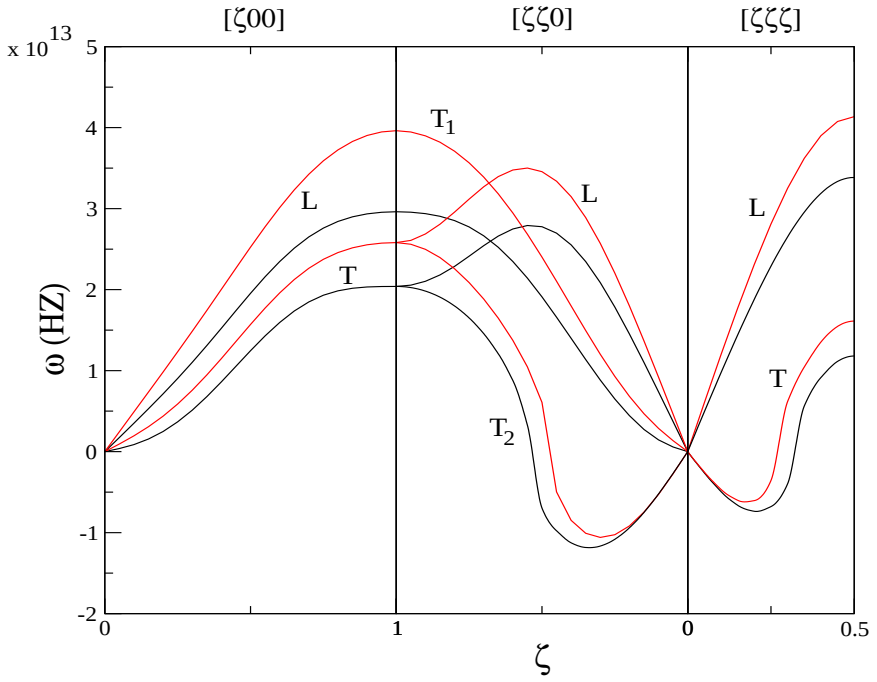


FIGURE 3.2: Calculated LDA (black lines) and GGA (red lines) phonon dispersion curves of Fe in the FCC phase, both computed at the experimental lattice constant of $Pd_{0.90}Fe_{0.1}$.

the GGA frequencies are larger than those of the LDA. Since our only aim was to show that the dynamical instability of the Fe at the FCC phase and at the given lattice constant is independent of the exchangecorrelation functional, the quantitative values of the phonon frequencies are irrelevant for the discussion. The results clearly demonstrate that the use of the LDA exchange-correlation functional is justified in the present case. The reason LDA works in the present case, although it even fails to produce the ferromagnetic ground state for the BCC structure, is the following: here we have done computations on the ferromagnetic-FCC phase of iron and at a lattice constant of 7.31 au. Wang *et al* [131] had earlier demonstrated that at the FCC phase the lowest energy state of the Fe is a high-spin ferromagnetic state beyond the lattice constant of 6.8 au and that the existence of this state is consistent with the experimental observation that FCC Fe precipitates in Cu-Au alloys (lattice constant = 7.11 au) [132]. Their calculations were done with the LDA functional. Therefore, for FCC Fe at the lattice constants considered for our study, the LDA functional can be used safely. Similar to this case, we see the identical qualitative features in LDA and GGA phonon dispersion results for Fe at the lattice constant of $Pd_{0.96}Fe_{0.04}$ as well, which demonstrates that the Fe is also dynamically unstable at this lattice constant. Consequently, the nearest-neighbor force

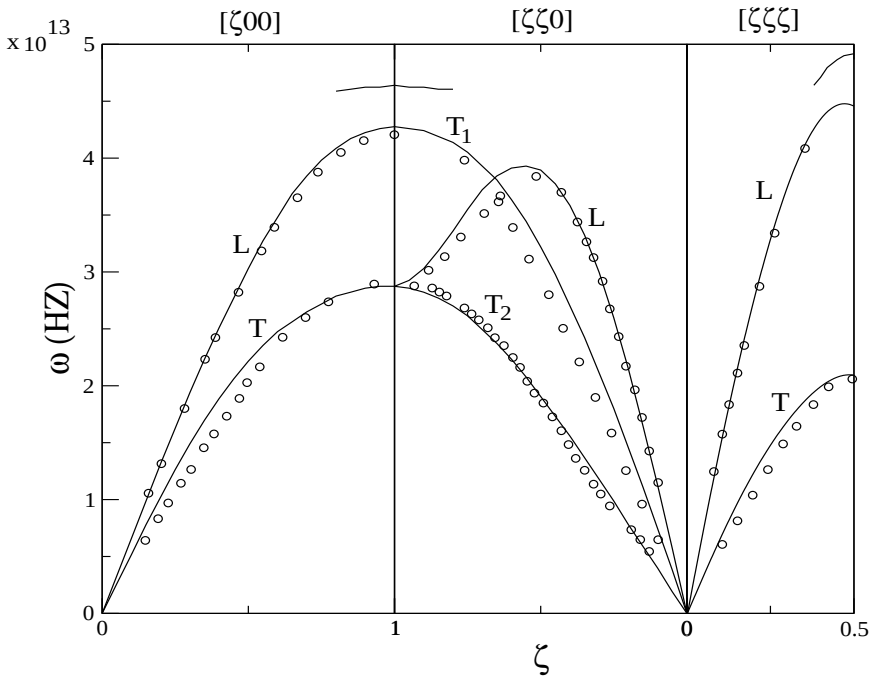


FIGURE 3.3: Dispersion curves for $Pd_{0.96}Fe_{0.04}$ calculated in the ICPA. The Fe-Pd force constants are the concentration-averaged ones. The circles are the experimental points.

constants (longitudinal and transverse) as shown in Table 3.1 are much softer than the corresponding ones in the case of pure Pd calculated at the same lattice constants. This is only to be expected as has been discussed before. This softness of the Fe-Fe interactions are expected to remain in the alloys studied as well because of the same lattice structure of the element and the alloy and because of the dependence of longitudinal (stretching) and transverse (bending) force constants on bond distances alone [116]. Therefore, the Fe-Fe interactions as portrayed in the model potential based method are far from reality.

In what follows, we calculate the phonon dispersion curves of these two alloys by the ICPA using the *ab initio* Fe-Fe and Pd-Pd force constants. As a first approximation, the Fe-Pd force constants are taken to be simple concentration averages of the Fe-Fe and Pd-Pd force constants, as was done in the calculations with the model potentials [119, 120]. The results for $Pd_{96}Fe_4$ and $Pd_{90}Fe_{10}$, calculated with these set of force constants, are presented in Fig. 3.3 and 3.4 respectively. The phonon frequencies are obtained from the peaks of the coherent scattering structure factor as defined in Eq. 2.3. The results show good agreement with experimental results for the major part of the spectrum for both the alloys. However, near the zone boundary, spurious splittings in the dispersion curves are observed. This kind of splitting in dispersion curves is a typical feature of a strong force constant disorder. In [91], the

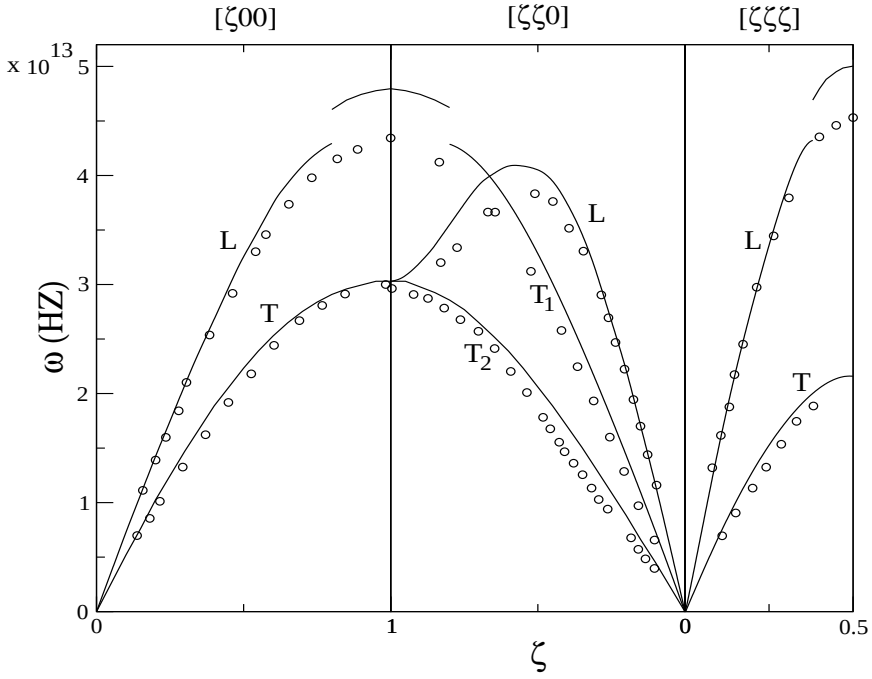


FIGURE 3.4: Dispersion curves for $Pd_{0.9}Fe_{0.1}$ calculated by the ICPA. The Fe-Pd force constants are the concentration-averaged ones. The circles are the experimental points.

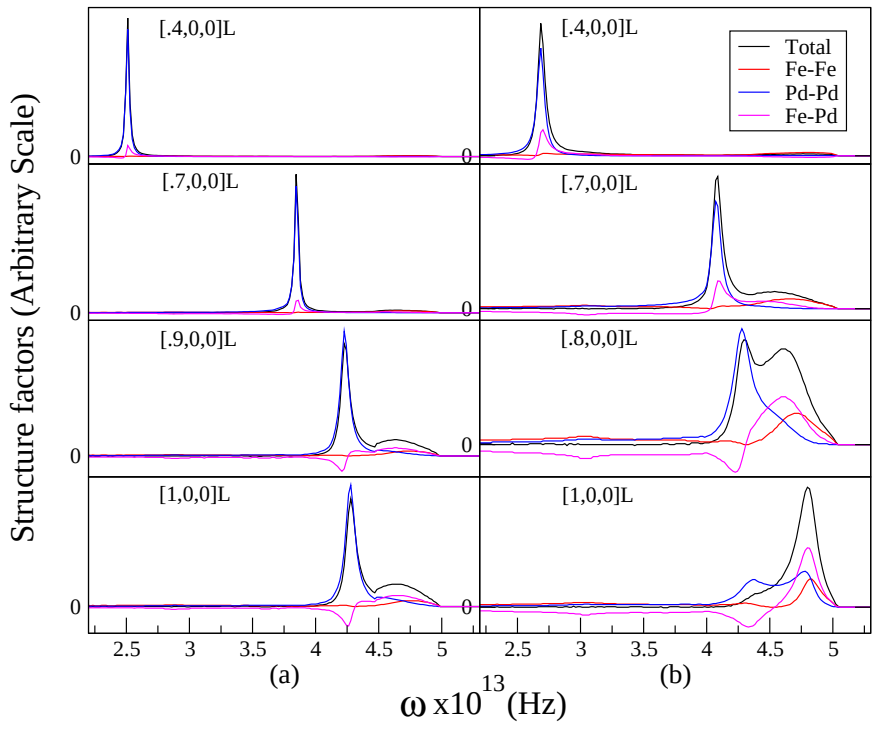


FIGURE 3.5: Partial and total structure factors calculated by the ICPA for various $\zeta$ values in the [$\zeta$,0,0] direction in (a) $Pd_{0.96}Fe_{0.04}$ and (b) $Pd_{0.9}Fe_{0.1}$ using the concentration averaged Fe-Pd force constants. All the curves are for longitudinal modes.

splitting in the dispersion curve for the $Ni_{50}Pt_{50}$ alloy was found to be due to the interplay of the Ni-Ni, Pt-Pt and Ni-Pt force constants whereas in [107], a spurious splitting like the present case was observed in the $Fe_{50}Pd_{50}$ alloy which was due to an overestimation of the Pd-Pd force constants. To understand the sources of the unphysical splittings in our cases, we take recourse in the partial and the average structure factors. In Fig. 3.5, we present results for the structure factors along the $[\zeta 00]$ direction and for the longitudinal branch at some selected $\zeta$ values. For $Pd_{0.96}Fe_{0.04}$ (Fig. 3.5(a)), we observe that the contributions of the Fe pairs to the total structure factors are minuscule and the spectrum is dominated mainly by the Pd pairs. However, the structure factor at the zone boundary has a two peak structure where the small hump-like peak at a higher frequency is due to substantial contributions from the Fe-Pd pairs. This is the reason behind the existence of the extra longitudinal branches in the dispersion curves. For $Pd_{0.9}Fe_{0.1}$(Fig. 3.5(b)), the peaks in the structure factors are mostly due to the Pd pairs with some contribution from the Fe-Pd pairs for smaller $\zeta$ values. However, as one moves towards the zone boundary, a hump starts to show up at higher frequencies, as is seen in case of $[0.7, 0, 0]$ longitudinal branch. The hump originates mainly from the Fe-Pd contributions. At the zone boundary, the main peak in the structure factor shifts substantially towards high frequency, producing a split in the dispersion curve. The new peak is now dominated by the Fe-Pd contributions along with contributions from the Pd pairs and Fe pairs. It is interesting to note that, on the lower frequency side where Pd-Pd had dominant contributions, no peak is observed because of the fact that the Fe-Pd contributions have neutralized the Pd-Pd contributions completely. The observations in the structure factor results suggest that, for high $\zeta$ values, the Fe-Pd interactions are competing with the Pd-Pd interactions producing the anomalous new branch in the phonon spectrum. That the Fe-Pd interactions are as strong as the Pd-Pd interactions can be understood from the force constants provided in table 3.1. We can therefore conclude that the Fe-Pd interactions calculated from simple concentration averages of the Fe-Fe and Pd-Pd interactions do not provide a correct picture of the microscopic interactions.

In our endeavor to model the inter-atomic interactions correctly with the help of the *ab initio* force constants, we next try to model the Fe-Pd force constants making use of the following intuitive argument: the basic assumption on which we calculated the Fe-Fe and Pd-Pd force constants at the alloy lattice constants was that the inter-atomic longitudinal and transverse force constants are dependent upon bond distances alone. In the same spirit, the Fe-Pd force constants can, therefore, not be of nearly the same magnitude as the Pd-Pd ones.

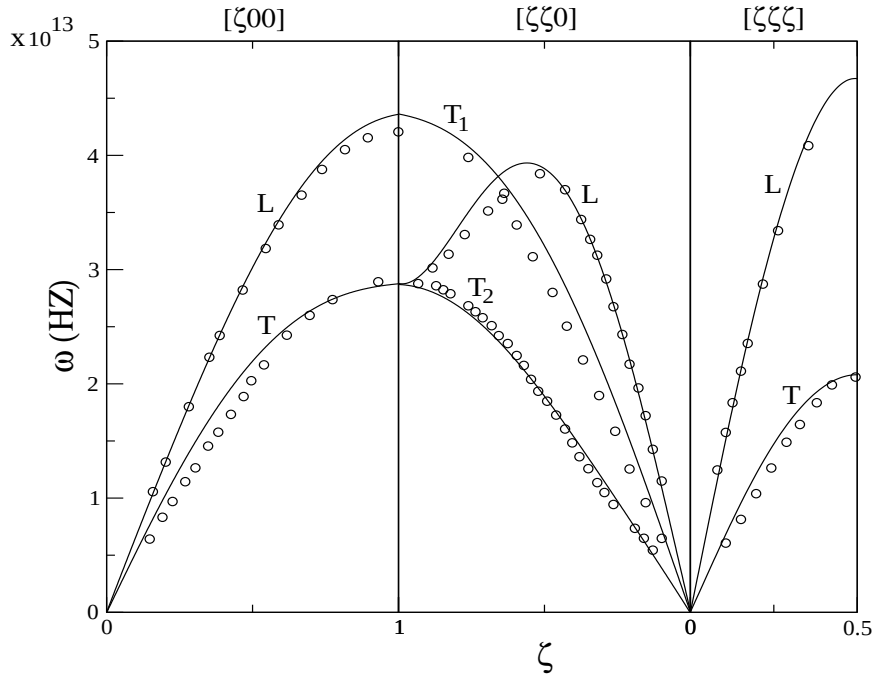


FIGURE 3.6: Dispersion curves for $Pd_{0.96}Fe_{0.04}$ with 20% reduced Fe-Pd force constants obtained from the ICPA calculations. The circles are the experimental points.

TABLE 3.1: Computed force constants (in units of $dyn\ cm^{-1}$) for $Pd_xFe_{1-x}$. Fe-Fe and Pd-Pd force constants are obtained from DFPT calculations. Fe-Pd (averaged) force constants are the ones obtained by performing concentration averages on Fe-Fe and Pd-Pd force constants. Fe-Pd (reduced) force constants are the ones reduced by 20% from the Fe-Pd (averaged) values. L and T represent the longitudinal and the transverse force constants respectively.

| Pair type | Conc.(x) | L | T |
|---|---|---|---|
| Fe-Fe | 0.96 | 13365.62 | -566.05 |
| Pd-Pd | 0.96 | 45925.46 | -2423.68 |
| Fe-Pd (averaged) | 0.96 | 44623.07 | -2349.37 |
| Fe-Pd (reduced) | 0.96 | 35698.46 | -1879.50 |
| Fe-Fe | 0.90 | 14495.28 | -609.35 |
| Pd-Pd | 0.90 | 48767.67 | -2698.84 |
| Fe-Pd (averaged) | 0.90 | 45340.43 | -2489.89 |
| Fe-Pd (reduced) | 0.90 | 36272.34 | -1991.91 |

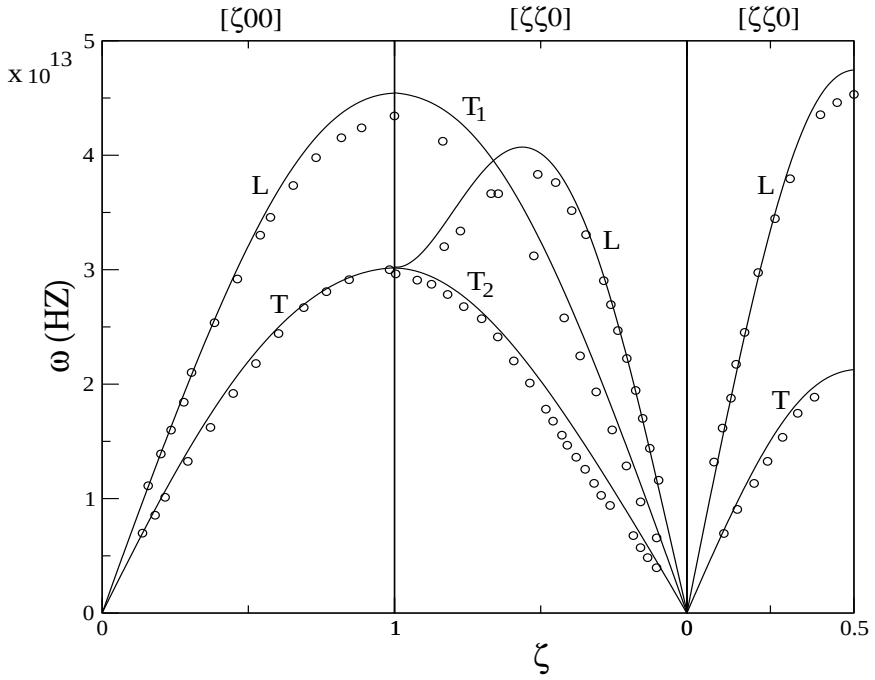


FIGURE 3.7: Dispersion curves for $Pd_{0.9}Fe_{0.1}$ with 20% reduced Fe-Pd force constants obtained from the ICPA calculations. The circles are the experimental points.

This intuitive argument is based upon the fact that, in both the alloys considered here, the Fe concentration is very low; therefore in the sample the Pd atoms would find themselves mostly surrounded by Pd atoms, making the average bond distances of Fe-Pd larger than that of Pd-Pd, resulting in the softening of the Fe-Pd interactions in comparison to the Pd-Pd ones.

Based on this intuitive argument, we now reduce the Fe-Pd force constants from the concentration averaged values, keeping the Fe-Fe and Pd-Pd ones intact. The anomalies in the phonon spectrum completely disappear by 20% reduction of the Fe-Pd force constants from the concentration averaged values. In Figs. 3.6 and 3.7, we present the dispersion curves calculated by the ICPA using these new sets of force constants for $Pd_{0.96}Fe_{0.04}$ and $Pd_{0.9}Fe_{0.1}$, respectively. We observe substantially good agreement between the ICPA results and the experimental results for both cases. Corresponding structure factors for [100] longitudinal branches are shown in Figs. 3.8 and 3.9, respectively. Unlike the previous structure factors (Fig. 3.5), no dual peak structures appear in these cases. For both alloys, the Fe-Pd contributions are significantly weaker than the Pd-Pd ones and at the zone boundary, the Fe-Pd contributions only add more weight to the single peak dominated by the Pd-Pd contributions. The extra peaks which were observed with the concentration averaged Fe-Pd force constants are now shifted to the lower frequencies and merge with the main peak.

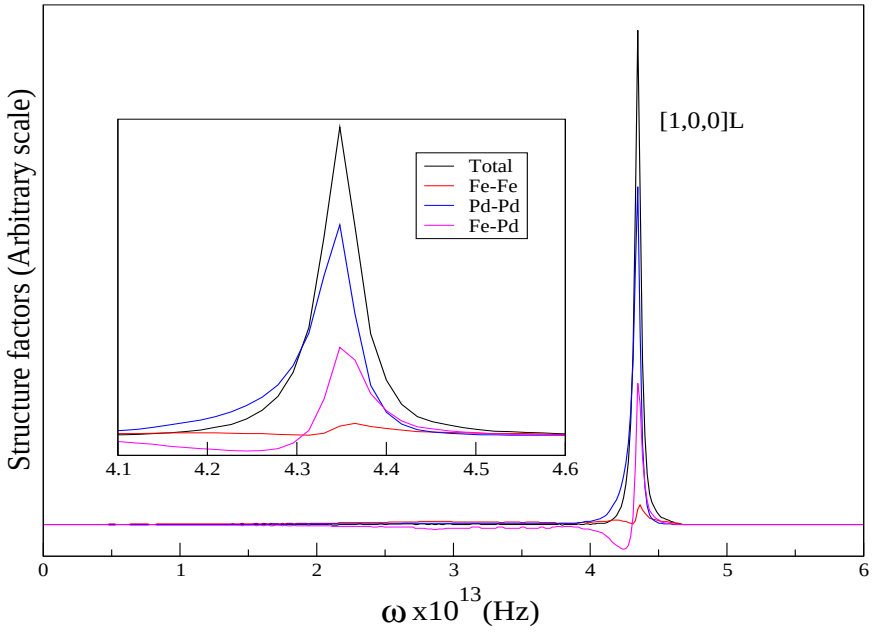


FIGURE 3.8: Partial and total structure factors calculated in the ICPA with 20% reduced Fe-Pd force constants for $\zeta = 1$ in the [$\zeta$,0,0] direction in $Pd_{0.96}Fe_{0.04}$. All the curves are for longitudinal modes. The inset shows the contributions from various pairs near the peak.

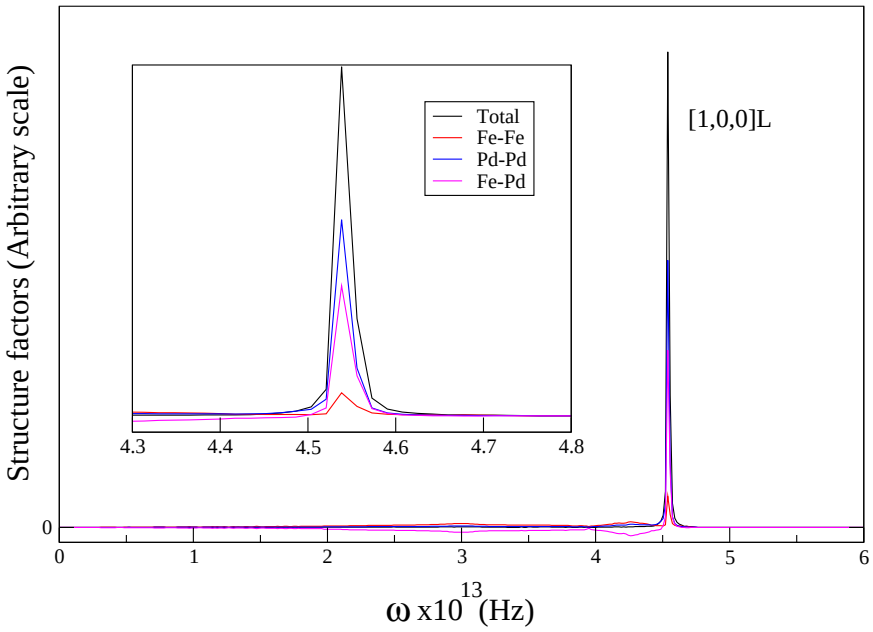


FIGURE 3.9: Partial and total structure factors calculated in the ICPA with 20% reduced Fe-Pd force constants for $\zeta = 1$ in the [$\zeta$,0,0] direction in $Pd_{0.9}Fe_{0.1}$. All the curves are for longitudinal modes. The inset shows the contributions from various pairs near the peak.

TABLE 3.2: Computed elastic constants (in units of Mbar) for $Pd_xFe_{1-x}$.

| | $Pd_{0.96}Fe_{0.04}$ | | | $Pd_{0.9}Fe_{0.1}$ | | |
|---|---|---|---|---|---|---|
| | Theo [our calc.] | Theo [119] | Expt. [123] | Theo. [our calc.] | Theo. [119] | Expt. [123] |
| $C_{11}$ | 1.97 | 1.716 | 2.3 | 2.24 | 1.724 | 2.29 |
| $C_{12}$ | 1.25 | 1.273 | 1.53 | 1.41 | 1.292 | 1.65 |
| $C_{44}$ | 1.26 | 1.015 | 0.78 | 1.12 | 1.004 | 0.86 |

Finally, we calculate the elastic constants in these alloys from the slopes of the phonon dispersion curves in order to check the accuracy and the quality of the phonon frequencies obtained by the modeling strategy adopted here. The results are given in Table 3.2. Results obtained from the model potential calculations [119] and the experiments [123] are also presented for comparison. We observe an overall better agreement of our results with the experimental values than those of the model potential approach. The only significant discrepancy is observed for $C_{44}$ in the case of $Pd_{0.96}Fe_{0.04}$. The average deviation between our results and the experimental ones is about 16%, indicating reasonably good agreement.

### 3.4.2 Limitations of the modeling strategy

In the present approach, we have tried to model the inter-atomic force constants for $Pd_{0.96}Fe_{0.04}$ and $Pd_{0.9}Fe_{0.1}$ by calculating the Pd-Pd and Fe-Fe force constants in pure Pd and pure Fe lattices with the alloy lattice constants. The basic assumption behind such approach is that the effect of environment on these force constants are expected to be less due to the high concentration of one of the constituents. The Fe-Pd interaction has also been modelled by hand-adjustment starting from the concentration averaged values. Although the results on phonon spectrum have good agreement with the experiments, these choices are purely arbitrary and thus do not have a robust physical meaning. Moreover, the non-incorporation of environment effects has limited its applicability for an arbitrary concentration. Hence, we need to find an alternative modeling strategy for random alloys so that the local environment effects are incorporated in the calculated force constants.

Recently a new model to calculate the inter-atomic force constants in random alloys has been proposed by Axel van de Walle and Gerbrand Ceder [116, 117]. Based on the idea of

bond length dependent transferable force constants across different environment, this model has all the necessary ingredients to overcome the limitations associated with the present modeling strategy. We discuss the essential features of this approach in the next section.

## 3.5 Transferable force-constant (TFC) model

The computational burden associated in the computation of force-constant tensors from first principles electronic structure calculations would be enormously reduced if the force constants determined in one structure could be used to predict force constants in another structure. The idea of using transferable force constants to reduce computational expense is, therefore, tremendously appealing and had been applied in the past for different class of systems [133–136]. However, it was observed in these calculations that the force-constants obtained from one structure are not directly transferable to another structure. Nevertheless, a simple modification of the transferable force constant approach yields substantial improvements in precision. Initially defined for the transferability of force constants for a particular pair type, between different chemical environments [134], van de Walle and Ceder have recently introduced the idea of using bond length dependent transferable force constants [116–118]. Their calculations on a number of systems [53, 57, 116–118] had revealed that magnitudes of the force constants are strongly correlated with the corresponding bond lengths. This suggests that most of the variation in the stiffness of a given chemical bond across different structures can be explained by changes in bond length alone and as a result, the 'force constant versus bond length' relationships exhibit better transferability than the force constants themselves.

In the TFC approach, three assumptions are made to obtain the desired transferable properties. Only the nearest neighbor interactions are considered because the longer ranged force constants are ill-suited for the purpose. However, no serious error is expected to occur due to this because of the fact that in the alloys considered, the distant neighbor force-constants are orders of magnitude smaller than the nearest-neighbor ones. The bending stiffness $b$ are averaged over various spatial directions in order to obtain effective isotropic bending stiffness and the off-diagonal terms in the force-constant tensor $\mathbf{\Phi}$ are constrained to be zero. Thus, the resulting force-constant tensor has only two independent terms, the stretching stiffness $s$ and

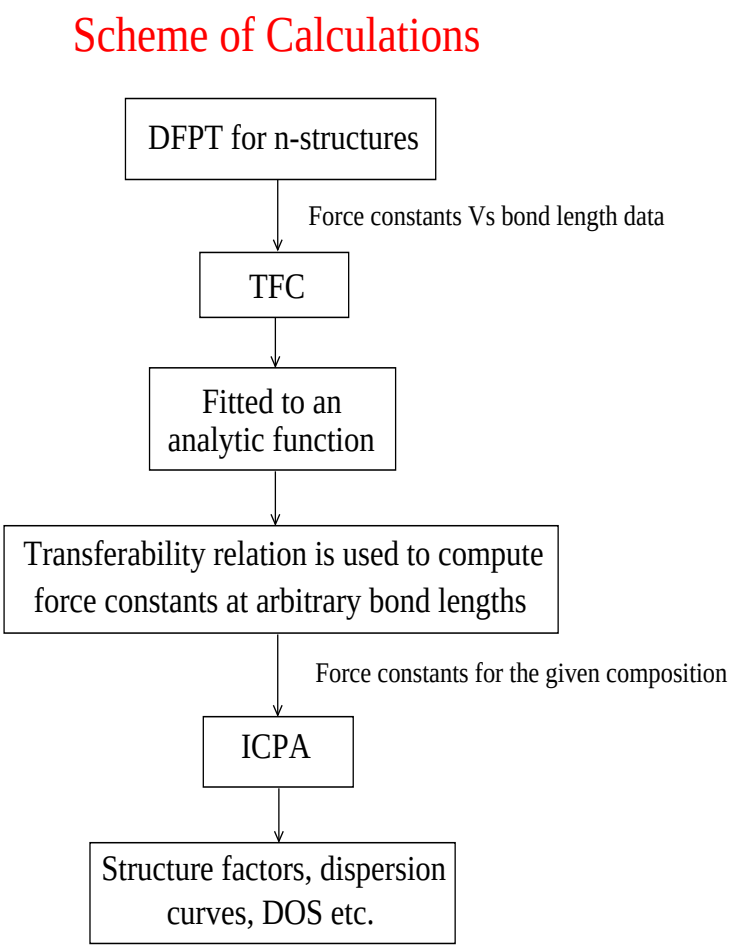


FIGURE 3.10: Scheme of calculations by the DFPT-TFC-ICPA method

the isotropic bending stiffness $b$:

$$\Phi(i,j) = \begin{pmatrix} b & 0 & 0 \\ 0 & b & 0 \\ 0 & 0 & s \end{pmatrix}.$$

Here the coordinate system is transformed such that the $z$ axis is aligned along the direction connecting atoms $i$ and $j$. This symmetrization ensures that the force constants never have a symmetry which is lower than the environment into which it is transferred. The force constants generated via the TFC method satisfy two important invariance properties. First, the TFC tensors are invariant under symmetry operations of the crystal's space group and second, the energy change associated with an infinitesimal translation is zero.

The TFC model provides a very simplistic and computationally feasible way to determine the inter-atomic force constants in random alloys. The 'force constant vs bond length' relationship can be easily determined first by calculating the elements of stretching-bending force-constant tensor for a set of ordered structures so that enough dispersions of different bond distances are obtained and then by fitting these elements to an analytic function. Once this is done, the inter-atomic force constants of any other structure can be determined solely from the knowledge of its equilibrium geometry. Previously, this approach had been used to calculate the vibrational entropies of $L1_2$-ordered and disordered phases in $Au_3Cu$, $Cu_3Au$, $Au_3Pd$, $Pd_3Au$, $Cu_3Pd$ and $Cu_3Pt$. In this thesis, we combine the ICPA with the state-of-the-art first-principles density-functional theory (DFT) based density functional perturbation theory (DFPT) and the transferable force constant (TFC) model to construct a new first-principles based computational tool to calculate the phonon dispersions in disordered alloys at arbitrary compositions. We name it as 'DFPT-TFC-ICPA' method. In Fig. 3.10, we present a scheme of calculations by this method. The applicability of this tool for a wide variety systems will be discussed in the next chapter.

## 3.6 Summary

In this chapter, we have introduced a new approach to understand the influences of inter-atomic interactions between various pairs of specie in a random binary alloy on the lattice dynamics of such systems both qualitatively and quantitatively using $Pd_xFe_{1-x}$ alloys as an example case. The modeling of inter-atomic interactions is based upon the results of *ab initio* calculations and the intuitive argument about dependence of stretching and bending force constants on bond lengths. This strategy has incorporated the important electronic structure effects which influence the interplay of forces at the microscopic level and thus provides a realistic and accurate picture which was absent in the approach based upon construction of model potentials. The ICPA, on the other hand, has performed the configuration averaging in a self-consistent way taking into account the disorder fluctuations in both mass and force constants. These issues were not addressed in the model potential approach and hence modeling the random alloy to a mean crystal like one could not provide the realistic picture of disordered fluctuations producing significant differences with the experimental results which can only get exaggerated for a system with stronger mass and force constant disorder like the

NiPt. Our methodology, a combination of accurate *ab initio* electronic structure tool and an efficient self-consistent method for configuration averaging, on the other hand, has been able to systematically investigate the influences of the force constant fluctuations on the phonon spectrum and therefore, understand the microscopic origin of the lattice dynamics in $Pd_xFe_{1-x}$ alloys. The calculated phonon frequencies and the elastic constants agree very well with the experiments, thus justifying the modeling strategy adopted.

In spite of its success in case of the PdFe alloys with high Pd content, the crude approximations involved in our modeling scheme has reduced its applicability for random alloys in general and at arbitrary concentrations. Thus, we have proposed a combination of density functional perturbation theory (DFPT) and transferable force constant (TFC) model as a new first-principles based tool which has the ability to calculate inter-atomic force constants for arbitrary compositions taking into account environmental effects.

# Chapter 4

# Applications of DFPT-TFC-ICPA method for binary alloys

## 4.1 Introduction

Study of phonon excitations in solids offer interesting perspectives regarding materials properties and behavior. Useful insight about the ordering behavior, phase stability and elastic properties, to name a few, can be obtained from the phonon dispersion relations of solids. The microscopic understanding of the material properties and the novel phenomena in materials from their lattice dynamics require robust and accurate theoretical tools. In the previous chapter, we have proposed DFPT-TFC-ICPA as a first-principles based method to compute lattice dynamics in substitutionally disordered alloys. In all previous calculations with the transferable force-constant (TFC) model, the focus had been on calculations of vibrational entropy contributions in the context of relative stability of various ordered and disordered phases [118]. The complete phonon spectra and related material properties, like the elastic constants, were never calculated using this approach. The reliability of the TFC model can't be completely satisfactory unless one computes the complete phonon spectra in disordered phases and at arbitrary compositions. This is because of the fact that in cases of calculation of vibrational entropies or their differences, the key quantity is the vibrational densities of states, an integrated quantity and therefore, may average out errors through the integration process. The phonon frequencies, on the other hand, would reflect the errors due to the approximation,

in a proper way. To this end, we apply the new approach, DFPT-TFC-ICPA, to calculate the phonon spectra and associated properties for a variety of alloys. Starting with a magnetic type-II alloy ($Fe_xPd_{1-x}$), we mainly focus on alloys with significant mass and size differences among the constituents ($Cu_xAu_{1-x}$, $Cu_xAu_{1-x}$ and $Ni_xPt_{1-x}$). The reasons for choosing these alloy systems are explained below.

For validification of our new theoretical approach, we first choose the $FePd$ alloys [137]. There are two reasons to choose the system: first, the size-mismatch between the constituents is not substantial, thus, local relaxations would not have a significant impact. It is important for validification of a new methodology that it is first validated for simpler systems. Second, $FePd$ is a type-II alloy. It is a well-known fact that, for type-II alloys like the $FePt$ and $FePd$, where the constituents, inspite of crystallizing in different structures in their respective ground states, form a single solid solution upon alloying. These alloys at compositions near the Invar region exhibit an interplay of magnetism and lattice dynamics [138, 139]. The computation and understanding of phonon spectra in these alloys is, thus, necessary to understand the microscopic nature of magnetism-phonon interaction in these technologically important systems. We, therefore, compute the phonon spectra and elastic constants for the magnetic alloy $Pd_xFe_{1-x}$ with $x = 0.96, 0.9, 0.5$ and $0.28$. We compare our results with those obtained from earlier attempts where the force constants were either extracted empirically [93, 109] or from model inter-atomic potentials [119, 120] and in the process, we try to validate our DFPT-TFC-ICPA method as a reliable first-principles based method for calculating the phonon spectra and related properties for disordered alloys which takes care of the microscopic aspects of various types of disorder.

Our next applications involve alloys with constituents having significant size differences. There, we try to investigate the influence of size mismatch between the components of a disordered alloy on the phonon dispersions [140]. It is well known that on introduction of defects into a perfect crystal, the volume of the sample changes even in the low concentration limit of the impurity. This phenomenon of lattice relaxation is more pronounced in case of size mismatched alloys. When atoms of different sizes are constrained to coexist on a lattice, an atom of larger (smaller) size can experience compressive (tensile) stress that results in locally stiffer (softer) regions if it is surrounded with atoms of smaller (larger) sizes. These local relaxations produce dispersions in the bond lengths associated with different pairs of chemical specie in the alloy. Correspondingly, it is expected that the stiffness of a given bond would also fluctuate depending upon the environment surrounding it. Thus, for size mismatched

TABLE 4.1: Properties of Cu, Pd and Au

| | Cu | Pd | Au |
|---|---|---|---|
| Atomic number | 29 | 46 | 79 |
| Atomic mass(amu) | 63.55 | 106.4 | 196.9 |
| Atomic radius(pm) | 128 | 137 | 144 |
| Nearest neighbor force-constants(dyn/cm) | | | |
| 1XX | 13160[a] | 19337[a] | 16610[b] |
| 1XY | 14880[a] | 22423[a] | 19930[b] |
| 1ZZ | -1489[a] | -2832[a] | -6650[b] |

[a] Reference [141]

[b] Reference [142]

alloys, three different types of disorder: the mass disorder, the force-constant disorder and the environmental disorder; should affect the phonon dispersion relations. A significant insight into the lattice dynamics and related properties in this class of alloys can only be gained if a microscopic picture on the role of each of the factors affecting the phonon spectra is achieved.

Here, we have chosen Cu-Pd and Cu-Au alloys which satisfy the above criteria and are well suited for our investigation. A brief summary of their elementary properties which are relevant to our investigations are presented in Table 4.1. The mass ratio of Pd to Cu is, $M_{Pd}/M_{Cu}$=1.674, whereas, that of Au to Cu is, $M_{Au}/M_{Cu}$=3.098. On the other hand, force constants of Pd are, on an average, 50% larger than those of Cu, while, the Au force constants are about 30% larger than those of Cu. These large mass and force constant ratios between the various constituent elements make the above alloys potential examples of strong mass and force-constant disorder. Neutron scattering experimental results on the phonon dispersion relations are available for $Cu_{0.715}Pd_{0.285}$ [143, 144] and $Cu_{0.75}Au_{0.25}$ [145, 146] systems and thus we have chosen alloys with these compositions for the present study. Our motivation is to understand the features in the phonon dispersion results based upon analysis of the role of the mass fluctuations and the fluctuations in the inter-atomic force constants; the later is an estimation of the stiffness of a bond connecting a pair of atoms. This in turn would validate our computational technique for addressing alloys with higher degree of all possible disorders due to chemical substitution. In the analysis of neutron-scattering experimental results on phonon dispersions, the experimentally obtained normal mode frequencies are routinely fitted to a

Born-Von-Karman model and the inter-atomic force constants are thus extracted. However, this approach never provides a correct picture of the complex interplay of inter-atomic forces in a disordered alloy because the model assumes an average lattice and thus neglects any fluctuations due to the presence of specie with different chemical properties. In this work, we systematically show that the phonon spectra need to be understood in the light of these fluctuations. Our results also show that the consideration of the local lattice relaxations is necessary in these systems. Although we get excellent agreement with the experiments for $Cu_{0.715}Pd_{0.285}$, our results significantly differ with the experiments in case of $Cu_{0.75}Au_{0.25}$. We explain the reasons behind the discrepancy in the light of the inter-atomic force constants and thus provide a physically reasonable picture of the microscopic situation in this system.

Finally, we focus on *NiPt* alloys [147]. These alloys have received considerable attention over the past few decades because of the immense technological importance associated with these systems. There have been numerous investigations both on the experimental [148–150] and on the theoretical [151–153] front with the focus on the ordering tendency and the magnetism in these alloys. Atomic ordering at 3:1 and 1:1 compositions indicate influence of short range ordering [154]. The long-range ordering on the other hand has been found to influence the magnetism [152] in these alloys significantly which has been attributed to the complex nature of electronic structure in these systems. The crucial yet less explored aspect in these systems is the lattice dynamical behavior. The $Ni_xPt_{1-x}$ alloys possess several advantages regarding the investigation of lattice dynamics: first, Ni and Pt form a continuous series of FCC solid solutions [154], thereby, making it possible to study the variation of phonons in the whole concentration range, second, the melting points of these alloys are nearly constant over a wide range of concentrations which means that the homogeneous single crystals can be grown at nearly any concentration without zone-melting effects, making the system attractive for experimental study, third, the phonon excitations of elemental Ni and Pt metals have been well characterized both experimentally and theoretically [38, 141, 155]. The results show that the nearest-neighbor atomic force constants of Pt are roughly 55% larger than those of Ni, making the alloy system an ideal candidate to study the effect of force constant differences on the phonon dispersion relations and fourth, the large mass and size ratio on top of large force constant ratio between the alloy constituents suggest that upon alloying, novel composition dependent features in the phonon spectra can be observed. A brief summary of the relevant elementary properties of the constituents is presented in Table 4.2.

TABLE 4.2: Properties of Ni and Pt

| | Ni | Pt |
|---|---|---|
| Atomic number | 28 | 78 |
| Atomic mass(amu) | 58.71 | 195.09 |
| Atomic radius(pm) | 124 | 139 |
| Nearest neighbor force-constants(dyn/cm) | | |
| 1XX | 17319[a] | 26358[b] |
| 1XY | 19100[a] | 30317[b] |
| 1ZZ | -436[a] | -7040 [b] |

[a] Reference [155]

[b] Reference [141]

Tsunoda *et al.* [73, 156] carried out neutron-scattering experiments to investigate the phonon spectra in this alloy system for the entire concentration range for the first time. They observed the following noteworthy features: first, anomalous jumps in frequencies for all phonon propagation directions which they attributed to the usual resonance modes of heavy Pt atoms in light Ni matrix. However, a resonance-like behavior was observed for $Ni_{0.25}Pt_{0.75}$, a system with larger concentration of the heavier constituent where an impurity mode due to Ni was supposed to be observed; second, a branch dependence of the resonance frequency was observed. In order to explain these anomalies, they computed the phonon spectra by the CPA [72] which was unable to reproduce many features, observed in experiments, qualitatively as well as quantitatively. For example, the top band edge frequencies computed by the CPA were significantly larger than the experimental ones and the vibrational densities of states computed by the CPA even predicted a split-band behavior for concentrated alloys. The authors concluded that these disagreements are due to the effects of force-constant disorder which was not addressed in the CPA. Here, we explore the changes in the phonon spectra of $Ni_xPt_{1-x}$ alloys with the change in concentration $x$ over the entire concentration range. The motivation is twofold: first, to understand the anomalous features in the phonon spectra and their variations with compositions observed experimentally and second, in doing so, to test the accuracy of the newly developed first-principles based method when applied to an alloy with substantial mass and size ratio among the constituents for any arbitrary composition.

In the next section, we briefly present the computational details. The subsequent section

contains results and thorough discussions including experimental results as well as results obtained from previous theoretical work. Summary of the results along with the concluding remarks are presented in section 4.4.

## 4.2 Computational Details

First-principles Quantum-Espresso code [124], based upon a Plane wave Pseudopotential implementation of the DFPT [112], has been used to compute the force constants at different bond lengths with different ordered structures, the details of which are described in Figs. 4.1, 4.8, 4.12 and 4.20. Ultra-soft pseudo-potentials [125] with nonlinear core corrections [126] are used. While Perdew-Zunger parametrization of the local density approximation (LDA) [127] is used for $Fe_xPd_{1-x}$ alloys, Perdew-Burke-Ernzerhof (PBE-96) generalized gradient approximation (GGA) [128] functional is used for rest of the alloys, for the exchange-correlation part of the potential. Plane waves with energies up to 55 Ry are used in order to describe electron wave functions and Fourier components of the augmented charge density with cutoff energy up to 650 Ry are taken into account. The Brillouin-zone integrations are carried out with Methfessel-Paxton smearing [129] using a 14x14x14 **k**-point mesh. The value of the smearing parameter is 0.02 Ry. These parameters are found to yield phonon frequencies converged to within 5 percent.

After achieving the desired level of convergence for the electronic structure, the force constants are conveniently computed in reciprocal space on a 4x4x4 **q**-point grid and Fourier transformation is employed to obtain the real space force constants. The resulting force-constants versus bond distances data for each chemical bond is then fitted using a linear relationship according to the TFC model:

$$s(l) = s_0 + s_1(l - l_0) \tag{4.1}$$

$$b(l) = b_0 + b_1(l - l_0) \tag{4.2}$$

$s(l)$, $b(l)$ are the stretching and bending components of the force-constant tensor respectively [116], $l_0$ is the equilibrium length of a particular bond and $s_0$, $b_0$ are the stretching and the bending components of the stiffness (force-constant) of the bond at the equilibrium length

respectively. Once the transferability relation is obtained, the inter-atomic force constants of any other structure can be determined solely from the knowledge of its equilibrium geometry.

The all-important configuration averaging is then performed by employing the ICPA method. The disorder in the force constants were considered for nearest neighboring shell only and the calculations were done on 400 energy points. A small imaginary frequency part of -0.05 was used in the Green's functions. The Brillouin-zone integration was done over 356 **q**-points in the irreducible Brillouin zone. The simplest linear-mixing scheme was used to accelerate the convergence, with the number of iterations ranged from 5 to 15 for all the calculations. The phonon frequencies and the disorder-induced widths are obtained, respectively, from the peaks and from the widths of the coherent scattering structure factor as defined in Eq. 2.3. Also, the vibrational densities of states are calculated from the imaginary part of the configuration-averaged mass-weighted Green's function through Eqs. 2.4 and 2.5.

## 4.3 Results and Discussion

### 4.3.1 $\mathbf{Pd}_x\mathbf{Fe}_{1-x}$ for $x = 0.96$, 0.9, 0.5 and 0.28

Neutron-scattering results on phonon spectra for $Pd_{0.96}Fe_{0.04}$, $Pd_{0.9}Fe_{0.1}$ [123], $Pd_{0.5}Fe_{0.5}$ [157] and $Pd_{0.28}Fe_{0.72}$ [139] for all three symmetry directions are available along with the results on elastic constants. However, the measurements were done at different experimental conditions. While the measurements for $x = 0.96, 0.9$ and 0.28 ($x$ is the Pd concentration) were done at room temperatures, the measurements for $x = 0.5$ were done at 1020 K. Accordingly, we discuss our results in two separate subsections.

#### 4.3.1.1 $\mathbf{Pd}_{0.96}\mathbf{Fe}_{0.04}$, $\mathbf{Pd}_{0.9}\mathbf{Fe}_{0.1}$ and $\mathbf{Pd}_{0.28}\mathbf{Fe}_{0.72}$

The stretching and bending force constants for the alloy at the three concentrations are extracted from the fitted 'bond stiffness versus bond distance' relations as shown in Fig. 4.1. The curves in Fig. 4.1 show that the linear fitting is appropriate for the present case as the monotonic decrease of the force constants with the increasing bond distances is well captured

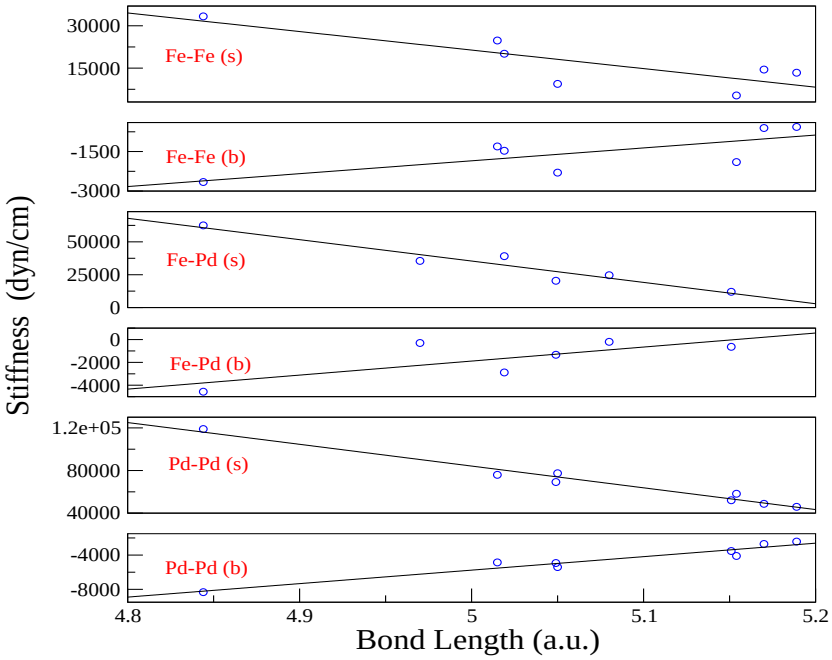


FIGURE 4.1: Nearest neighbor stretching and bending force constants for $Pd_xFe_{1-x}$ as a function of bond length. The solid lines are the fitted functions whereas the circles correspond to data obtained from *ab initio* calculations on one of a set of structures ($L1_2$ at four different volumes, $L1_0$ at two different volumes, FCC Fe and FCC Pd at three different volumes).

for all three pairs of inter-atomic force constants. The computed values of correlation coefficient for the straight line fitting of stretching components of the force constant matrices varies between 0.83 and 0.99 which can be considered to be a very good fit. The fit accuracy for the bending components is, however, a bit low with the calculated correlation coefficient varies between 0.74 and 0.97. But still, one can safely ignore this point as the bending components of force constant matrices are orders of magnitude smaller than the stretching components and therefore, play minimal role in determining the phonon frequencies. The stretching and bending force constants for the three concentrations obtained from the fitted results are presented in Table 4.3. The results show that for high Pd concentration systems, namely for $x = 0.96$ and 0.9, the Fe-Fe and Fe-Pd force constants are softer by an order of magnitude than that of the Pd-Pd ones, with the Fe-Pd force constants being the softest. This is only to be expected because of the following reason: in a Pd-rich alloy like the ones discussed here, the Fe atoms would find lesser numbers of Fe atoms in the nearest-neighbor environment compared to that of the elemental Fe. As a result, the Fe-Fe and Fe-Pd interactions would be much softer compared to the Pd-Pd ones due to the overwhelming domination of the later pair in the environment. In the previous chapter, we tried to model the inter-atomic force constants for these

TABLE 4.3: Computed force constants (in units of $dyn/cm$) for $Pd_xFe_{1-x}$ using the TFC model. Results from other calculations are also presented for comparison.

| Pair type | Conc. (x) | Bond length (a.u.) | *s* (TFC) | *b* (TFC) | *s* (Other work) | *b* (Other work) |
|---|---|---|---|---|---|---|
| Fe-Fe | 0.96 | 5.189 | 8990 | -930 | 13366[a] | -566[a] |
| Pd-Pd | 0.96 | 5.189 | 45641 | -2783 | 45925[a] | -2424[a] |
| Fe-Pd | 0.96 | 5.189 | 4720 | 432 | 35698[a] | -1879[a] |
| Fe-Fe | 0.90 | 5.170 | 10202 | -1020 | 14495[a] | -609[a] |
| Pd-Pd | 0.90 | 5.170 | 49404 | -3073 | 48768[a] | -2699[a] |
| Fe-Pd | 0.90 | 5.170 | 7718 | 206 | 36272[a] | -1992[a] |
| Fe-Fe | 0.28 | 5.019 | 20157 | -1760 | – | – |
| Pd-Pd | 0.28 | 5.019 | 80323 | -5457 | – | – |
| Fe-Pd | 0.28 | 5.019 | 32345 | -1655 | – | – |
| Fe-Fe | 0.50 | 5.12 | 13573 | -1271 | – | – |
| Pd-Pd | 0.50 | 5.12 | 59874 | -3880 | – | – |
| Fe-Pd | 0.50 | 5.12 | 16057 | -424 | – | – |
| Fe-Fe | 0.50 | 5.246 | 5230 | -651 | 15400[b] | -4100[b] |
| Pd-Pd | 0.50 | 5.246 | 33983 | -1883 | 41800[b] | -2900[b] |
| Fe-Pd | 0.50 | 5.07 | 24136 | -1035 | 30600[b] | -2500[b] |

[a] Chapter 3 of this thesis and Reference [109]

[b] Reference [107]

two systems by calculating the Pd-Pd and Fe-Fe force constants in pure Pd and Fe lattices respectively with the alloy lattice constant while the Fe-Pd interaction was modelled by hand-adjustment starting from the concentration averaged values. Although the results on phonon spectrum had good agreement with the experiments, these choices were purely arbitrary and neglecting the environment effects limited it's applicability for an arbitrary concentration. On the other hand, the TFC based approach captures the effects of environment and thus leads to the correct understanding of the relative nature of interactions between different specie pair. A comparison on the force-constants obtained from the TFC model and those from the modeling scheme presented in the previous chapter (Table 4.3) show that the Pd-Pd force constants have near perfect agreement while the Fe-Fe force constants obtained by the modeling scheme of previous chapter, are slightly stiffer. This definitely is an artifact of neglecting the role of

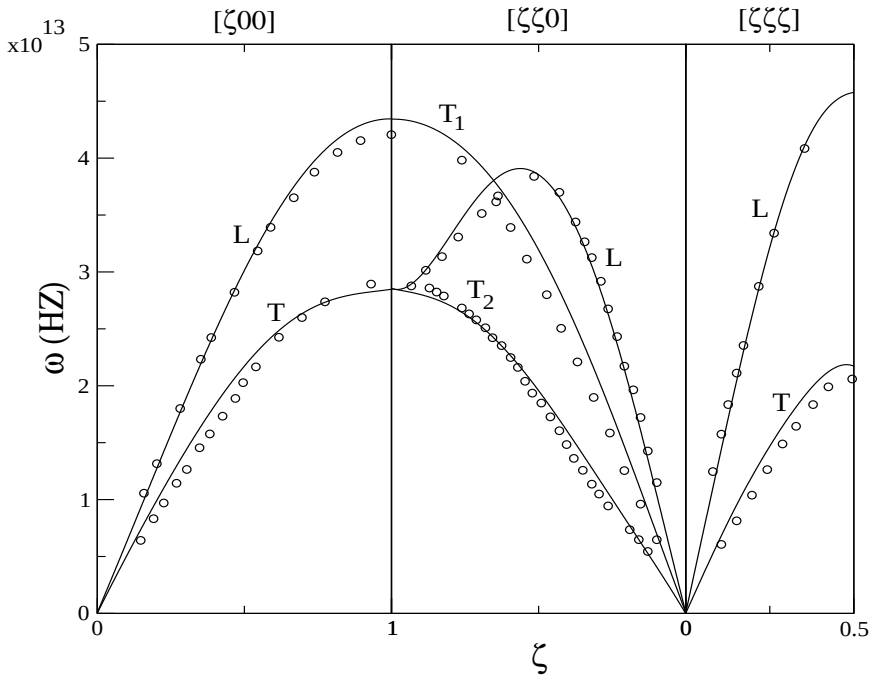


FIGURE 4.2: Dispersion curves (frequency $\omega$ vs reduced wave vector $\zeta$) ; $\zeta = \frac{|\vec{q}|}{|\vec{q}_{max}|}, \vec{q}$ the phonon wave-vector; for $Pd_{0.96}Fe_{0.04}$ calculated in the ICPA (solid lines) with the force constants obtained at the alloy bond length (5.189 a.u.) using 'bond stiffness vs bond length' method. The circles are the experimental data.

environment. In case of Fe-Pd force constants, we see a large difference. This is only to be expected as in the case of the modeling scheme of previous chapter, the force constants were obtained by adjusting from concentration-averaged values based upon empirical observations and thus didn't have a robust physical reasoning. On the other hand, the Fe-Pd interactions obtained by the TFC model have better reliability and accuracy because it is based upon the physical reality of transferability of the bond stiffness versus bond length relationship.

In the case of $Pd_{0.28}Fe_{0.72}$, the force constants obtained from the transferability relation as presented in Table 4.3 show hardening of all three inter-atomic force constants in comparison to Pd-rich alloys. This behavior follows the expectation. Since the bond distances are smaller than the Pd-rich alloys, all three bonds were expected to stiffen. The Fe-Fe interactions harden because the Fe atoms can now find more Fe atoms in the neighboring environment. The Pd-Pd bonds stiffen because of the fact that the larger Pd atoms find themselves in a cage of smaller Fe atoms and the Fe-Pd interactions harden because of presence of more unlike pairs in the nearest-neighbor environment.

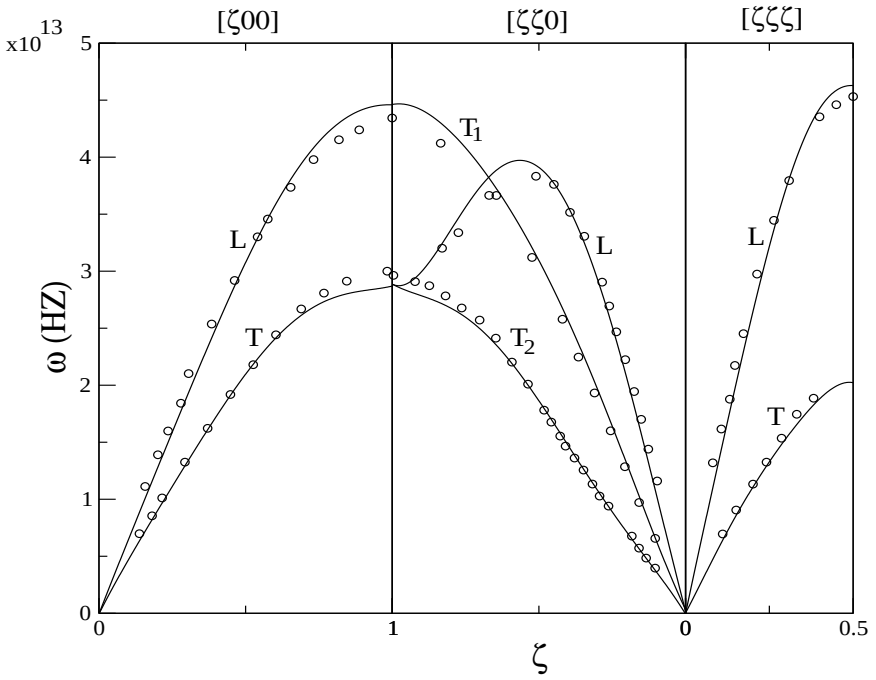


FIGURE 4.3: Dispersion curves (frequency $\omega$ vs reduced wave vector $\zeta$) ; $\zeta = \frac{|\vec{q}|}{|\vec{q}_{max}|}$, $\vec{q}$ the phonon wave-vector; for $Pd_{0.9}Fe_{0.1}$ calculated in the ICPA (solid lines) with the force constants obtained at the alloy bond length (5.17 a.u.) using 'bond stiffness vs bond length' method. The circles are the experimental data.

In what follows, we use the transferable force constants of Table 4.3 as inputs to the ICPA and calculate the phonon dispersion relations for the three alloys. The phonon dispersion results for $Pd_{0.96}Fe_{0.04}$, $Pd_{0.9}Fe_{0.1}$ and $Pd_{0.28}Fe_{0.72}$ calculated with these sets of force constants are presented in Figs. 4.2, 4.3 and 4.4, respectively. It can be seen that calculated and experimental results of phonon frequencies for $Pd_{0.96}Fe_{0.04}$ and $Pd_{0.9}Fe_{0.1}$ alloys are in excellent agreement for all the symmetry directions. The calculated phonon frequencies of the $Pd_{0.28}Fe_{0.72}$ alloy also agree reasonably well with experimental values except near the zone edges. This disagreement could be because of using the LDA as the exchange-correlation functional at the experimental lattice constant for a Fe-rich system. Earlier calculations with pure Fe [158] had shown that the calculated frequencies are underestimated if one uses the LDA at the experimental lattice constant which is larger than the LDA equilibrium lattice constant. Another noteworthy feature in the dispersion curves for $Pd_{0.28}Fe_{0.72}$ is that, near the zone edge, a splitting in the dispersion curves is observed in the longitudinal branch along the [$\zeta$,$\zeta$,$\zeta$] direction. This kind of splitting in the dispersion curves is a typical feature of strong force constant disorder and is seen in the past for some other alloys too [91]. However,

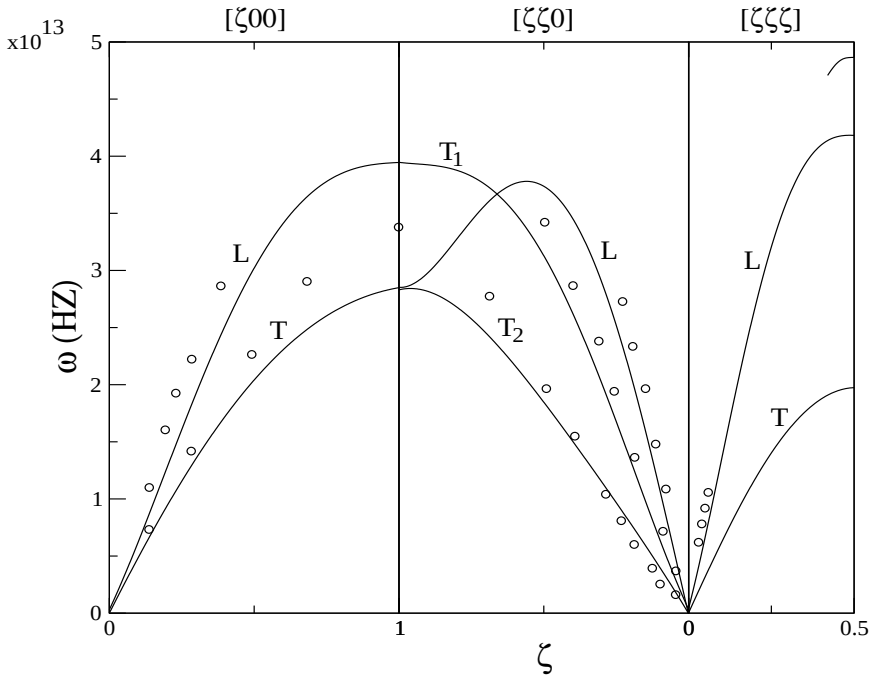


FIGURE 4.4: Dispersion curves (frequency $\omega$ vs reduced wave vector $\zeta$) ; $\zeta = \frac{|\vec{q}|}{|\vec{q}_{max}|}, \vec{q}$ the phonon wave-vector; for $Pd_{0.28}Fe_{0.72}$ calculated in the ICPA (solid lines) with the force constants obtained at the alloy bond length (5.019 a.u.) using 'bond stiffness vs bond length' method. The circles are the experimental data.

experimental data for high wavevectors are not available for confirmation.

The overall results, therefore, show that the phonon frequencies calculated by a combination of the TFC model and the ICPA agree well with the experimental results for both Pd-rich and Fe-rich alloys. To further validate the approach, we present results for elastic constants in Table 4.4. A comparison with the experimental results and our earlier calculations with empirical force constants is also done. The results show an overall improvement of all the elastic constants calculated in the present approach as compared to the approach with empirical force constants for $Pd_{0.96}Fe_{0.04}$ and $Pd_{0.9}Fe_{0.1}$. The calculated elastic constants for $Pd_{0.28}Fe_{0.72}$ have excellent agreement with experimental results as well.

#### 4.3.1.2 $\mathbf{Pd_{0.5}Fe_{0.5}}$

The system $Pd_{0.5}Fe_{0.5}$ needs separate attention from the point of view of comparison between experimental and theoretical results. This is because of the fact that, unlike the other systems considered so far, neutron-scattering measurements on this system were done at a high

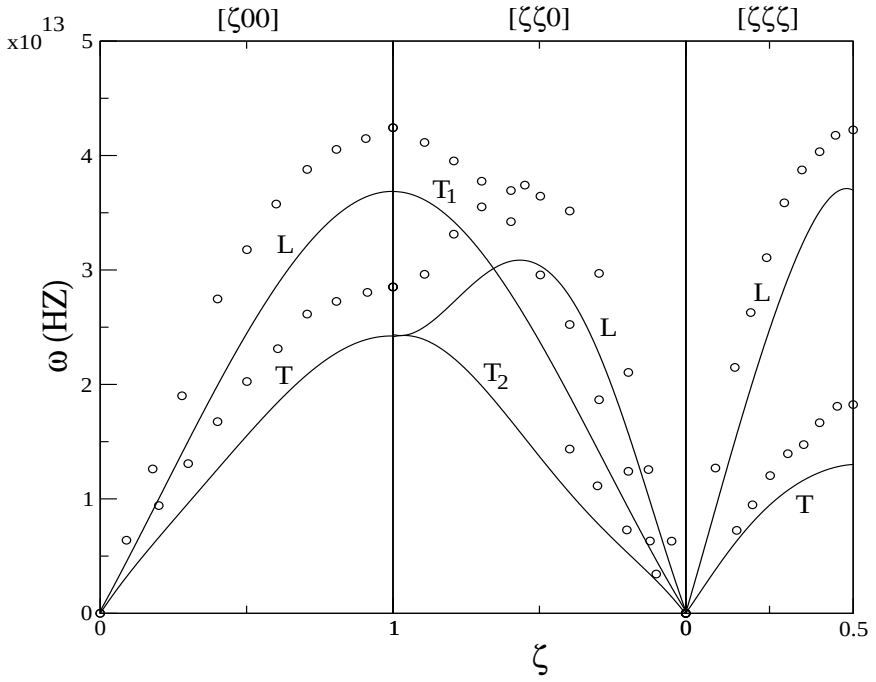


FIGURE 4.5: Dispersion curves (frequency $\omega$ vs reduced wave vector $\zeta$) ; $\zeta = \frac{|\vec{q}|}{|\vec{q}_{max}|}$, $\vec{q}$ the phonon wave-vector; for $Pd_{0.50}Fe_{0.50}$ calculated in the ICPA (solid lines) with the force constants obtained at the $L1_0$ bond length at 860 K(5.25 a.u. for Fe-Fe and Pd-Pd and 5.07 a.u. for Fe-Pd) using 'bond stiffness vs bond length' method. The circles are the experimental data.

TABLE 4.4: Computed elastic constants (in units of Mbar) for $Pd_xFe_{1-x}$.

| System | Elastic constant | TFC | Other method† | Expt. [123, 139] |
|---|---|---|---|---|
| $Pd_{0.96}Fe_{0.04}$ | $C_{11}$ | 2.17 | 1.97 | 2.3 |
| | $C_{12}$ | 1.62 | 1.25 | 1.53 |
| | $C_{44}$ | 1.09 | 1.26 | 0.78 |
| $Pd_{0.90}Fe_{0.10}$ | $C_{11}$ | 2.12 | 2.24 | 2.29 |
| | $C_{12}$ | 1.59 | 1.41 | 1.65 |
| | $C_{44}$ | 1.05 | 1.12 | 0.86 |
| $Pd_{0.28}Fe_{0.72}$ | $C_{11}$ | 1.50 | - | 1.40 ± 0.20 |
| | $C_{12}$ | 1.13 | - | 1.34 ± 0.18 |
| | $C_{44}$ | 0.75 | - | 0.80 ± 0.02 |

† Modeling scheme of chapter 3 of this thesis and Reference [109]

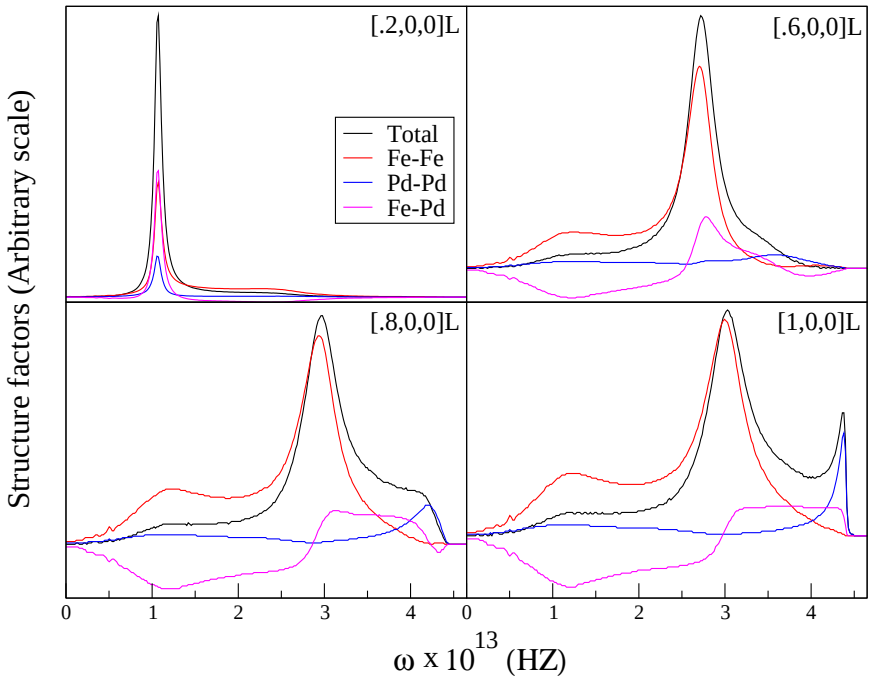


FIGURE 4.6: Partial and total structure factors calculated by the ICPA for various $\zeta$ values in the [$\zeta$,0,0] direction in $Pd_{0.50}Fe_{0.50}$ using the force constants extracted at the disordered alloy bond length (5.12 a.u.). The black lines are the total contributions, the red lines are the Fe-Fe contributions, the blue lines are the Pd-Pd contributions and the magenta lines are the Fe-Pd contributions. All the curves are for longitudinal modes.

temperature. It would, therefore, be interesting to see how far the present TFC model can address the complex interplay of inter-atomic forces between various species pairs since the construction of the TFC model did not take care of temperature effects. As is done in the cases for the alloys at other compositions, we calculate the phonon frequencies by the ICPA using the force constants extracted at the disordered alloy bond length (5.12 a.u.). To understand the contributions of each pair of species towards the normal modes, we look into the partial and the average structure factors. In Fig 4.6, we present results for the structure factors along [$\zeta$,0,0] direction and for the longitudinal branch at some selected $\zeta$ values. No anomalous behavior is observed for low and medium wavevectors for which single distinct peaks in the structure factors are observed. However, for [0.8,0,0] an additional peak begins to appear which is clearly visible at [1,0,0]. This, in turn, means that there would be existence of a split branch along the particular direction in the frequency spectrum. The partial structure factors show that the spurious high frequency peak is due to the Pd-Pd pairs and to a smaller extent due to Fe-Pd pairs. As is mentioned already, the splitting of the high frequency branch is a typical feature of strong force constant disorder and has been reported for some alloys. To

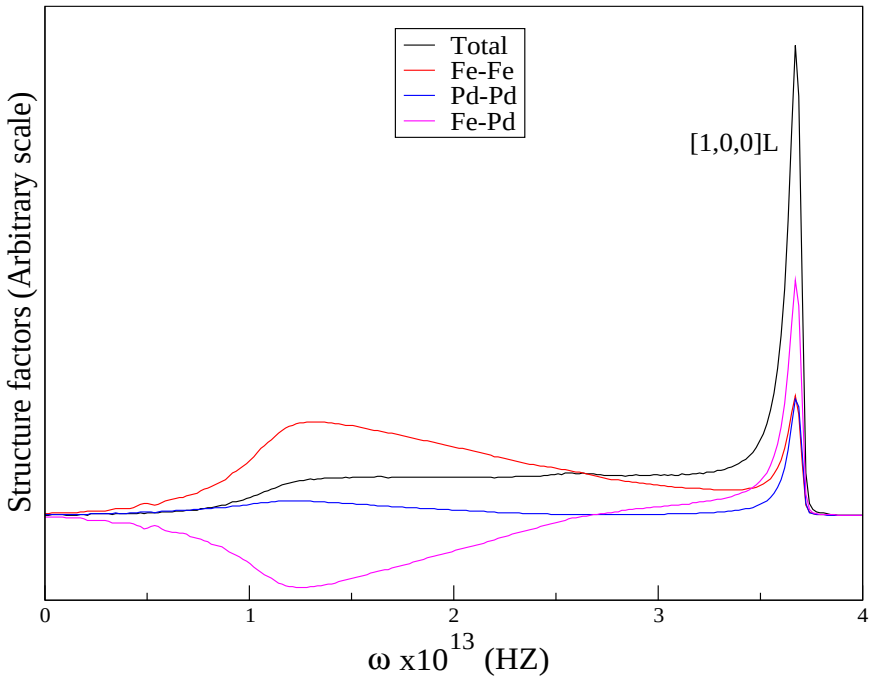


FIGURE 4.7: Partial and total structure factors calculated by the ICPA for $\zeta = 1$ in the [$\zeta$,0,0] direction in $Pd_{0.50}Fe_{0.50}$ with force constants extracted at the $L1_0$ bond lengths. The black lines are the total contributions, the red lines are the Fe-Fe contributions, the blue lines are the Pd-Pd contributions and the magenta lines are the Fe-Pd contributions. All the curves are for longitudinal modes.

understand its origin, we look at the force constants from Table 4.3. It is observed that the Fe-Fe and Fe-Pd force constants differ significantly from Pd-Pd force constants, thereby representing a situation of very strong disorder. We can, therefore, conclude that the strong force constant disorder causes the splitting of the high frequency branch. Since the experimental results [157] do not show any such splitting, these force constants do not represent the correct picture of the microscopic interactions in $Pd_{0.50}Fe_{0.50}$.

In [157], neutron-scattering experiments were done on ordered $L1_0$ FePd at room temperature and at a temperature close to the order-disorder transition. The force constants in the $L1_0$ structures at those temperatures were also extracted by fitting the measured frequencies to a Born-Von Karman model. In [107], the experimental force constants for $L1_0$ structure at 860 K, a temperature close to the order-disorder transition temperature 950 K, were used as the disordered alloy force-constants in the ICPA calculations and the results obtained were in excellent agreement with the experimental observations. It was, therefore, argued that the force constants at 860 K correctly represent the ones of the disordered alloy because of the

fact that, near the order-disorder transition temperature, the ordered and disordered states are expected to be in perfect equilibrium, with the disordered state possessing short-range order. To see whether this was indeed the case, we next use the inter-atomic bond distances of various pairs in the $L1_0$ structure at 860K to extract the fitted force constants. The results along with the ones used in [107] are presented in Table 4.3. It is observed that the Fe-Fe and Pd-Pd bonds soften in comparison to the ones at disordered alloy bond distances, with the Pd-Pd being mostly affected. The Fe-Pd bonds harden because of the shortening of the corresponding bond distances. However, all the bonds are significantly softer than the ones in [107]. To see whether the fitting to the $L1_0$ bond distances get rid of the spurious peak in the structure factors of Fig. 4.6 and thus wash away the split-peak behavior, we plot the structure factors for the [1 0 0] longitudinal branch in Fig. 4.7. Unlike the previous structure factors (Fig. 4.6), no dual peak structures appear in this case. The single high frequency peak is now mostly because of the Fe-Pd contribution; the Fe-Fe and Pd-Pd contributions only add more weights to the single peak. This signifies that Pd-Pd contributions were overestimated whereas the Fe-Pd contributions were grossly underestimated by the calculations at the disordered bond length. The corresponding dispersion curves are presented in Fig. 4.5. The results suggest that the consideration of the $L1_0$ bond distances produce the correct qualitative features as we do not see any peak splitting. Thus, the results *a posteriori* validate the approximation with reference to inter-atomic force constants in [107]. However, the qualitative agreement with the experimental results is far from satisfactory. The calculated frequencies are significantly underestimated in this case. This is a reflection of overall softening of the force constants as discussed above. The reason for this underestimation could be because of the non-incorporation of any temperature effect in the fitting model. This incorporation, however, is a non-trivial task and is beyond the scope of the present context.

### 4.3.2 $Cu_{0.715}Pd_{0.285}$ and $Cu_{0.75}Au_{0.25}$

We discuss our results on $Cu_{0.715}Pd_{0.285}$ and $Cu_{0.75}Au_{0.25}$ in two different subsections. Our calculations of the phonon dispersion relations are compared with the available experimental results. The interpretation of our results and the agreement (discrepancy) with experimental results are done with the help of the coherent scattering structure factors.

TABLE 4.5: Computed stretching ($s$) and bending ($b$) force constants, in units of $dyn/cm$ for $Cu_{0.715}Pd_{0.285}$ using 'bond stiffness vs bond length' approach.

| Pair type | Bond length (au) | s | b |
|---|---|---|---|
| Cu-Cu[a] | 4.9695 | 24610.62 | -1312.64 |
| Pd-Pd[a] | 4.9695 | 67824.28 | -2511.19 |
| Cu-Pd[a] | 4.9695 | 43582.46 | -1803.09 |
| Cu-Cu[b] | 4.989 | 23981.67 | -1289.29 |
| Pd-Pd[b] | 5.10 | 58285.63 | -2372.90 |
| Cu-Pd[b] | 5.037 | 37793.93 | -1528.49 |

[a] No relaxation is considered

[b] Relaxation is incorporated

#### 4.3.2.1 $Cu_{0.715}Pd_{0.285}$

In Fig. 4.8, we present the stretching (s) and bending (b) components of the nearest neighbor force constant tensors for CuPd systems as a function of bond length. The figure illustrates that the linear fitting is appropriate for the present case as the monotonic decrease of the force constants with the increasing bond distances is well captured for all three pairs of inter-atomic force constants. The computed values of correlation coefficients for the straight line fitting of stretching components of the force constant tensors varies between 0.96 to 0.98 which shows the fit to be very good. The fit accuracy for the bending components is, however, a bit low with the calculated correlation coefficient varying between 0.65 to 0.87. This, however, is acceptable, as the bending components of force constant matrices are order of magnitude smaller than the stretching components and therefore, play minimal role in affecting the results. The stretching and bending force constants for the alloy $Cu_{0.715}Pd_{0.285}$ at its experimental bond length, obtained from the fitted results, are presented in Table 4.5. The results show that the Cu-Cu and the Cu-Pd force constants are much softer than that of the Pd-Pd ones, with the Cu-Cu force constants being the softest. This is only to be expected as the equilibrium Pd-Pd bond-length in pure Pd (5.32 a.u.) is significantly larger than that in this alloy, thus making the Pd-Pd bonds stiffer than the other kinds in the alloy environment where the volume available for the Pd atoms is much less compared to pure Pd.

In what follows, we use the transferable force constants of Table 4.5 as inputs to the ICPA

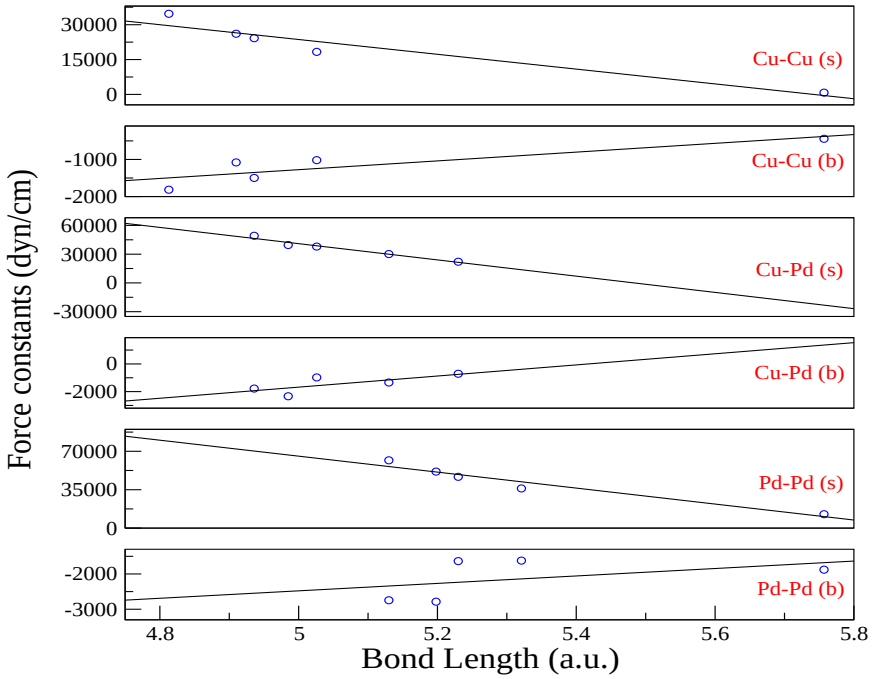


FIGURE 4.8: Nearest neighbor stretching ($s$) and bending ($b$) force constants for $Cu_xPd_{1-x}$ as a function of bond length. The solid lines are the fitted functions whereas the circles correspond to data obtained from *ab initio* calculations on one of a set of structures ($L1_2$ at four different volumes, $L1_0$ at two different volumes, FCC Cu and FCC Pd at two different volumes).

and calculate the phonon dispersion curves for the alloy which are presented in the top panel of Fig 4.9. It can be seen that the calculated and experimental results of phonon frequencies agree reasonably well except near the zone edges where a frequency shift in the dispersion curves is observed in the longitudinal branches along all the symmetry directions. This is a typical resonance-like behavior at around $\nu = 6.65$ THz associated with a large density of states contributed by the Pd atoms. This kind of frequency shift in the dispersion curves, which is altogether absent in the experimental results is generally associated with a very strong force constant disorder and is seen in the past for some other alloys too (for example, Ni-Pt alloy [156]). To find out whether the disorder in the force constants is the possible reason for this anomalous frequency shift obtained from our calculations, we look into the partial and the total structure factors and try to understand the contributions of each pair of species towards the normal modes. In Fig 4.10, we present results for the structure factors along [$\zeta$,0,0] direction and for the longitudinal branch at some selected $\zeta$ values. No anomalous behavior is observed for wave vectors up to $\zeta$=0.7 with a single distinct peak in the structure factors. However, near [0.75,0,0], the peaks due to Cu-Pd and Pd-Pd tend to shift towards higher frequency region, whereas, the Cu-Cu peak remains static at a lower frequency. This

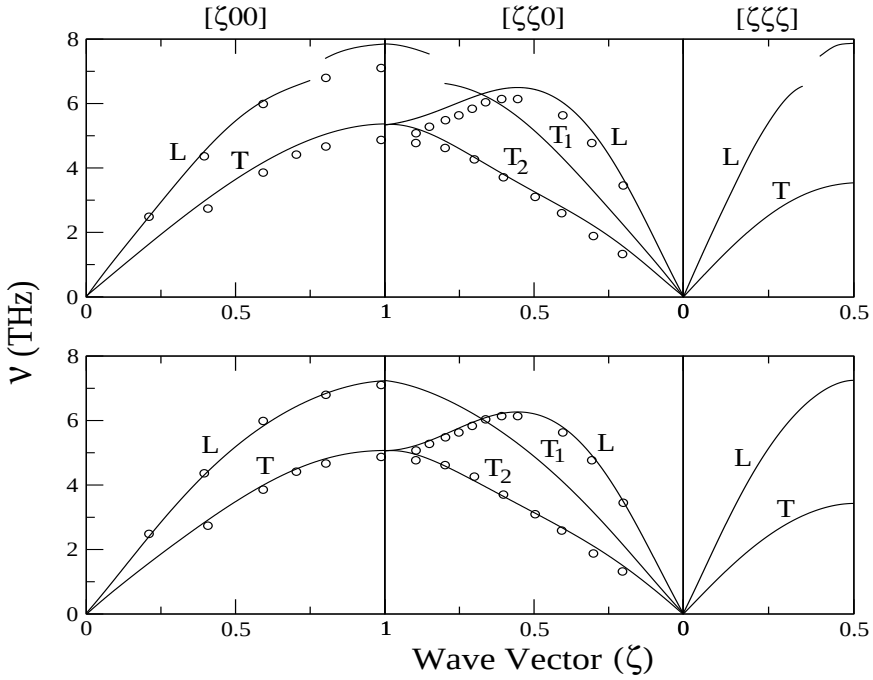


FIGURE 4.9: Dispersion curves (frequency $\nu$ vs reduced wave vector $\zeta$) ; $\zeta = \frac{|\vec{q}|}{|\vec{q}_{max}|}$, $\vec{q}$ the phonon wave-vector; for $Cu_{0.715}Pd_{0.285}$ calculated in the ICPA (solid lines). The upper panel corresponds to the results obtained with the force constants extracted at the alloy bond length (4.9695 a.u.) using 'bond stiffness vs bond length' method while the lower panel corresponds to the results obtained with the force constants extracted at the relaxed bond lengths (mentioned in Table 4.5) using the same method. The circles are the experimental data.

in turn increases the phonon line width and the line becomes gradually asymmetric in shape. This scenario is portrayed more clearly in the structure factors for [0.80,0,0] and [0.90,0,0] where the peak position of the phonon line is shifted to a high frequency value with a small shoulder remaining in the low frequency side which is entirely due to the contribution from the Cu-Cu pair. This behavior must be responsible for the jump in frequency in the phonon dispersion curves near the zone boundary. It can be stated in this context that the peak position at high wave vectors is dominated by Cu-Pd pair with some contribution from Pd-Pd pair which indicates that Cu-Pd and Pd-Pd force constants are overestimated in the present case leading to the anomalous splitting in the dispersion curves. Hence, these set of force constants do not depict the correct nature of bond stiffness's in this alloy. This spurious effect was earlier observed in case of Fe-Pd alloys where an erroneous estimation of inter-atomic force constants in random environment led to anomalous splitting of phonon branches and the origin of such anomaly could be understood based upon an analysis of partial and total structure factors [107, 109].

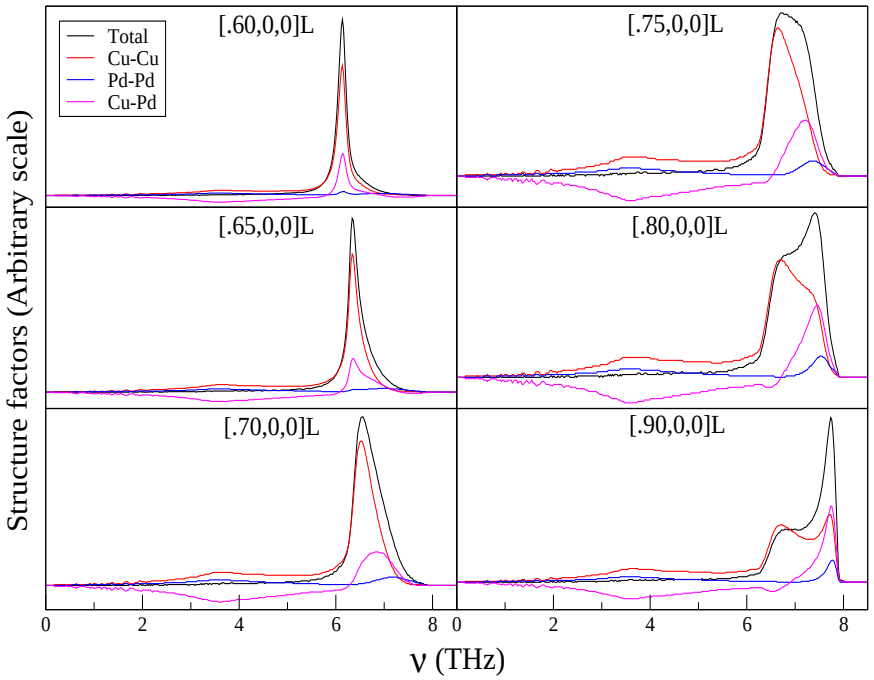


FIGURE 4.10: Partial and total structure factors calculated by the ICPA for various $\zeta$ values in the [$\zeta$,0,0] direction in $Cu_{0.715}Pd_{0.285}$ with force constants calculated at the alloy bond length. The black lines are the total contributions, the red lines are the Cu-Cu contributions, the blue lines are the Pd-Pd contributions and the magenta lines are the Cu-Pd contributions. All the curves are for longitudinal modes.

As already discussed, the size mismatch of the constituent elements should have a significant effect on the vibrational properties of an alloy. As the alloy expands (or contracts) locally on introduction of disorder into the system, the lengths of all chemical bonds decrease (or increase) affecting the stiffness's of the corresponding bonds. For $Cu_{0.715}Pd_{0.285}$, it can be observed from Table 4.1 that there is notable size difference between Cu and Pd in their elemental phases. Therefore, using the force constants for all three types of bonds at the experimental bond length of the alloy, we have neglected the local relaxations around atoms of different sizes forcing over-stiffening of the bonds involved with larger Pd-atoms. Thus, to address the real nature of microscopic interactions among various pairs of species in the alloy, it is essential to incorporate the lattice relaxation effects into our scheme of calculations. In this regard, Mousseau and Thrope had performed a study [159] on bond length distribution associated with a pair of chemical specie with compositions for a number of FCC based binary metallic alloys which included $Cu_xPd_{1-x}$ as well. It had been observed by the authors of Reference [159] that in our coveted alloy, the nearest neighbor bond distances between different pairs of species differ a lot from the average or mean bond distance. We have estimated the

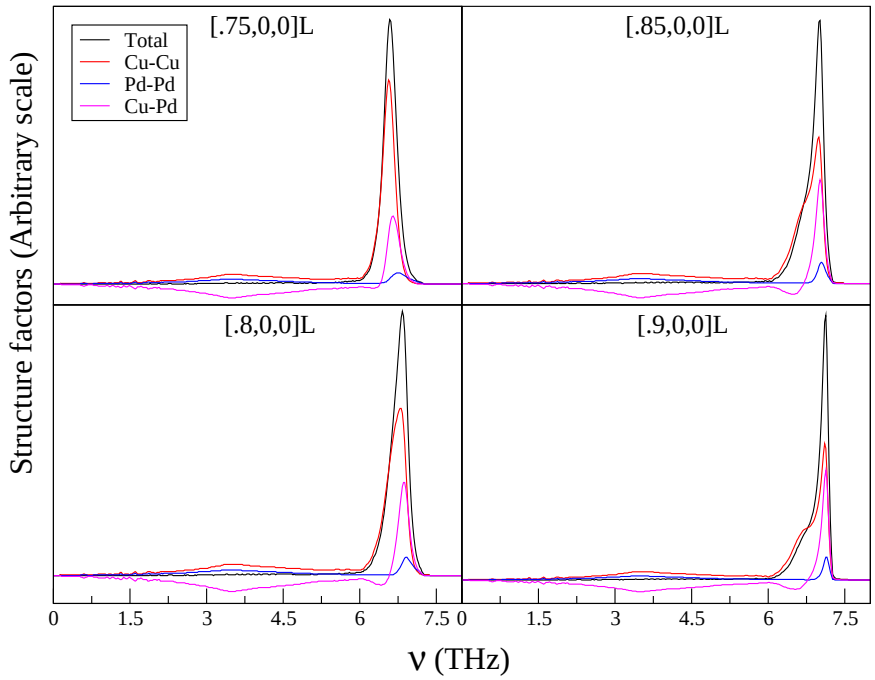


FIGURE 4.11: Partial and total structure factors calculated by the ICPA for various $\zeta$ values in the [$\zeta$,0,0] direction in $Cu_{0.715}Pd_{0.285}$ with force constants calculated at the relaxed bond lengths. The black lines are the total contributions, the red lines are the Cu-Cu contributions, the blue lines are the Pd-Pd contributions and the magenta lines are the Cu-Pd contributions. All the curves are for longitudinal modes.

relative variation of bond lengths for each pair with respect to the mean distance as mentioned in the paper and introduced the same in our calculation. The new relaxed bond lengths are being worked out by incorporating the same relative changes as per the above scheme to our computed mean distance which is about 5.0277 a.u.. The relaxed bond-lengths and the corresponding force constants are presented in Table 4.5 for comparison. It is observed that the bond lengths involving the larger Pd atoms are larger than the average bond length while there is a contraction of the lattice in the neighborhood involving Cu atoms only. Consequently, the Cu-Pd and Pd-Pd force constants reduce by a significant amount compared to the un-relaxed lattice force constants while the Cu-Cu ones remain almost unaltered because of very minimal change in Cu-Cu bond distances with respect to the un-relaxed lattice. This indicates that on incorporation of lattice relaxation into our calculation, the Cu-Pd and Pd-Pd interactions soften noticeably. To see whether this relaxation gets rid of the spurious frequency shift in the phonon dispersion curves, we plot the dispersion curves with the new set of force constants in the bottom panel of Fig 4.9 and the corresponding structure factors in Fig 4.11.

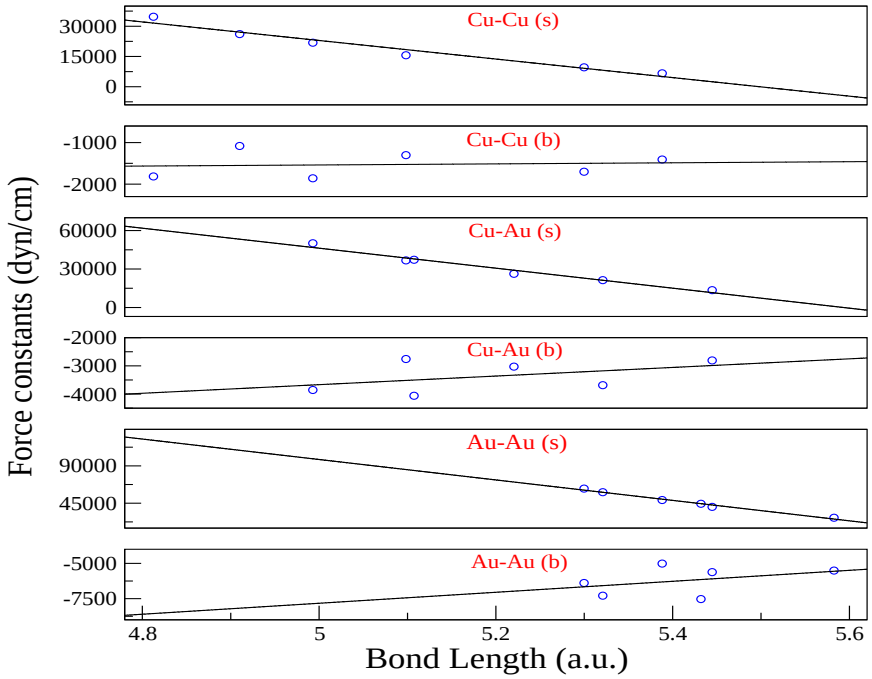


FIGURE 4.12: Nearest neighbor stretching ($s$) and bending ($b$) force constants for $Cu_xAu_{1-x}$ as a function of bond length. The solid lines are the fitted functions whereas the circles correspond to data obtained from *ab initio* calculations on one of a set of structures ($L1_2$ at four different volumes, $L1_0$ at two different volumes, FCC Cu and FCC Au at two different volumes).

The results of phonon frequencies in the bottom panel of Fig 4.9 show that the shift in frequency as observed in the previous case in the top panel of the same figure has disappeared completely and an excellent agreement between the theoretical and the experimental results is obtained. To understand the reason, we look into the partial and total structure factors for the longitudinal branch along [$\zeta$,0,0] direction in Fig 4.11. Here, no sudden shift in the peak position is observed around $\zeta$=0.75 because the peaks in the structure factors from all three pairs of species occur at the same frequency, unlike the case with the un-relaxed lattice where the over-stiffening of the bonds involving Pd atoms shifted the contributions from Cu-Pd and Pd-Pd pairs towards higher frequencies. Hence, we conclude that apart from the mass and the force-constant disorders, the local lattice relaxation and thus the environmental effects play an important role in the $Cu_xPd_{1-x}$ alloy and one must consider it in an appropriate manner to understand the lattice dynamics of the system properly. The first-principles based TFC-ICPA model has, thus, been successful in not only obtaining the accurate dispersion relations but also in interpreting the microscopic picture leading to it.

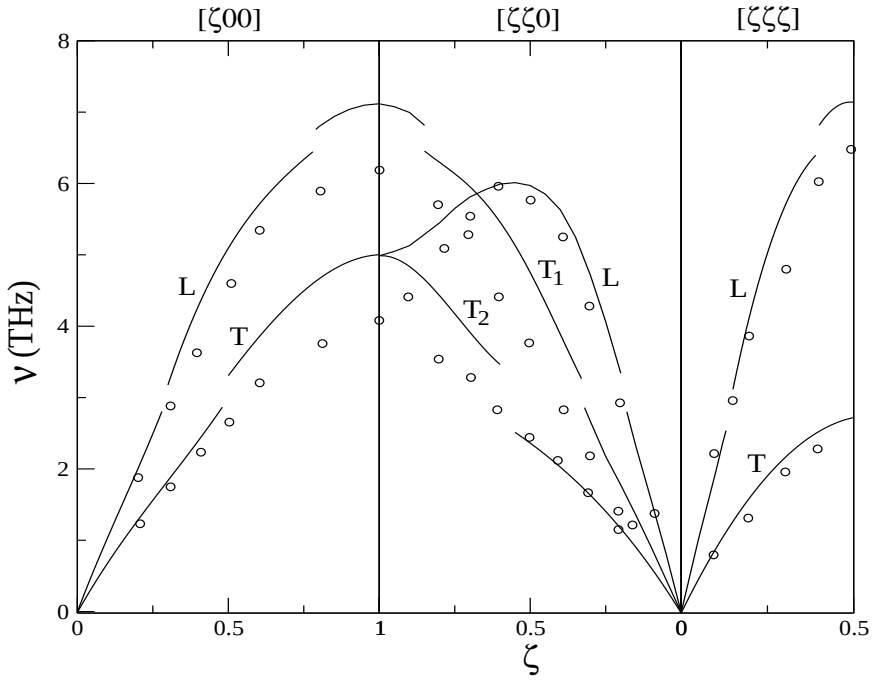


FIGURE 4.13: Dispersion curves (frequency $\nu$ vs reduced wave vector $\zeta$) ; $\zeta = \frac{|\vec{q}|}{|\vec{q}_{max}|}$, $\vec{q}$ the phonon wave-vector; for $Cu_{0.75}Au_{0.25}$ calculated in the ICPA (solid lines) with the force constants obtained at the alloy bond length (5.0098 a.u.) using 'bond stiffness vs bond length' method. The circles are the experimental data.

#### 4.3.2.2 $Cu_{0.75}Au_{0.25}$

Next, we discuss the Cu-Au alloy where several experimental and theoretical investigations [160–162] in the low concentration limits of Au have been reported. Previous studies on this system revealed that the lattice constant changes substantially with changes in compositions which implies a variation in the inter-atomic force constants even between the like atoms in the alloy environment with respect to the pure elements. To begin with, we present in Fig. 4.12, the stretching (s) and bending (b) components of the nearest neighbor force constant tensors for CuAu as a function of bond length. As was the case with the CuPd, the linear fitting is found to be appropriate for the present case. The stretching and bending components of the force constant tensors for the alloy $Cu_{0.75}Au_{0.25}$ at its experimental bond length obtained from the fitted results are presented in Table 4.6. The Au-Au force constants are about 300% larger in magnitude than that of the Cu-Cu ones, whereas, the Cu-Au ones are on an average 100% larger than the corresponding Cu-Cu force constants. This represents a situation of huge mass and force constant disorder and one should anticipate significant effect of these disorders on the phonon dispersion curves. The huge differences in the magnitude of force

constants must be an artifact of forcing the larger Au atoms to vibrate in a lattice much smaller compared to the equilibrium lattice of Au in its elemental phase (bond length=5.58 a.u.). As a result of this, Au-Au bonds get stiffer. The Cu-Cu bond stiffness, on the other hand, do not differ significantly from that found in $Cu_{0.715}Pd_{0.285}$ because of the comparable Cu-Cu bond lengths in both cases. The phonon dispersion curve for the alloy is presented in Fig. 4.13. A resonance behaviour is observed around $\nu = 2.9$ THz for all the branches except the [$\zeta$,$\zeta$,$\zeta$]T branch. In addition to that a secondary resonance is observed around $\nu = 6.65$ THz only along the longitudinal branch for all the symmetry directions. This kind of secondary resonance is previously observed in $Ni_xPt_{1-x}$, characterized by a high density of phonon states near the resonance frequency, and for the similar concentration ratio of larger and smaller atom [156]. However, the experimental results available for the present alloy do not show any signature of resonance like behavior. This is somewhat puzzling as the mass and size ratio between the constituent elements in $Ni_xPt_{1-x}$ is almost identical as that of $Cu_xAu_{1-x}$ alloy and hence, one should expect similar qualitative features in both the alloys. To find out the possible reasons of the discrepancy between the theoretical and the experimental results, we investigate the partial and the total structure factors and analyze the role played by each specie pair towards the normal modes. In Fig. 4.14, we present the structure factors for the longitudinal branch at some relevant reduced wave vectors along [$\zeta$,0,0] direction. The left panel of the figure shows that at $\zeta$=0.25, the contributions to the structure factor from vibrations of all three pairs of atoms occur at same frequency, while at around $\zeta$=0.3 where the first resonance occurs, the contributions from the Cu-Cu pairs to the structure factor start to shift towards higher frequencies compared to the Au-Au and Cu-Au ones, thereby, increasing the phonon line width and producing asymmetric line shapes. At higher wave vectors, we again see a resonance-like behaviour as a result of strong force-constant disorder. The right panel of Fig. 4.14 suggests that for wave vectors beyond $\zeta$=0.75, significant contributions from Cu-Au and Au-Au pairs start to build up at frequencies higher than those where the vibrations from Cu-Cu pairs contribute. This moves the phonon peak positions at higher frequencies as can be clearly be seen by comparing the structure factors at $\zeta$=0.75 and at $\zeta$=0.80. This demonstrates the fact that the overestimations of the Cu-Au and the Au-Au force constants are responsible for this splitting of the dispersion curves at higher frequencies and hence, the force constants extracted at the experimental bond length of the alloy do not represent the correct nature of inter-atomic interactions in this alloy.

There is significant mass and size difference between Cu and Au atoms with the latter

TABLE 4.6: Computed force constants, in units of $dyn/cm$ for $Cu_{0.75}Au_{0.25}$ using 'bond stiffness vs bond length' approach.

| Pair type | Bond length (au) | s | b |
|---|---|---|---|
| Cu-Cu[a] | 5.0098 | 22486.36 | -1537.38 |
| Au-Au[a] | 5.0098 | 96460.75 | -7788.05 |
| Cu-Au[a] | 5.0098 | 45481.08 | -3651.43 |
| Cu-Cu[b] | 5.0065 | 22639.54 | -1537.81 |
| Au-Au[b] | 5.2523 | 66595.32 | -6844.91 |
| Cu-Au[b] | 5.0788 | 40107.48 | -3546.24 |
| Cu-Cu(Expt) | - | 34890.00[c] | -3060.00[c] |
| Au-Au(Expt) | - | 34890.00[c] | -3060.00[c] |
| Cu-Au(Expt) | - | 34890.00[c] | -3060.00[c] |

[a] No relaxation is considered

[b] Relaxation is incorporated

[c] Reference [146]

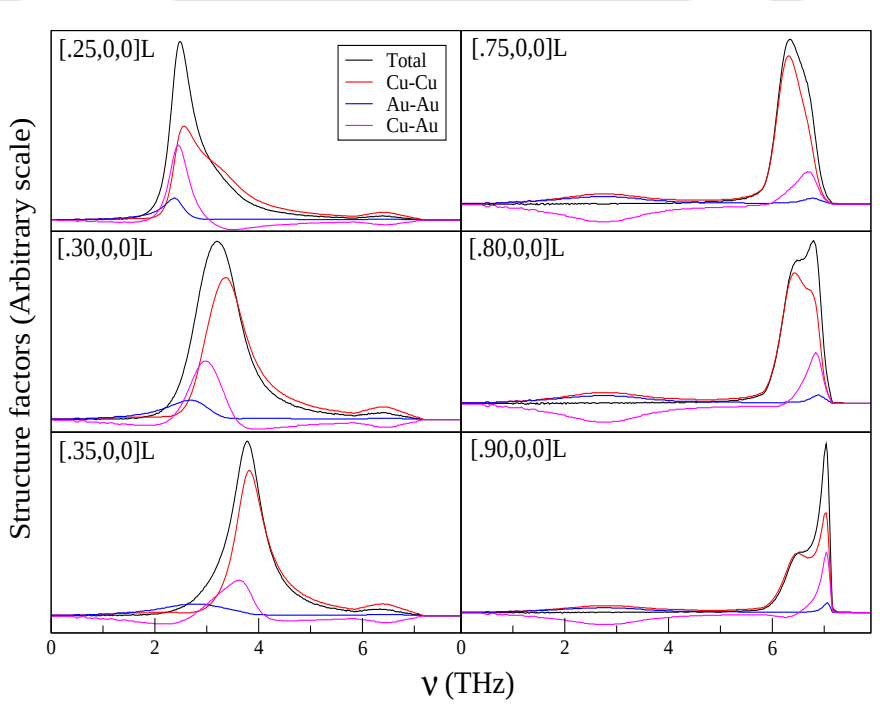


FIGURE 4.14: Partial and total structure factors calculated by the ICPA for various $\zeta$ values in the [$\zeta$,0,0] direction in $Cu_{0.75}Au_{0.25}$ with force constants calculated at the alloy bond length. The black lines are the total contributions, the red lines are the Cu-Cu contributions, the blue lines are the Au-Au contributions and the magenta lines are the Cu-Au contributions. All the curves are for longitudinal modes.

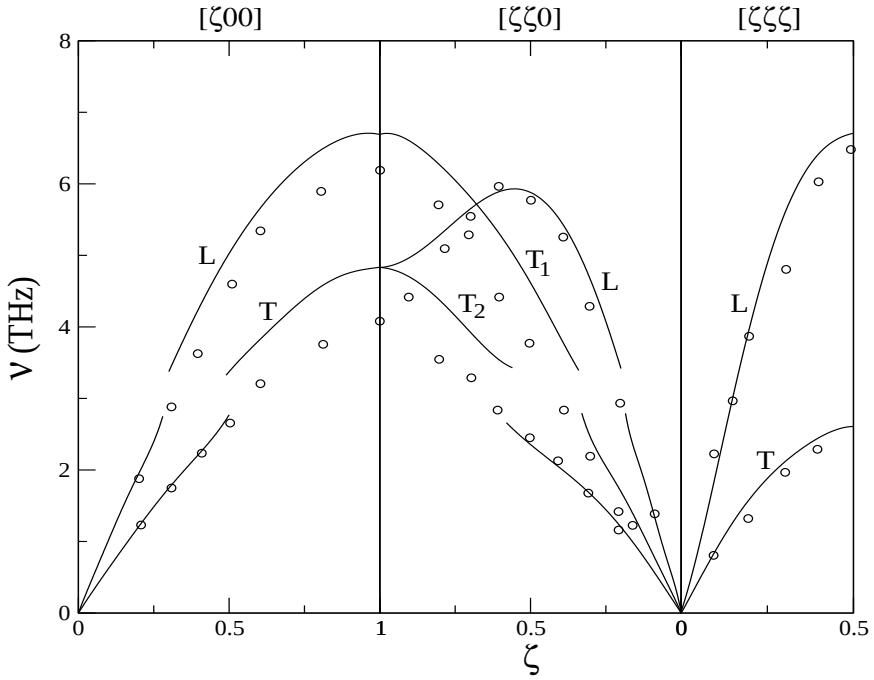


FIGURE 4.15: Dispersion curves (frequency $\nu$ vs reduced wave vector $\zeta$) ; $\zeta = \frac{|\vec{q}|}{|\vec{q}_{max}|}, \vec{q}$ the phonon wave-vector; for $Cu_{0.75}Au_{0.25}$ calculated in the ICPA (solid lines) with the force constants obtained at the new relaxed bond lengths (mentioned in Table 4.6) using 'bond stiffness vs bond length' method. The circles are the experimental data.

being the heavier and larger of the two as can be seen from Table 4.1. This would most obviously result in an enhanced overlap of the heavy Au atoms with their nearest neighbors, because of their larger size and the situation would be vastly different from that of a lattice with identical bond length for all the pairs of species. As a corrective measure, we adopt the same strategy as we have already successfully implemented for Cu-Pd system. Mousseau and Thrope, in their paper have shown the dispersion of bond lengths for various pairs of specie in the $Cu_xAu_{1-x}$ alloy. As is done for the $Cu_{0.715}Pd_{0.285}$ system, we incorporate the relative changes to our theoretically calculated average bond length which is about 5.0788 a.u. and get three distinct bond lengths for the three different pairs of species in the alloy. Force constants corresponding to these new bond lengths are extracted from the fitted relationships of Fig. 4.12 and are presented in Table 4.6. It can be seen that in comparison to the un-relaxed case, the Au-Au and the Cu-Au force constants have been softened by a large amount. On the other hand, the Cu-Cu force constants remains almost unchanged in comparison to the un-relaxed ones, as was the case for the Cu-Pd alloy. To study the effect of the relaxed environment involving the chemical bonds on the phonon spectra, we plot the dispersion

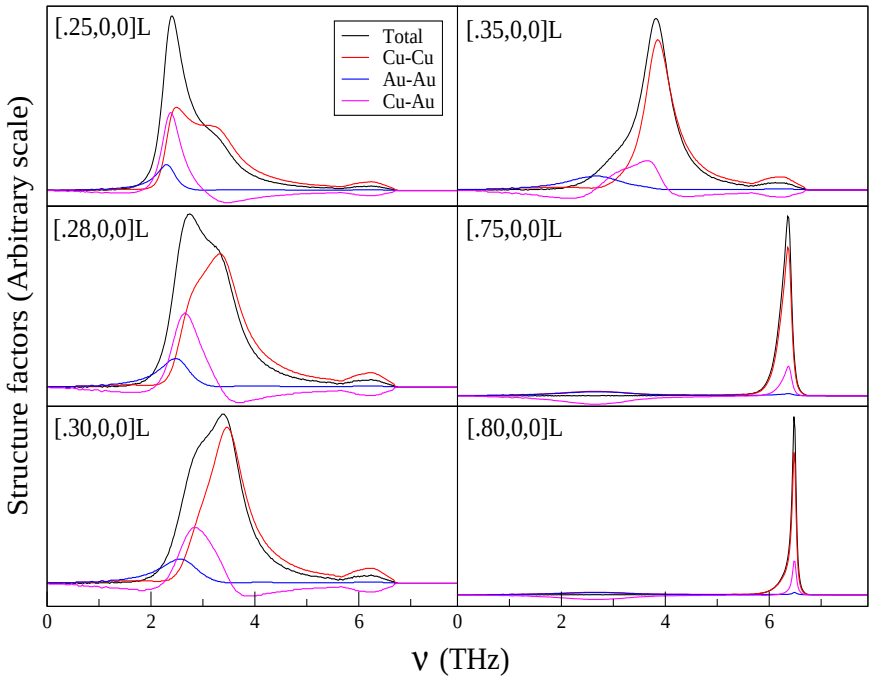


FIGURE 4.16: Partial and total structure factors calculated by the ICPA for various $\zeta$ values in the [$\zeta$,0,0] direction in $Cu_{0.75}Au_{0.25}$ with force constants calculated at the relaxed bond lengths. The black lines are the total contributions, the red lines are the Cu-Cu contributions, the blue lines are the Au-Au contributions and the magenta lines are the Cu-Au contributions. All the curves are for longitudinal modes.

curves obtained with the relaxed force constants in Fig. 4.15. It can be seen that the secondary resonance-like splitting in the dispersion curves has disappeared and that the frequencies near the zone boundary have shifted towards lower values in comparison to the un-relaxed case, thus improving the agreement between theory and experiment. This, thus is an artifact of the softer Cu-Au and Au-Au force constants due to the expansion of bonds associated with the Au atoms. However, the resonance mode at frequency around 2.9 THz still persists along [$\zeta$,0,0] and [$\zeta$,$\zeta$,0] directions, whereas, it is not observable along [$\zeta$,$\zeta$,$\zeta$] direction which indicates a direction dependent resonant behavior. For deeper analysis, we look into the partial and the total structure factors for the longitudinal branch along [$\zeta$,0,0] direction in Fig 4.16. For lower values of $\zeta$ and around the resonance, we see no qualitative difference between the un-relaxed case and the relaxed case. For higher $\zeta$ values, we observe that the contributions from all three pairs occur at the same frequency, unlike the un-relaxed case. These suggest that the resonance-like behavior at higher $\zeta$ values stem from the over-stiffening of the bonds involving bigger Au atoms and that the incorporation of relaxations took care of it. However, the resonance behavior at lower $\zeta$ region has no correlation with the local lattice relaxations.

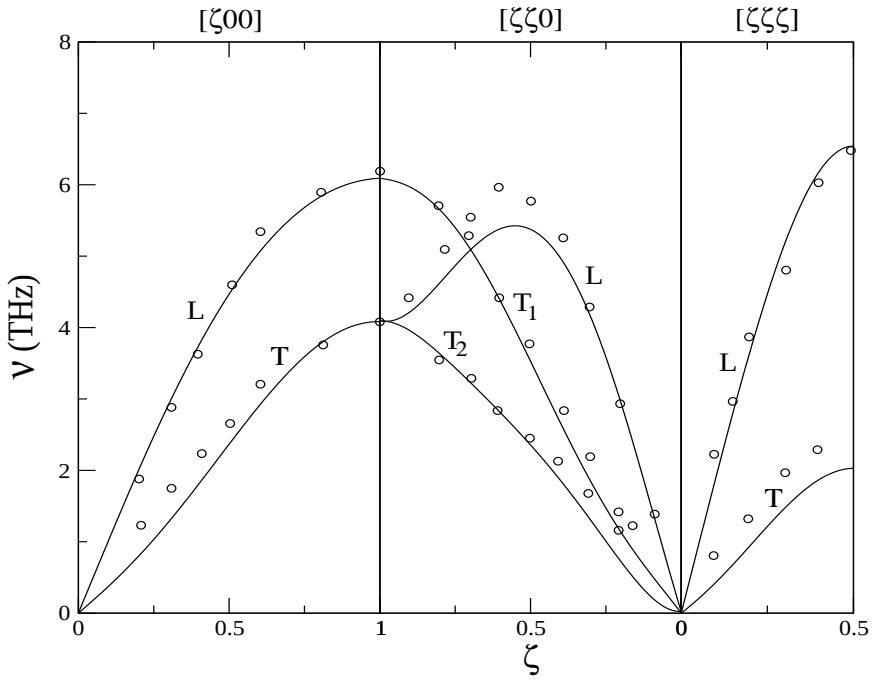


FIGURE 4.17: Dispersion curves (frequency $\nu$ vs reduced wave vector $\zeta$) ; $\zeta = \frac{|\vec{q}|}{|\vec{q}_{max}|}$, $\vec{q}$ the phonon wave-vector; for $Cu_{0.75}Au_{0.25}$ calculated in the VCA (solid lines) with the force constants obtained by fitting experimental frequencies to the Born-von Karman model (mentioned in Table 4.6). The circles are the experimental data.

Thus, in spite of the incorporation of bond relaxations improving the agreement between theoretically calculated and experimentally observed phonon dispersion curves, the qualitative difference because of the existence of a resonance mode at around $\nu = 2.9$ THz is still an enigma that has to be resolved. Katano *et al.* in Ref. [146] had performed a fourth neighbor Born-von Karman fit to the experimentally measured phonon frequencies and extracted the inter-atomic force constants. Surprisingly, they achieved an excellent fit to the experimental results using this model which only assumes an average rigid lattice and neglect any mass and force-constant fluctuations. This was quite a puzzle because it suggested that the large mass and size ratio had little effect on the phonon frequencies. In an attempt to solve the above puzzle, we have carried out calculations with the Coherent potential approximation (CPA) and the Virtual crystal approximation (VCA) using force constants as reported by Katano *et al.* [146] in both calculations. Our motivation behind this is to systematically explore the effect of each type of disorder on phonon spectra starting from the average lattice (no disorder) and thus understand the reason behind the success of the 'average lattice model' for a system supposed to have strong disorders in mass, force-constants and environment. The

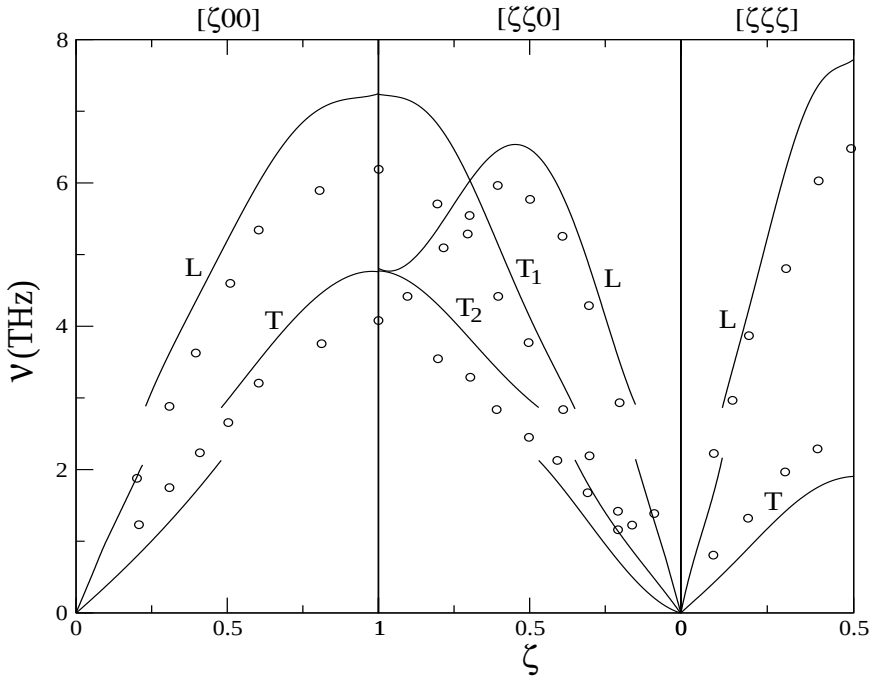


FIGURE 4.18: Dispersion curves (frequency $\nu$ vs reduced wave vector $\zeta$) ; $\zeta = \frac{|\vec{q}|}{|\vec{q}_{max}|}$, $\vec{q}$ the phonon wave-vector; for $Cu_{0.75}Au_{0.25}$ calculated in the CPA (solid lines) with the force constants obtained by fitting experimental frequencies to the Born-von Karman model (mentioned in Table 4.6). The circles are the experimental data.

force constants for the nearest neighbors as obtained by the fit to the experimental frequency is listed in Table 4.6 for comparison. Fig. 4.17 shows that an excellent agreement between theory and experiment for all the symmetry directions is achieved using the VCA. However, the same qualitative disagreement between the theory and the experimental results that was observed in case with mass and force-constant disorders on a relaxed lattice (Fig. 4.15) persists in case of calculations with the CPA as well, shown in Fig. 4.18. Quantitatively, the results with the CPA are far worse than those obtained with the ICPA on a relaxed lattice. In the long wave length region, the CPA calculated frequencies are substantially underestimated in comparison to the experimentally observed values, whereas, for high wave vectors the calculated frequencies are significantly overestimated in comparison to the experimental ones. This result, thus, suggests that both the mass and the force-constant disorder have significant role in the lattice dynamics in this system and thus, neglecting any one of them would provide a qualitatively wrong picture of the microscopic physics. This can be realized more clearly from CPA results. For high wave vectors and thus higher frequencies, the normal modes would be dominated by the vibrations of lighter Cu atoms. For low wave vectors and lower frequencies, heavier Au

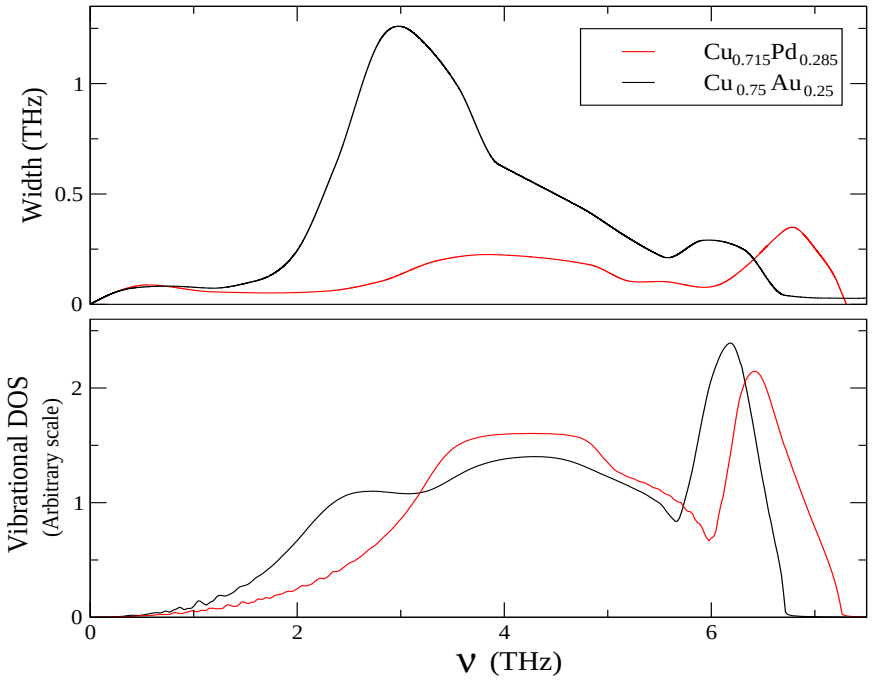


FIGURE 4.19: Top panel shows the disorder-induced widths in $Cu_{0.75}Au_{0.25}$ (black line) and in $Cu_{0.715}Pd_{0.285}$ (red line) along [$\zeta$,0,0] direction for the longitudinal branch calculated in the ICPA using the force constants obtained at their respective relaxed bond lengths. The corresponding vibrational densities of states for $Cu_{0.75}Au_{0.25}$ (black line) and $Cu_{0.715}Pd_{0.285}$ (red line) are presented in the bottom panel.

atoms will contribute most towards the normal modes. The average force constants used in the CPA calculations are way too large compared to the Cu-Cu force constants obtained by the TFC upon considering local lattice relaxations. This, therefore, pushes the frequencies further up at higher wave vectors. On the other hand, the Au-Au force constants obtained by the TFC incorporating relaxations are much larger than the average force constants. Thus, in the low wave-vector region, the CPA calculated frequencies are pulled down. In the VCA or the average lattice model, the average mass used, is higher (lower) than the mass of Cu (Au). A higher (lower) mass in the high (low) wave-vector region, in comparison to the CPA, compensates for the stiffer (softer) bonds, and thus pulls the frequencies down (up) making a perfect agreement with the experiments. This points to the fact that the error introduced due to consideration of an average mass is compensated by the erroneous set of force constants; a classic case of cancellation of errors leading to perfect agreement with experiments.

These results, thus, clearly show that the mass disorder, the force-constant disorder and the local lattice relaxations, together make up the phonon dispersions in this alloy, being

correctly addressed by the first-principles based DFPT-TFC-ICPA method and that the non-appearance of the resonance mode in the experiments could be due to the limitations in the measurements. These propositions have solid grounds because of the fact that similar branch dependent resonance modes have been experimentally observed for $Cu_{0.97}Au_{0.03}$ [161] and $Cu_{0.91}Au_{0.09}$ [160]. Large values of natural line widths which contain information about the disorder effects were observed in these systems around the resonance frequency. A mass-disorder only theory for impurities, although worked reasonably well for $Cu_{0.97}Au_{0.03}$, failed to explain the frequency shifts and large disorder-induced widths near the resonance frequency [160], thus indicating that the fluctuations in force-constant are a must to understand the phonon spectra in these alloys. Thus, the resonance behavior in $Cu_{0.75}Au_{0.25}$ is expected. To further validate our arguments, we have calculated the disorder-induced widths. Results for the longitudinal branch along [$\zeta$,0,0] direction for $Cu_{0.75}Au_{0.25}$ are shown in the top panel of Fig. 4.19. Results for the $Cu_{0.715}Pd_{0.285}$ system are also shown for comparison. The behavior of the widths are similar for other directions and thus we refrain from showing them. It can be seen in Fig. 4.19 that at around $\nu = 2.9$ THz, an anomalously large width is observed in case of $Cu_{0.75}Au_{0.25}$ , coinciding with the region where the resonance occurs. No such anomalously large width is obtained for $Cu_{0.715}Pd_{0.285}$ which indicates the absence of a resonance mode. That this anomalously large width is indeed a signature of the resonance mode is further reinforced by the results on the vibrational densities of states. In case of alloys made up by the heavier impurity in a lighter host, the states with lower frequencies are dominated by the heavier atoms which gradually merge with the main host band. However, the occurrence of resonance in such alloys is marked by a large densities of states of the heavier atoms near the resonance frequencies and subsequent decay of the states into the main host band. This extra scattering induced by the impurity atoms in the host band produces a large width near the resonance frequency. The bottom panel of Fig. 4.19 shows the vibrational densities of states of these two systems under considerations. Around the resonance frequency according to our calculations, the $Cu_{0.75}Au_{0.25}$ system has larger densities of states as compared to that of $Cu_{0.715}Pd_{0.285}$. The large contributions are all due to the heavier Au states which form a broad peak between 2.5 and 3 THz before decaying into the host Cu band. Such a phenomenon has been observed in the past for $Ni_xPt_{1-x}$ alloys [156], a system with similar degree of mass and force-constant disorder as $Cu_{0.75}Au_{0.25}$. In case of $Cu_{0.715}Pd_{0.285}$ alloy, we do not observe any broad peak in the densities of states in the low-frequency part of the spectrum and the densities of states curve looks more like that of pure Cu. The absence of any such peak in the vibrational densities of states along with the absence of an anomalously large line width

in the low-frequency part of the spectrum in $Cu_{0.715}Pd_{0.285}$ can be attributed to the lesser mass and size ratio of the constituents in this alloy compared to that in $Cu_{0.75}Au_{0.25}$ and is the reason behind the qualitative differences in the phonon dispersion relations between these two systems.

### 4.3.3 $Ni_xPt_{1-x}$ for $x = 0.95, 0.70, 0.50$ and $0.25$

In this work, we have computed the phonon dispersions in $Ni_{0.95}Pt_{0.05}$, $Ni_{0.70}Pt_{0.30}$, $Ni_{0.50}Pt_{0.50}$ and $Ni_{0.25}Pt_{0.75}$ for which inelastic neutron scattering results are available [156]. Fig. 4.20 presents the stretching ($s$) and bending ($b$) components of the nearest neighbor force constant tensor for the alloy $Ni_xPt_{1-x}$ as a function of $x$, computed by the DFPT-TFC method. The results show that for systems with high Ni concentration, namely x = 0.95 and 0.70 (x is the Ni concentration in the alloy), the Pt-Pt bonds are stiffer by an order of magnitude than that of the Ni-Ni and Ni-Pt ones, with the Ni-Ni bonds being the softest. The huge differences in the stiffnesses of the bonds are artifact of forcing the larger Pt atoms to vibrate in a lattice much smaller compared to the equilibrium lattice of Pt in its elemental phase. With increase in Pt concentration in the alloy, all three bonds soften with Pt-Pt being the most affected. This is expected as the atoms now have an expanded lattice and considerably larger bond distances. The effect on Pt-Pt pairs is larger than the other pairs due to the fact that with decreasing $x$, the bond distances tend to get closer to the Pt-Pt bond distances in it's elemental phase. The bending components of the force-constant tensors do not vary significantly with $x$, in comparison to the stretching components and they being order of magnitude smaller than the stretching components, are expected to play little role in affecting the lattice dynamics. In what follows, we use these set of force constants as inputs to the ICPA and calculate the phonon dispersions for the alloy. We discuss our results for each composition in different subsections.

#### 4.3.3.1 $Ni_{0.95}Pt_{0.05}$

The results obtained for the dispersion curves along all the symmetry directions are shown in Fig. 4.21(a). The calculated and the experimental results of phonon frequencies agree reasonably well both qualitatively and quantitatively along [$\zeta$,0,0] direction where the resonance behavior, observed experimentally around a frequency of 3.3 THz is well reproduced by our

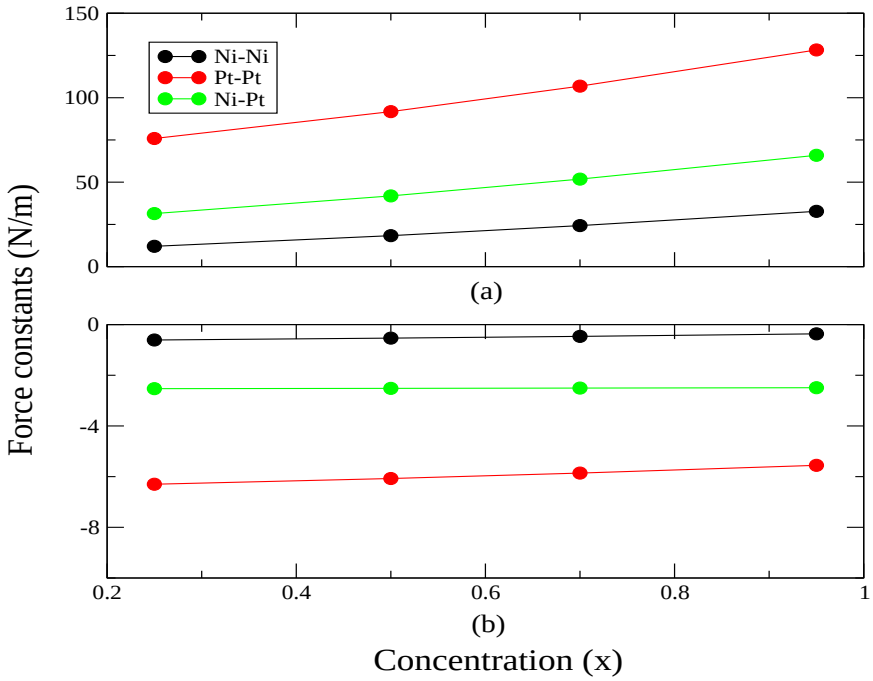


FIGURE 4.20: Nearest neighbor (a) stretching and (b) bending force constants for $Ni_xPt_{1-x}$ as a function of $x$, the Ni concentration. The force constants are computed by the DFPT-TFC method with *ab initio* calculations performed on a set of structures ($L1_2$ at four different volumes, $L1_0$ at two different volumes, FCC Ni and FCC Pt at two different volumes).

calculations. However, the resonance mode along [$\zeta$,$\zeta$,0] direction can only be observed for $T_2$ branch, whereas, it is not at all observable along [$\zeta$,$\zeta$,$\zeta$] direction where no experimental data is available for comparison. Around the resonance frequency which corresponds to $\zeta$=0.23 for the [$\zeta$,0,0]L branch and to $\zeta$=0.37 for the [$\zeta$,0,0]T branch, we observe a frequency shift in the dispersion curves. This kind of frequency shift in the dispersion curves is generally associated with a strong force constant disorder which holds true for the present system. To find out whether the disorder in the force constants is the possible reason for this anomalous frequency shift obtained from our calculations, we look into the partial and the total structure factors. In Fig. 4.22, we present results for the partial and the total coherent scattering structure factors along [$\zeta$,0,0] direction and for the transverse branch at some selected $\zeta$ values. We find that the Ni-Ni pairs contributed the most to the structure factors while there are small but significant contributions from the Ni-Pt pairs around the wave vectors near resonance which die down gradually with increasing $\zeta$. This corroborates the assumption of Tsunoda *et al.* [156] that the lower value of the resonance frequency obtained from the calculations by the mass-disordered CPA, in comparison to the experimentally measured one, is due to the larger

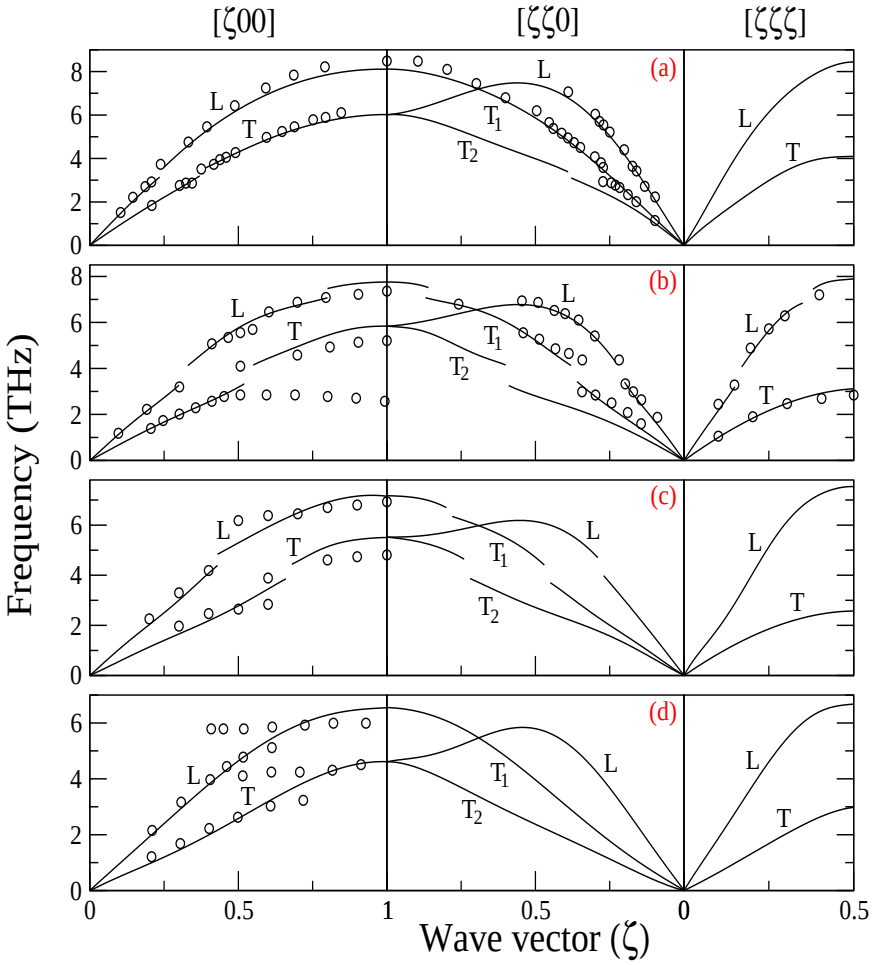


FIGURE 4.21: Dispersion curves (frequency $\omega$ vs reduced wave vector $\zeta$) ; $\zeta = \frac{|\vec{q}|}{|\vec{q}_{max}|}$, $\vec{q}$ the phonon wave-vector; for $Ni_xPt_{1-x}$ (where, (a) x=0.95, (b) x=0.70, (c) x=0.50 and (d) x=0.25) calculated in the ICPA (solid lines) with the force constants obtained by the DFPT-TFC method [109, 137]. The circles are the experimental data of Reference [156].

value of the Ni-Pt force constants than the Ni-Ni ones. Our computations of the structure factors show that indeed the Ni-Pt pairs contribute to the structure factors near resonance. This finding, together with the results on the force constants from Fig. 4.20, demonstrates that the resonance frequency is influenced by the vibrations of the Ni-Pt pairs. From Fig. 4.22, it is observed that at $\zeta = 0.3$, the peaks due to Ni-Ni and Ni-Pt contributions occur at the same frequency. However, at $\zeta = 0.35$, the peak due to the contributions from the Ni-Ni pairs tends to shift towards higher frequency compared to the Ni-Pt one, making the spectral lines wide and effecting a split in the phonon branches. However, since the alloy is Ni-rich, the effect is not much pronounced. That this behavior signifies resonance due to the vibrations of Pt atoms is demonstrated by the disorder-induced widths as shown in Fig. 4.23(a). Fig. 4.23(a) suggests

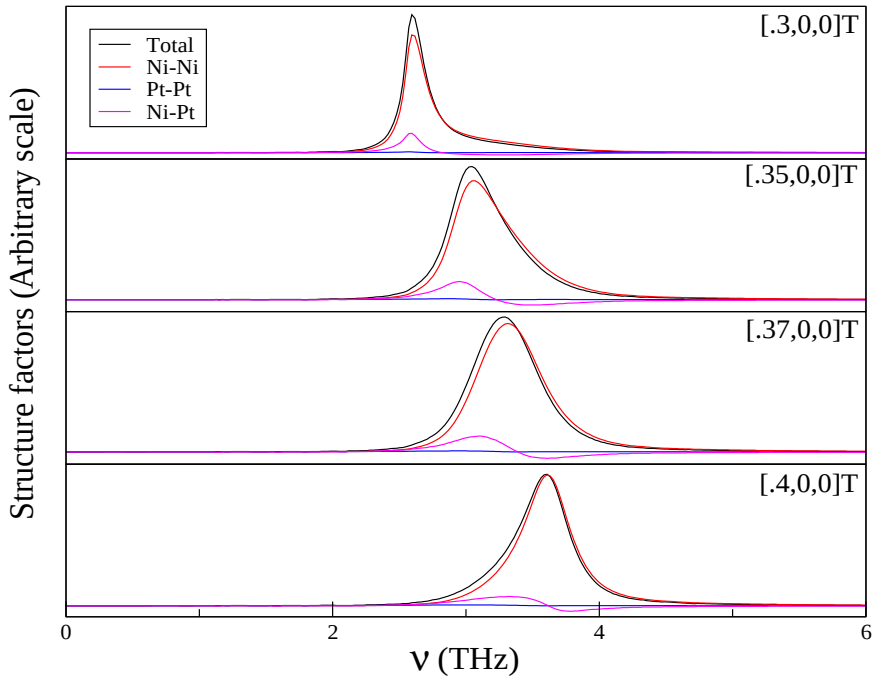


FIGURE 4.22: Partial and total structure factors calculated by the DFPT-TFC-ICPA method for various $\zeta$ values in the [$\zeta$,0,0] direction in $Ni_{0.95}Pt_{0.05}$. The black lines are the total contributions, the red lines are the Ni-Ni contributions, the blue lines are the Pt-Pt contributions and the magenta lines are the Ni-Pt contributions. All the curves are for transverse modes.

that there is an anomalously large width at $\zeta$=0.24 for the longitudinal branch, and at $\zeta$ = 0.36 for the transverse branch. These wave vectors correspond to the regions where resonance occurs. Such anomalously large widths near the resonance frequencies have also been observed experimentally for $Cu_{0.97}Au_{0.03}$ and $Cu_{0.91}Au_{0.09}$ alloys [160–162]. These anomalously large widths at a particular wave vector or frequency denote smaller phonon life-times and are due to the metastable phonon modes of Pt impurities in the main Ni band as is demonstrated by the contributions of the Ni-Pt pairs to the structure factors near the resonance frequency and their subsequent decay with increasing phonon energy. A noteworthy difference between our computed line shapes and the experimental ones is the absence of double peak structures in the line shapes from our calculations. The experimental line shapes near the resonance frequencies had double peak structures, although one of the peaks was always much less intense compared to the main one. The absence of this secondary peak in the structure factors computed by us could be due to the fact that we have weighted the line shapes by the corresponding coherent scattering lengths resulting in the redistribution of weights. In spite of these qualitative differences, there is excellent agreement between the experiment and theory regarding the resonance frequency and qualitative features of the dispersion curves.

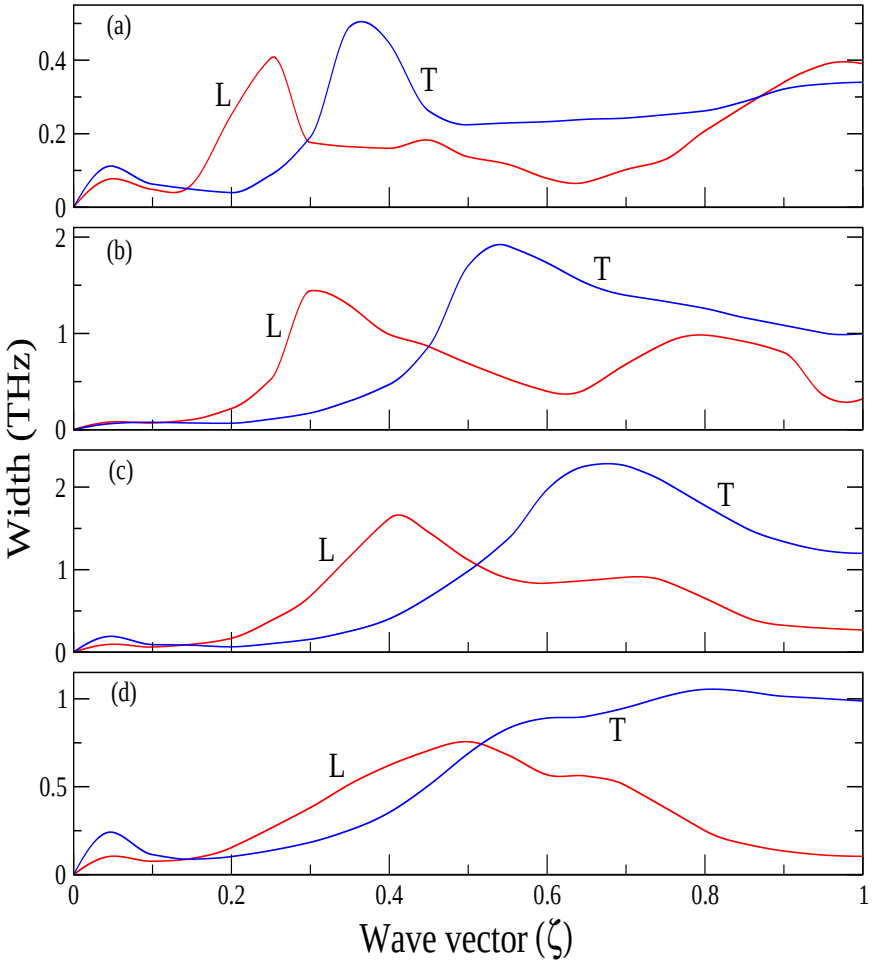


FIGURE 4.23: Disorder-induced widths in $Ni_xPt_{1-x}$ (where, (a) x=0.95, (b) x=0.70, (c) x=0.50 and (d) x=0.25) along [$\zeta$,0,0] direction for both the longitudinal (red line) and the transverse (blue line) branches calculated by the DFPT-TFC-ICPA method.

#### 4.3.3.2 $Ni_{0.70}Pt_{0.30}$

In Fig. 4.21(b), we present our computed dispersion curves for all symmetry directions and compare with the experiments. The qualitative features of dispersion curves agree reasonably well with experiments except that the double peaks in the region from $\zeta$=0.4 to the zone boundary observed experimentally for the [$\zeta$,0,0]T branch are missing in our results. It is to be noted that the peaks at the higher frequency observed experimentally [156] are rather poorly defined and have very large widths. The CPA calculations by Tsunoda also reproduced the double peak structures in the line shapes. However, a double peak structure in the CPA is only natural because non-consideration of variations in the force-constants between different pairs of species may effect a separation of bands associated with the two constituents having

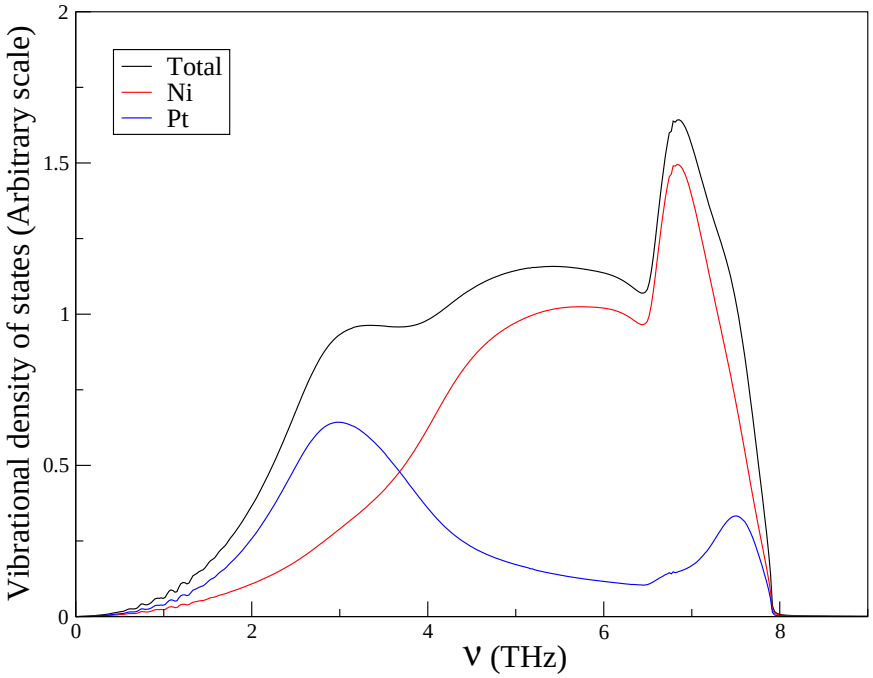


FIGURE 4.24: Vibrational densities of states for $Ni_{0.70}Pt_{0.30}$ calculated by the DFPT-TFC-ICPA method.

a large mass difference, giving rise to two well separated peaks in the line shapes as seen in Ref. [91]. Thus, a double peak structure of the line shapes obtained from the experiments for the transverse branches could be an artifact of the limitations in the experimental setup. The resonance behavior is found to be more pronounced in this sample as compared to $Ni_{0.95}Pt_{0.05}$. Fig. 4.21(b) shows a splitting in the dispersion curves at $\nu \approx 3.5$ THz for all the branches except the [$\zeta$,$\zeta$,$\zeta$]T branch which, as in the experimental results, does not show any anomalous feature. This resonance frequency is in perfect agreement with the experimental results for the transverse branches, whereas, the resonance behavior for the longitudinal branches were observed experimentally at a slightly higher frequency which is approximately 4.0 THz. In addition, a secondary splitting is observed near $\nu \approx 7.05$ THz for [$\zeta$,0,0]L, [$\zeta$,$\zeta$,0]$T_1$ and [$\zeta$,$\zeta$,$\zeta$]L branches, although the experimental results show this additional feature only for the [$\zeta$,0,0]L direction and at a frequency around 6.0 THz which is considerably lower than the theoretically calculated value. Such a secondary resonance is due to extra scattering induced by impurity at higher frequencies causing resonance modes to decay into the host phonon density of states and hence increasing the line widths. To interpret the underlying mechanism of secondary resonance more clearly, we present the partial and the total vibrational densities of states in Fig. 4.24. The plot indicates a maximum for Pt densities of states at $\nu$=3.0 THz

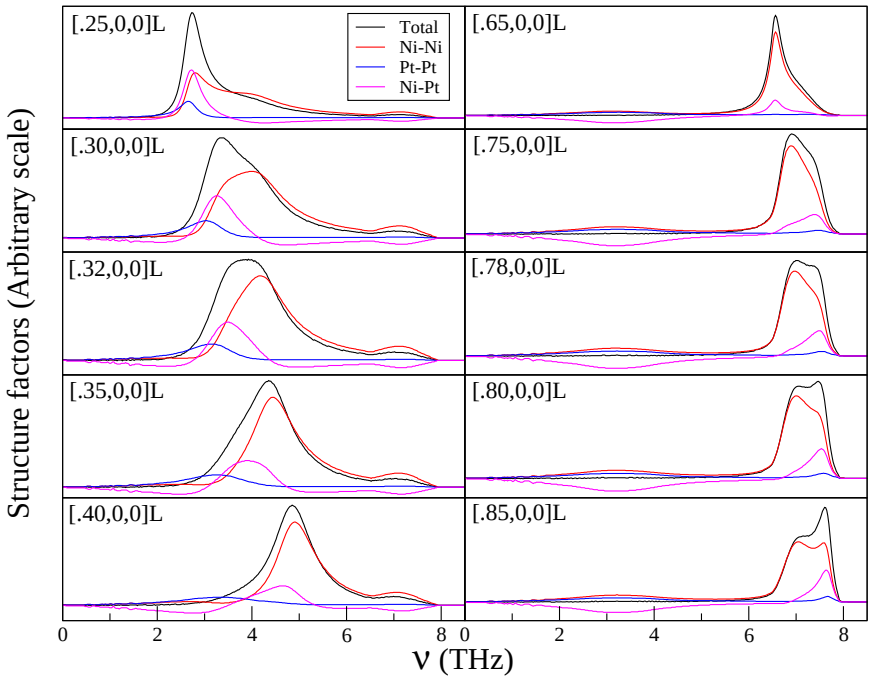


FIGURE 4.25: Partial and total structure factors calculated by the DFPT-TFC-ICPA method for various $\zeta$ values in the [$\zeta$,0,0] direction in $Ni_{0.70}Pt_{0.30}$. The black lines are the total contributions, the red lines are the Ni-Ni contributions, the blue lines are the Pt-Pt contributions and the magenta lines are the Ni-Pt contributions. All the curves are for longitudinal modes.

which in addition shows a second maximum at $\nu$=7.4 THz. This 2nd maximum in the densities of states for impurity Pt in the high frequency region is responsible for the occurrence of secondary resonance. Since it occurs at a frequency much higher in magnitude than the maximum frequency of the transverse branches, hence, we do not see any secondary resonance for this branch. This anomalous phenomena of secondary resonance can also be extracted from the disorder-induced-widths shown in Fig. 4.23(b). The results show large widths at $\zeta \approx 0.30$ and $\zeta \approx 0.78$ for the longitudinal branch, whereas, it is observed only once and at $\zeta = 0.52$ for the transverse branch. The position of the peaks coincide with the regions around which resonance occurs along [$\zeta$,0,0] direction.

For a deeper analysis about the contribution of each specie pair towards normal modes of vibrations and to explain the discrepancies between theoretical and experimental results regarding the frequency of the secondary resonance, we look into the partial and the total structure factors for the longitudinal branch along [$\zeta$,0,0] direction in Fig. 4.25. Unlike in $Ni_{0.95}Pt_{0.05}$, it can be seen that the Pt-Pt pairs have significant contributions in this case at low wave vectors along with the Ni-Pt contribution. At $\zeta$=0.25, contributions from all three pairs

have peaks at the same frequency. However, at $\zeta \approx 0.30$ where the first resonance occurs, the peak due to the contributions from the Ni-Ni pairs to the structure factor starts to shift towards higher frequencies compared to the other pairs, thereby increasing the phonon line width. This is visible more clearly at $\zeta$=0.32, where we see that the peak for the total structure factor has been rather flat. The right panel of Fig. 4.25 suggests that for $\zeta \approx 0.75$, the phonon line shape begins to be asymmetric in shape. This happens because of sudden shift of Ni-Pt peak towards high frequency side as compared to that of Ni-Ni peak which, as a result, tends to shift the peak of the total structure factor to a high frequency. This feature demonstrates two things: first, the Ni-Pt pairs play an increasingly important role in the phonon dispersion relations and thus a theory like the CPA which does not take into account the dispersion in the force constants between different specie pair cannot explain the anomalous features in an alloy like the present one, and second, the discrepancy between our results and the experimental results regarding the frequency of the secondary resonance can also be understood in the following way: a higher value of the frequency obtained from our calculations suggest that the Ni-Pt interactions which is responsible for the secondary resonance, could be overestimated in our methodology. The reasons for this overestimation could be twofold: one, we have not considered any local lattice relaxation which may make the Ni-Pt bonds softer in comparison to that in a rigid lattice, thus pushing the positions of the peaks of Ni-Pt structure factors towards lower frequency and bringing in closer agreement to the experiments and two, we have not incorporated any short-range order in our formalism. Tsunoda [156] has pointed out that it is very difficult to get rid of short-range order in this alloy near the 1:3 atomic ordering. Since short-range order would mean greater influence of the unlike pairs of species, the Ni-Pt force constants considered in our calculations could be very different than those in a homogeneously random alloy, thus affecting the results.

#### 4.3.3.3 $\mathbf{Ni_{0.50}Pt_{0.50}}$

Tsunoda *et al.* [156] had observed that the most significant failure of the mass-disordered CPA was in case of $Ni_{0.5}Pt_{0.5}$ alloy where the vibrations of the unlike atom pairs are expected to play a more significant role. The vibrational densities of states for this alloy, calculated by the CPA, had predicted a split-band behavior. That the force-constant disorder is necessary to understand and even reproduce the experimentally observed phonon spectra, was later established by the ICPA calculations [91]. However, the set of force-constants used in Ref.

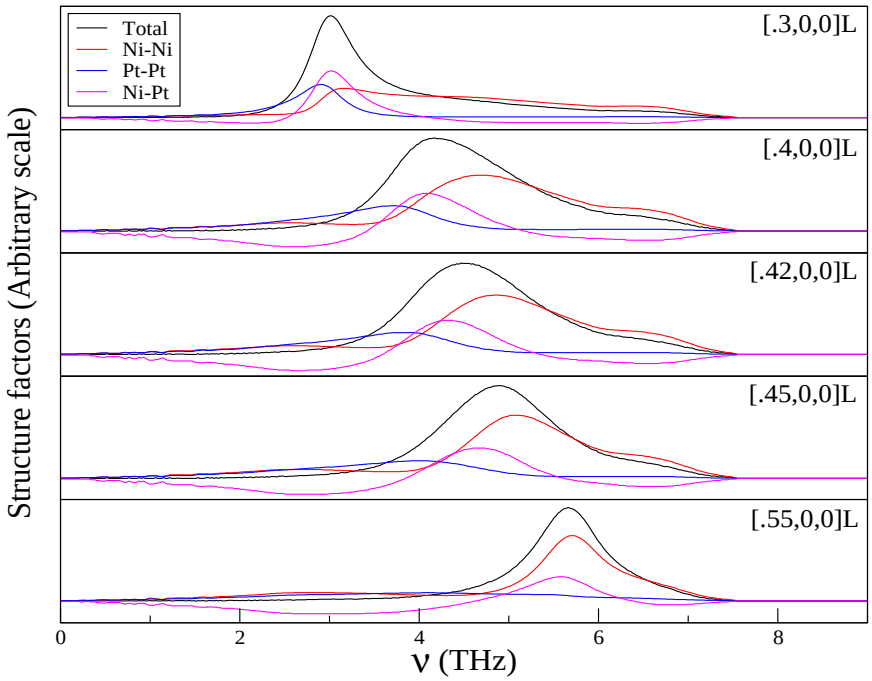


FIGURE 4.26: Partial and total structure factors calculated by the DFPT-TFC-ICPA method for various $\zeta$ values in the [$\zeta$,0,0] direction in $Ni_{0.50}Pt_{0.50}$. The black lines are the total contributions, the red lines are the Ni-Ni contributions, the blue lines are the Pt-Pt contributions and the magenta lines are the Ni-Pt contributions. All the curves are for longitudinal modes.

[91] were intuitive and thus their accuracies were questionable. Therefore, in Fig. 4.21(c), we present the phonon dispersions calculated with our first-principles based formalism which is supposed to model the inter-atomic bond stiffnesses accurately. We find an overall fair agreement between our calculations and the experiments. Good agreement is obtained for the low frequency branches along [$\zeta$ 0 0] direction. For the high frequency branches, there are quantitative differences between our calculations and the experiments. The calculated resonance frequency for the [$\zeta$,0,0]T branch is 3.9 THz ($\zeta \approx 0.67$), which is a bit higher than that of the experimental data ($\approx$ 3.5 THz). However, as described by Tsunoda *et al.* [156], there might be some ambiguity in the estimation of resonance frequency as the peaks for $\zeta \approx 0.7$ were quite broad and were superimposed on an uneven background caused by the incoherent inelastic scattering. There is also some discrepancy over the position of resonance for the [$\zeta$,0,0]L branch. The experimental results show resonance for this branch at a frequency, $\nu \approx 5.2$ THz, whereas, the calculations predict it to be at $\nu$=4.5 THZ. Experimental interpretation, however, was very difficult in this region because of the very large widths. No well-defined peaks were observed experimentally near $\zeta \approx 0.45$, presumably due to extreme line broadening. As was observed earlier for $x = 0.95$ and $x = 0.7$, the disorder-induced widths [Fig. 4.23(c)] for

both branches show anomalously large values at certain wave vectors which coincide with the wave vectors corresponding to the resonance, thus validating the results obtained from the positions of the peaks in the structure factors. It is also observed that the phonon frequencies from our calculations for the high frequencies are higher in magnitude than the experimental frequencies. A comparison with the earlier ICPA calculations with empirical force-constants [91], however, suggests that quantitatively, the present results are in better agreement with the experiments. To understand these observations, we present the structure factors in Fig. 4.26 for the [$\zeta$ 0 0]L branch at selected $\zeta$ values. Similar to $Ni_{0.7}Pt_{0.3}$, we find that the Ni-Pt pairs have substantial contributions in this alloy system. Near $\zeta = 0.4$, the wave vector around which the resonance occurs for [$\zeta$ 0 0]L branch, the peak due to the Ni-Ni contributions start to shift towards higher frequencies compared to the peaks due to the contributions from other two pairs. As a result, the phonon line shapes become asymmetric and the widths increase significantly. With increasing $\zeta$, the positions of the Ni-Pt and the Ni-Ni peaks start to get closer and move towards higher frequencies as compared to the Pt-Pt peaks with gradually diminishing contributions of the Pt-Pt pairs to the total structure factors. At $\zeta = 0.55$, the Ni-Ni and Ni-Pt peaks appear at the same frequency with Pt-Pt pairs contributing very little to the structure factors. For $\zeta > 0.55$, the Pt-Pt pairs practically have no significant contributions and the structure factors are dominated by the vibrations of the Ni-Ni and Ni-Pt pairs. The reasons behind the better agreement of the present calculations with the experiments in comparison to the results of Ref. [91] can be understood from the features in the structure factors discussed. In Ref. [91], it was assumed that the Ni-Pt force constants would be softer than the Ni-Ni ones. Thus, the Ni-Ni bond stiffnesses in Ref. [91] were overestimated. Since the high frequency phonon branches are dominated by the Ni-Ni contributions as seen in Fig. 4.26, such overestimation resulted in larger phonon frequencies. With our present first-principles based methodology, on the other hand, we have found that the Ni-Ni bond stiffnesses are softer than the Ni-Pt ones. This correct depiction of the relative strengths of the Ni-Ni and Ni-Pt bonds, has brought in a better agreement between the present calculations and the experiments.

In Ref. [156], the measurements were carried out for [$\zeta$ 0 0] direction only because the authors, from the observations on $Ni_{0.95}Pt_{0.05}$ and on $Ni_{0.7}Pt_{0.3}$ alloys, inferred that the anomalous features of the lattice dynamics do not depend very sensitively on the phonon propagation directions. However, for the $Ni_{0.5}Pt_{0.5}$ alloy, we do find a dependence of the anomalous features on the propagation directions. For the [$\zeta$,$\zeta$,0]L and [$\zeta$,$\zeta$,0]$T_2$ branches, resonance occurs at $\nu \approx$3.95 THz, while the same can be seen for the [$\zeta$,$\zeta$,0]$T_1$ branch at 3.75

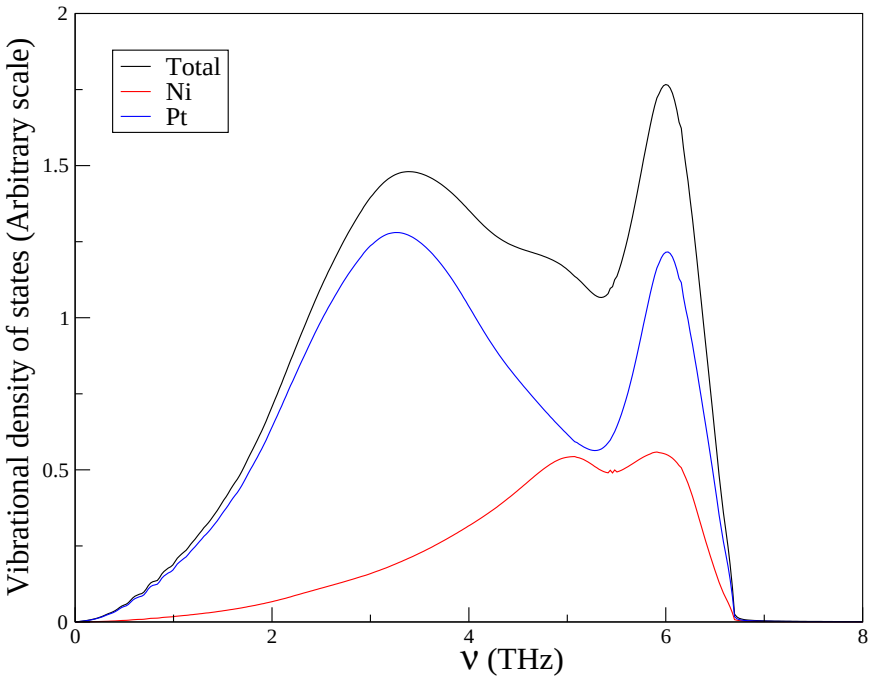


FIGURE 4.27: Vibrational densities of states for $Ni_{0.25}Pt_{0.75}$ calculated by the DFPT-TFC-ICPA method.

THz. An extra feature in the form of secondary resonance is also observed for the [$\zeta$,$\zeta$,0]$T_1$ branch at 6.40 THz. For the [$\zeta$,$\zeta$,$\zeta$] direction, we do not see resonance for either of the directions. This suggests the need for further experimental studies for these two directions of phonon propagation.

#### 4.3.3.4 $Ni_{0.25}Pt_{0.75}$

A substantial qualitative disagreement between the theoretical and the experimental results is observed for this alloy composition. The experimental results along [$\zeta$,0,0] direction for this specimen showed double-peaked structures reminiscent of resonant behavior for the longitudinal branch at $\zeta \approx 0.4$, whereas, for the transverse branch, resonance was observed at $\zeta \approx 0.5$. For $\zeta$ larger than 0.55, the frequencies of the longitudinal branch were almost independent of wave vector which is typically observed for localized phonon. These results, however, have limitations as the phonon peaks at higher frequencies were superimposed on the uneven incoherent background, thereby, making it difficult to identify the peak positions properly. Our calculated dispersion curves are presented in Fig. 4.21(d). Contrary to the experimental observations, we do not see resonance like behavior for any of the branches. No frequency shift

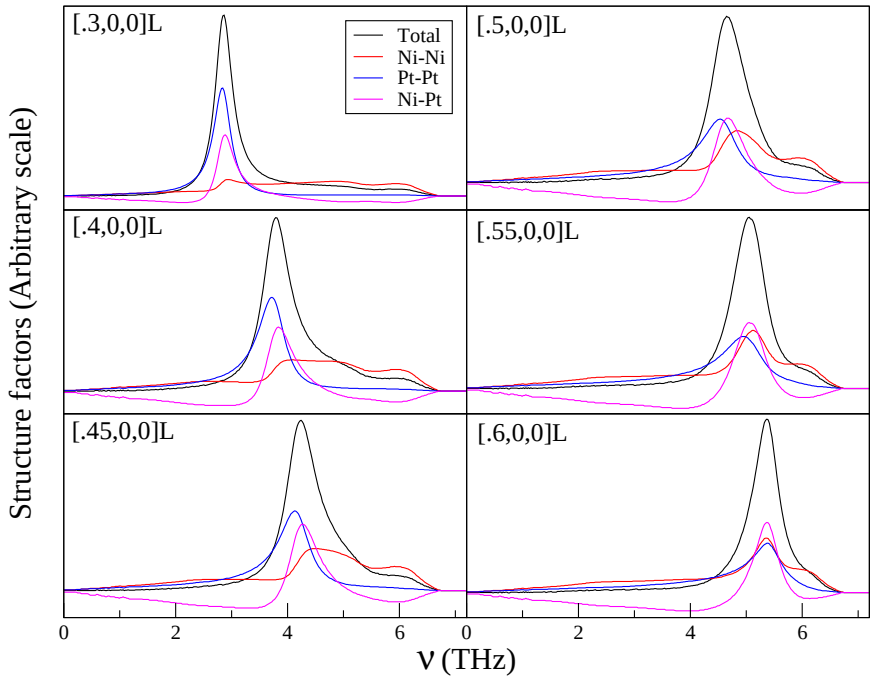


FIGURE 4.28: Partial and total structure factors calculated by the DFPT-TFC-ICPA method for various $\zeta$ values in the [$\zeta$,0,0] direction in $Ni_{0.25}Pt_{0.75}$. The black lines are the total contributions, the red lines are the Ni-Ni contributions, the blue lines are the Pt-Pt contributions and the magenta lines are the Ni-Pt contributions. All the curves are for longitudinal modes.

reminiscent of resonant behavior is observed in the theoretically calculated phonon dispersion curves. The calculated dispersion curves rather resemble those of the pure Pt. The calculated disorder-induced-widths [Fig. 4.23(d)] do not show any anomalously large value at any wave vector or frequency, unlike the other compositions considered so far, indicating a qualitative difference between the lattice dynamics of the alloy at this composition and at other compositions we studied. To understand the reasons behind these significant discrepancies, we take recourse to the vibrational densities of states (Fig. 4.27) and the structure factors (Fig. 4.28). The vibrational densities of states show that the Pt atoms play the dominant role throughout the band with Ni atoms adding weight to it at higher frequencies. This, thus corroborates the experimental observation of the localized impurity mode not splitting off from the main phonon band. It is to be noted that the mass-disordered CPA predicted [156] a splitting of the impurity Ni band from the main phonon band. The origin of these contradicting predictions can be traced by analyzing the calculated structure factors in Fig. 4.28. For higher values of $\zeta$ in case of [$\zeta$ 0 0]L, we find that the contributions from all three pairs of atoms are important and that they vibrate at the same frequency (the peaks of the partial structure factors occur at same frequencies) with the maximum frequency being lower than the frequency of the phonon

band-edge. This is due to the consideration of the force-constant disorder, or in other words, due to the incorporation of the fact that the Ni-Pt pairs decide the lattice dynamics at high frequencies and that the Ni-Pt bond stiffness's are significantly less than the Pt-Pt bond stiffness's. There was no such possibility within the framework of the mass-disorder CPA and thus consideration of a single force constant for all pairs resulted in severe overestimation of the frequencies leading to the splitting of the impurity mode from the host band.

The results of Fig. 4.28 also suggest a possible clue to the disagreement between our calculations and the experimental results. A closer look at the structure factors reveal that for $\zeta$=0.45-0.55, there is a small hump around 6 THz due to the Ni-Ni vibrations. The small peak due to this is completely diminished due to the contributions from the Ni-Pt pairs, resulting in only single-peak structure factors. Clearly, our calculated structure factors also would have two-peak structures resulting in qualitative agreement between the theory and the experiment, had this hump persisted. Thus, a couple of reasons could be thought of behind this disagreement: one, it could be that due to the non-consideration of short-range order in our calculations, the Ni-Pt contributions have gained more weight and inclusion of the short-range order may re-distribute the weights of the contributions associated with the three pairs of species, resulting in two-peak structure factors and two, the limitations in the determination of the peak positions from neutron group data for high frequencies as described in Ref. [156] could lead to the spurious splitting of the dispersion curves, thus giving rise to the disagreement between our calculations and the experiments. Therefore, a theoretical calculation incorporating short-range order in our formalism and a careful neutron- scattering experiment should be performed for this composition of the alloy.

## 4.4 Summary

A combination of the transferable force constant model based upon first-principles DFPT calculations and the ICPA has been proposed as a first-principles based tool to calculate the phonon spectrum and related properties for disordered alloys at any arbitrary concentration. The TFC model has been applied for the first time to calculate the complete phonon spectra of disordered alloys. The reliability of the model has also been examined for a wide variety of alloys. To begin with, we have chosen magnetic type-II alloys $Pd_xFe_{1-x}$, for which the phonon dispersion curves and elastic constants agree very well with the experiments at

low temperatures. For $Pd_{0.5}Fe_{0.5}$ alloy, inspite of producing qualitatively correct inter-atomic force constants by this approach, a noticeable deviation of the calculated phonon frequencies from the experimental results is observed which could be attributed to the non-incorporation of any temperature effect in calculating the force-constants. We have also investigated the role of size-mismatch of end point components on the lattice dynamics of binary alloys by considering the illustrative examples of $Cu_{0.715}Pd_{0.285}$ and $Cu_{0.75}Au_{0.25}$ systems. On incorporation of bond length fluctuations for the alloy $Cu_{0.715}Pd_{0.285}$, the phonon dispersion curves agree very well with the experimental results. In case of $Cu_{0.75}Au_{0.25}$ we find a resonance mode at around 2.9 THz which is not observed in the experiments. A systematic investigation reveals that this alloy presents a case where both the mass and the force constant disorders play significant role in determining the phonon frequencies. The good agreement obtained with the average mass and average set of force constants extracted by fitting the experimental frequencies to a Born-Von Karman model, is indicative of cancellation of errors emanating from the mass and the force constants. Presence of resonance modes in the experimental results for the Cu-Au alloy at even smaller concentrations of Au suggest that the results obtained by us with relaxed bond lengths indeed capture the real picture of complex interplay of various types of disorders influencing the phonon dispersions in $Cu_{0.75}Au_{0.25}$ and that a more careful experiment has to be performed so as to produce the disorder induced effects properly for this alloy. In addition to these alloy systems, we have studied the complete phonon spectra for substitutional disordered alloys $Ni_xPt_{1-x}$, in which a systematic investigation reveals the importance of force constant disorder in determining the phonon frequencies for these alloys which justifies the failure of mass disorder only CPA theory for the alloys considered. The agreement between the theoretically calculated and the experimentally observed results is reasonably good except for the case of $Ni_{0.25}Pt_{0.75}$ where we see qualitative difference between the two in the phonon dispersion curves. Unlike experimental results, no split in the dispersion curves suggesting the occurrence of resonance is observed for this composition which is apparently clear from the behavior of the phonon line width. The dispersion curves are like pure Pt which is evident from the vibrational density of states. The only other notable discrepancy between our results and the experimental ones is that we do not obtain the experimentally observed double peaks in phonon lines for the [$\zeta$,0,0]T branch for $Ni_{0.70}Pt_{0.30}$ in the region from $\zeta$=0.4 to the zone boundary. For rest of the compositions, no such discrepancy is seen and our results successfully predict the resonance behavior around the experimentally observed regions. Although we have not observed any double-peaked structure reminiscent of resonance, however, the sudden jumps in the peak positions of the phonon lines and the associated large

widths strictly indicates the occurrence of resonance. It is worth mentioning at this point that the experimental results were ambiguous at certain places because of the uneven background caused by the incoherent scattering. This resulted in broad peaks which made it difficult to identify the peak positions accurately. Our calculated results are devoid of any such uncertainties. However, our calculations have not incorporated any short-range order, which, given the fact that the Ni-Pt bond stiffness's have been demonstrated to be playing the key role in affecting the lattice dynamics with the change in compositions, may turn out to be important in resolving the observed discrepancies. Thus, a calculation with the short-range order being incorporated in the formalism and a more careful experiment should be performed to settle the issues completely.

# Chapter 5

# Incorporation of the local environment effects

## 5.1 Introduction

The DFPT-TFC method [137] to calculate force constants corresponding to an inter-atomic bond in random alloys involves fitting of 'force constant vs bond length' data, obtained for the same bond in different chemical environments, to a suitable analytic function. Therefore, the reliability of the inter-atomic force constants between a pair of species calculated by this scheme heavily depends upon the accuracy of the fitting. Moreover, the approach fails to incorporate the effects of strong environmental disorders like the short-range order which may play important roles in governing the lattice dynamics of many real systems. For example, presence of short-range order in the system would mean more influence of the unlike pair of species and the inter-atomic force constants would be significantly different from that of a homogeneously disordered system. Hence, our quest is to find a suitable first-principles based theory to compute lattice dynamics in random alloys which is devoid of any of parameter fitting and has the ability to address the issue of environmental disorder correctly in addition to mass and force constant disorders.

In this chapter, we present a new first-principles based formalism [163] to compute the lattice dynamics of substitutional disordered alloys which incorporates the effects of disorder in mass, force constant and environment. We demonstrate the formalism by computing the

phonon dispersion spectra of homogeneously disordered $Ni_{0.5}Pt_{0.5}$ alloy. This alloy is chosen as an illustrative example due to the fact that its constituents have large mass differences (Pt is 3 times heavier than Ni), large size differences ($\sim$ 11%) and large force constant differences (Pt-Pt force constants being $\sim$ 55 % larger than the Ni-Ni ones) and thus significant effects of all three kinds of disorder on the lattice dynamics can be expected. As has been discussed in the previous chapter that the alloy with this composition exhibits certain anomalous features in its phonon dispersion and thus is interesting as a test case for any new formalism. Although, we had investigated this system with DFPT-TFC-ICPA method and results were discussed in the previous chapter, in this chapter we are not attempting any comparison of the results obtained with our new formalism with that obtained from the DFPT-TFC-ICPA method, neither are we attempting any calculation incorporating short-range order. Rather, our motivation is to discuss the nitty-gritties of the new formalism and stress upon its potential utility in handling the environment disorder. Thus, the only comparison of results we attempt is between the results obtained by this new formalism and the results obtained with other theoretical models where the effects of environments were somewhat neglected. To this end, we have compared the results of this new formalism with those from the CPA and from the ICPA in conjunction with the empirical set of force constants, the last one eventually having fairly good agreement with the experimental results.

## 5.2 Methodology

Our formalism has **three** important components: the structural model of substitutional disorder, the averaging procedure of the force constant tensor to recover the original symmetry of the solid solution and the ICPA for performing averaging over configurations. In the following sub-sections, we briefly describe the first two components of the formalism, whereas, the details of the ICPA method are already discussed in Chapter 2.

### 5.2.1 Structural model

Within the framework of first-principles calculations, some degree of translational symmetry is always assumed. Systems with long-range disorder must therefore be treated approximately, usually by averaging properties over several ordered configurations. Current computational capabilities limit the size of each configuration, as well as the number of configurations sampled. Recently, Zunger *et. al.* developed a computationally tractable approach to model the disorder through the introduction of a "special quasirandom structure" (SQS) [164–166], an $N$-atom per cell periodic structure designed so that their distinct correlation functions $\Pi_{k,m}$ best match the ensemble-averaged correlation-functions $\ll \Pi_{k,m} \gg$ of the random alloy. Here $(k, m)$ corresponds to the figure defined by the number of $k$ of atoms located on its vertices ($k$=2, 3, 4.... are pairs, triangles, tetrahedra etc.) with m being the order of neighbor distances separating them ($m$=1, 2....are first, second neighbors etc.). This approach creates a distribution of distinct local environments whose average corresponds to the random medium which is contrary to the requirement of mean-field theories (*e.g.* CPA) [71, 167–169] in which each atom is influenced by an identical, average medium. It has been used extensively to study the equilibrium volumes, density of states, band gaps, formation enthalpies and optical properties in semiconductor alloys [164–166]. Moreover, the approach has also been applied to investigate the local lattice relaxations in size-mismatched transition metal alloys [170–173] and to predict the formation enthalpies of Al-based FCC alloys [174]. The biggest advantage of the SQS over a conventional supercell to model positional disorder is that the former uses the knowledge of the pair-correlation functions, a key property of the random alloys, to decide the positions of the atoms in the unit cell, instead of inserting them randomly as is done in the conventional supercell technique, and thus is guaranteed to provide a better description of the environments in an actual random alloy.

### 5.2.2 Averaging procedure for force-constants

Since the relaxation of atomic positions produce a distribution of nearest neighbor distances for any pair of atoms, the nearest neighbor force constants, too, have a distribution, depending on the bond distances. However, since the symmetry of the SQS is lower than the symmetry of the actual lattice of the alloy which is most often cubic in case of binary systems, the force constant matrices look more complicated. For construction of the Green's function for the

actual alloy with it's underlying symmetry and for the computation of configuration-averaged quantities in an inexpensive way, one thus need to recover the actual symmetry in nearest neighbor force constant matrices through proper averaging of the SQS force constant matrices obtained from first-principles calculations done on the SQS. The retrieval of force constants with cubic symmetry from the SQS force constants is possible because of the fact that the SQS is indeed a superstructure of the underlying lattice of the actual disordered alloy. We, here, demonstrate a smart procedure to retrieve the average force constants with the symmetry of the real binary alloy. For the sake of convenience, we demonstrate the averaging procedure for a FCC lattice.

In a FCC lattice, the distances between a given atom and its 12 nearest neighbors are specifieded by the vectors $(\pm\frac{1}{2}, \pm\frac{1}{2}, 0)a$, $(\pm\frac{1}{2}, 0, \pm\frac{1}{2})a$ and $(0, \pm\frac{1}{2}, \pm\frac{1}{2})a$; $a$ being the lattice constant. The force constant matrix for two atoms separated by the vector $(\frac{1}{2}, \frac{1}{2}, 0)a$ is of the form

$$\begin{pmatrix} a & b & 0 \\ b & a & 0 \\ 0 & 0 & c \end{pmatrix}$$

The other nearest neighbor force constant matrices are of the same form and are related by point group operations. However, when the atoms are allowed to relax, the vector separating a pair of nearest neighbor atoms are modified to $(\frac{1}{2} \pm \delta_1, \frac{1}{2} \pm \delta_2, \delta_3)a$ and the matrix of force constants corresponding to a given pair of atoms reflects the loss of symmetry, taking the general form

$$\Phi = \begin{pmatrix} a_1 & b_1 & a_3 \\ b_2 & a_2 & a_4 \\ a_6 & a_5 & c \end{pmatrix} \tag{5.1}$$

For a particular set of $\delta_1$, $\delta_2$ and $\delta_3$, one needs to perform the averaging such that we obtain the following force constant matrix:

$$\Phi' = \begin{pmatrix} a' & b' & 0 \\ b' & a' & 0 \\ 0 & 0 & c' \end{pmatrix} \tag{5.2}$$

To achieve this, one needs to pick up the relevant ones out of the 48 symmetry operations corresponding to the cubic group which transform the force constant matrices to one displaying the symmetry of the FCC structure. To elaborate on this, we provide the following example:

Suppose, two atoms are separated by the separation vector $\vec{R} = \{\frac{1}{2} - \delta_1, -(\frac{1}{2} + \delta_2), -\delta_3\}a$. The force constant matrix obtained from first-principles calculations on the SQS is given by Eq. 5.1. To recover the symmetry of the FCC force constants, we need to find out the transformations that transform the separation vector $\vec{R}$ to a new separation vector $\vec{R}' = \{\frac{1}{2} - \delta_1, \frac{1}{2} + \delta_2, -\delta_3\}a$ and $\{\frac{1}{2} + \delta_2, \frac{1}{2} - \delta_1, -\delta_3\}a$. These transformations, in this particular case, mimic the nearest neighbor separation $(\frac{1}{2}, \frac{1}{2}, 0)a$ for the unrelaxed FCC lattice. They are:

$$\begin{aligned} (x, y, z) &\longrightarrow (y, -x, z) \\ (x, y, z) &\longrightarrow (x, -y, z) \\ (x, y, z) &\longrightarrow (y, -x, -z) \\ (x, y, z) &\longrightarrow (x, -y, -z). \end{aligned} \tag{5.3}$$

Corresponding to each of these transformation, there is a transformation matrix $U$. We transform the SQS force-constant matrix $\Phi$ to the FCC force-constant matrix $\Phi'$ by performing the operation $U^T \Phi U$ in each of the 4 cases and then adding them. This simple procedure produces $a' = 2(a_1 + a_2)$, $b' = -2(b_1 + b_2)$ and $c' = 4c$. All other off-diagonal elements vanish due to this symmetrization and the FCC symmetry is recovered. This procedure is repeated for all pairs of force constants and an arithmetic average is finally computed.

The methodology, therefore, consists of the following components:

(a) computations of the dynamical matrices and real-space force constant tensors on an N-atom SQS,

(b) the averaging procedure is employed so that the resulting force-constants tensors have the original symmetry of the underlying crystal structure,

(c) the averaged force-constants are then used in the ICPA calculations for computations of the phonon dispersions and densities of states.

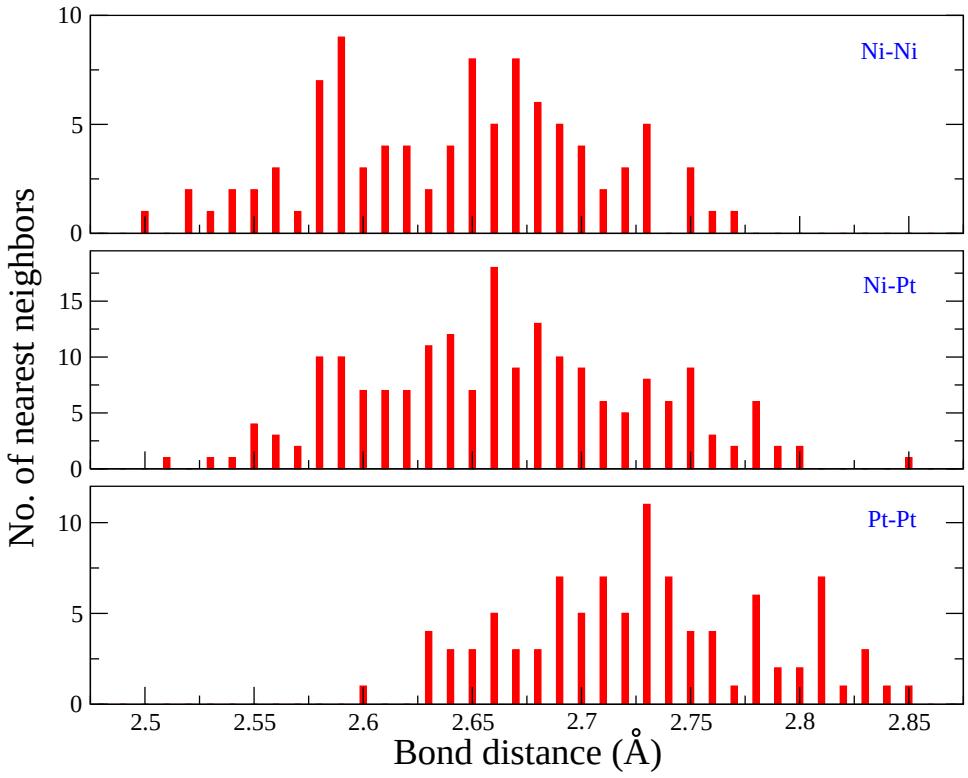


FIGURE 5.1: Dispersion of bond distances for three pairs of atoms computed by the SQS.

## 5.3 Example: $Ni_{0.5}Pt_{0.5}$

We illustrate the novelty of this formalism by computing phonon dispersions for $Ni_{0.5}Pt_{0.5}$ alloy. A 64 atom SQS is constructed to represent the random alloy. We employ first-principles plane wave projector augmented wave method as implemented in the VASP code [175, 176] for calculation of the electronic structure for the 64-atom SQS. The dynamical matrices and the real-space force constants are calculated using the PHON code [177]. The cut-off energy for the electronic wave functions is 400 eV. The structure is fully relaxed till the forces are converged to $10^{-4}$ eV/$\AA$. For the configuration-averaging, the disorder is considered in the nearest-neighbor shell only as the further neighbors have force-constants a order of magnitude less. The ICPA calculations are done with a $25 \times 25 \times 25$ $k$-mesh and 1000 energy points.

In Fig. 5.1, the variations of the nearest-neighbor bond distances for a given pair of specie with the variations in the environment are plotted. It is observed that the inter-atomic bond distances for a given chemical specie pair depend sensitively on the number of unlike atoms i.e. the fluctuations in the environment. As a result of this, the inter-atomic force constants

TABLE 5.1: Real-space nearest neighbor force constants $\Phi^{\alpha\beta}$ (in units of dyn/cm) for $Ni_{0.5}Pt_{0.5}$ obtained by averaging the SQS force constants; the force constants used for CPA calculations and the empirical force constants [91] are also included for comparison. The last column indicates the Cartesian components of $\Phi^{\alpha\beta}$.

| Pair | SQS | CPA | Empirical | $\alpha\beta$ |
|---|---|---|---|---|
| Ni-Ni | 8231 | 19365 | 15587 | *xx* |
| Ni-Pt | 17868 | 19365 | 13855 | ” |
| Pt-Pt | 33494 | 19365 | 28993 | ” |
| Ni-Ni | -525 | -3255 | -436 | *zz* |
| Ni-Pt | -2820 | -3255 | -348 | ” |
| Pt-Pt | -6854 | -3255 | -7040 | ” |
| Ni-Ni | 9580 | 22679 | 19100 | *xy* |
| Ni-Pt | 20740 | 22679 | 15280 | ” |
| Pt-Pt | 39655 | 22679 | 30317 | ” |

too undergo variations with the fluctuations in the environment. First-principles calculations on the SQS structure show that the average Ni-Ni bond distance is 2.64 Å, the average Ni-Pt bond distance is 2.66 Å and the average Pt-Pt bond distance is 2.73 Å which means that there is significant dispersions among the three pairs of bonds. It is to be noted that the Ni-Pt bond distance is exactly equal to the unrelaxed alloy bond distance while the Ni-Ni bond distance is less than 1% smaller than the unrelaxed alloy bond distance and the Pt-Pt bond distance is 2.6% larger than the unrelaxed alloy bond distance. The effects of such dispersions in inter-specie bond distances on the relevant force constants are presented in Table 5.1 where a comparison is made between three different models of disorder: the SQS-averaged, the empirical [91] and the CPA. It is to be noted that the empirical force constants used in Ref. [91] were obtained based upon intuitive arguments about relative bond strengths of the three specie pairs and their quantifications based upon the fit to the upper band edge of the experimental phonon spectra. There, it was argued that the Ni-Ni bonds in the alloy are softer compared to those in pure Ni, the Pt-Pt bonds are stiffer compared to those in pure Pt and Ni-Pt bonds are even softer than the Ni-Ni ones because the Ni-Pt bond distances were thought to be the largest. A comparison between the force constants obtained by the SQS-averaged and by this empirical scheme shows that the Ni-Ni force constants computed by the SQS-averaging scheme are 50% softer, the Ni-Pt and the Pt-Pt force constants are 25% and 23% harder on an average. More importantly, the Ni-Pt force constants computed by

the SQS-averaging scheme are harder than the Ni-Ni ones, a result in contradiction with the empirical scheme. This is due to non-consideration of the environmental disorder resulting in incorrect considerations of the relative strengths of the stiffnesses of the three types of inter-specie bonds. In the empirical model, the Ni-Ni alloy force constants were taken to be only 10% softer than the Ni-Ni force constants in the pure Ni. While the Ni-Ni bond distances in the alloy under consideration are about 6% larger than that in the pure Ni, consideration of only 10% softening was a gross overestimation of the Ni-Ni interactions in the random alloy environment. Due to a significantcant increase in the Ni-Ni average bond distances, the Ni-Ni interactions should suffer more severe dilution which is correctly addressed upon consideration of the random environment and subsequent atomic relaxations under the SQS model of positional disorder. The Pt-Pt alloy bond distances on the other hand reduce only by about 1% as compared to the pure Pt-Pt bond distance. Thus, the effect on the Pt-Pt force constants should be much less. Under the SQS-averaging scheme, the actual stiffening of the Pt-Pt bonds in the alloy is found to be about 25% compared to the pure Pt. The stiffer Ni-Pt bonds with respect to the Ni-Ni ones, as computed by the SQS, inspite of nearly same bond distances, is the consequence of the fact that the Ni atoms find the much larger Pt atoms as their nearest neighbors, roughly within the same available space as that of Ni atoms as nearest neighbors and as a result, the nearest-neighbor interactions become harder as the smaller Ni atoms try to accommodate the bigger Pt atoms within the same volume as that of their like pairs.

In what follows, we calculate the phonon dispersion curves of $Ni_{0.5}Pt_{0.5}$ alloy using force constants obtained by these three models of compositional disorder, the results of which are presented in Fig. 5.2. The configuration averaging in case of the SQS-averaging and the empirical scheme are done by the ICPA. The results indicate that the SQS-ICPA shows the best agreement with the experiments as compared to the CPA and the empirical-ICPA [91]. The disorder-induced widths computed by the SQS-ICPA method (the shaded region in Fig. 5.2) also agree reasonably well with the experimental results. It is to be noted that the comparisons with the experiments could be possible only for the [$\zeta$00] direction because experimental results were not available for other directions. A closer look at Fig. 5.2 reveals that for the low-frequency branches, the results of the empirical-ICPA and the SQS-ICPA methods are in close agreement while there are significant differences for the high frequency branches. The mass-disorder treated in CPA, on the other hand, fails to reproduce the experimental features of the dispersion relations both qualitatively and quantitatively. The frequencies of the

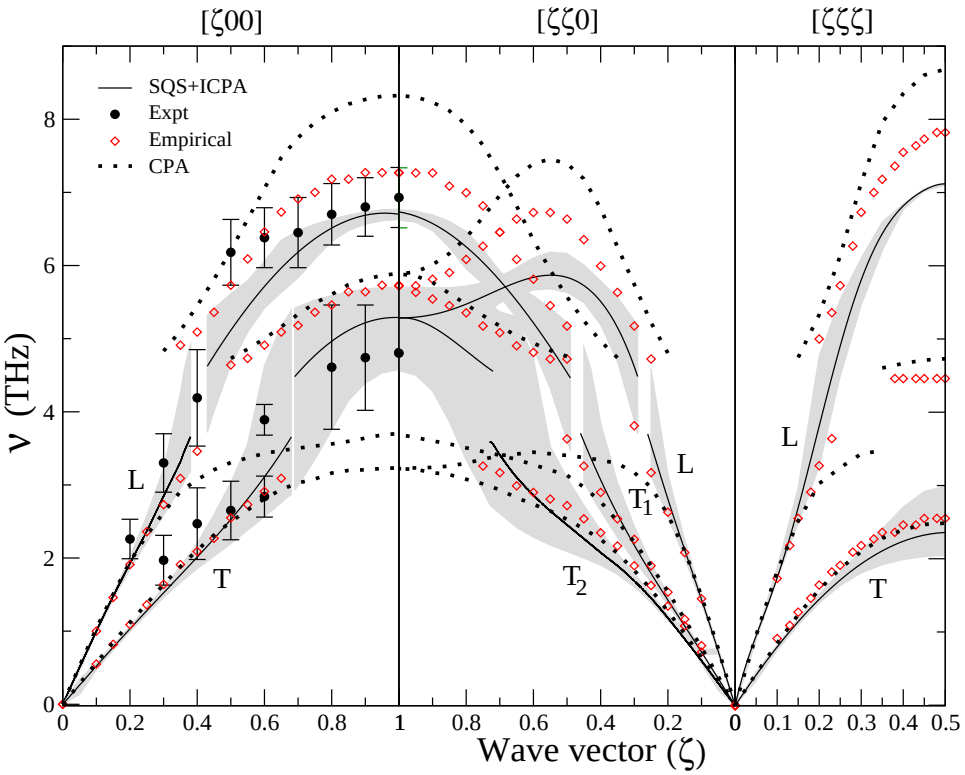


FIGURE 5.2: Phonon dispersion in $Ni_{0.5}Pt_{0.5}$ alloy computed by the SQS-ICPA (solid line), the CPA (dotted line) and the empirical-ICPA [91] (red diamonds) methods. The circles indicate the experimental results. The shaded regions indicate the disorder-induced widths calculated by the SQS-ICPA.

high frequency branches (both transverse and longitudinal) computed by the CPA are severely overestimated while the lower frequency branches extend all the way to the zone boundary, thus displaying a split-band behavior in the phonon dispersions which is not observed experimentally.

All these observations can be understood in terms of the inter-atomic force constants (shown in Table 5.1) which in turn are influenced by the fluctuations in the local environments. In the CPA, the fluctuations in the force constants are completely neglected and hence Ni-Ni, Ni-Pt and Pt-Pt pairs have the same force constants. In earlier studies [91, 156], the force constants used in the CPA were those of pure Ni ones obtained experimentally [141]. In this study, we have used a more realistic set of force constants for the CPA calculations which are $\Phi^{\alpha\beta} = x^2\Phi^{\alpha\beta}_{Ni-Ni} + (1-x)^2\,\Phi^{\alpha\beta}_{Pt-Pt} + 2x(1-x)\,\Phi^{\alpha\beta}_{Ni-Pt}$ where $\alpha,\beta$ are the Cartesian directions and $x$ is the concentration of Ni. The $\Phi^{\alpha\beta}_{ss'}$ are the SQS-averaged force constants. Such a choice of force constants have been used in order to incorporate, in an average way,

the effects of alloy environment. The results, nevertheless, suggest that unless the fluctuations in the force constants are incorporated, the results do not even agree qualitatively with the measurements. The frequencies of the upper branches of longitudinal and transverse modes computed by CPA are too high as compared to the experiments while the frequencies of the lower branches are lower than the experimental ones. The reason being that the Ni-Ni vibrations dominate the higher frequency branches and the average force constants being too high pushes the frequencies away from the ones measured by neutron-scattering while the lower frequency branches being solely due to the Pt-Pt vibrations have frequencies lower as compared to neutron-scattering results because of the underestimation of the Pt-Pt force constants. The empirical-ICPA results on the other hand agree qualitatively with the experimental results because there is no split-band like behavior as was seen in the CPA. This is due to the consideration of the Ni-Pt correlated vibrations which renormalize the spectral weights associated with the contributions from Ni-Ni and Pt-Pt pairs [91]. Moreover, the splitting around $\zeta = 0.55$, a signature of existence of resonance mode, is reproduced and the frequencies of the high-frequency branches came out to be better as compared to the CPA. The Ni-Ni (Pt-Pt) force constants in the empirical model as shown in Table 5.1 are softer (harder) as compared to the CPA ones explaining the reason for better agreement of the phonon frequencies computed by the empirical-ICPA model with the experimental results. However, the overestimation (underestimation) of the Ni-Ni (Pt-Pt) interactions and an incorrect qualitative estimation of the Ni-Pt interactions as compared to the Ni-Ni ones gives rise to significant discrepancies for the high-frequency longitudinal and optical branches. The consideration of precise variations in the force constants between a given specie pair in the SQS-ICPA method makes the quantitative agreement between theory and experiments much better as seen in Fig. 5.2. The high-frequency branches for both longitudinal and transverse vibrations computed by the SQS-ICPA method agree substantially with the experimental results. The normal mode frequencies for these branches are dominated by the vibrations of the Ni pairs and thus a softening of the Ni-Ni bonds as computed by the SQS pushes the frequencies downwards compared to the empirical model making a better agreement with the experiments. Similarly, the relaxations of the Pt atoms results in the stiffening of the Pt-Pt bonds, thus pushing the frequencies slightly upwards. However, the high-frequency transverse branch computed by the SQS-ICPA model is still overestimated. In the neutron-scattering measurements [156], there were some ambiguities in determining the peak positions of the line shapes for the high-frequency transverse modes and thus the experimental results for this branch had larger uncertainties. Given this fact, the agreement between the theory and the experiment can be considered to be fairly

good. Another noteworthy feature is that inspite of a qualitatively incorrect estimation of the relative stiffnesses of the Ni-Ni and Ni-Pt bonds in the empirical model, there is no significant qualitative discrepancy between the results computed by the empirical-ICPA and the SQS-ICPA methods. The reason behind this is that the vibrations of Ni-Pt pairs only renormalize the relative spectral weights associated with the vibrations of the Ni-Ni and Pt-Pt pairs. Since the relative differences in the stiffnesses of the Ni-Pt bonds used in the two models are much less compared to that for Ni-Ni bonds, the qualitative features of the phonon dispersions are not affected.

## 5.4 Summary

We have developed a reliable first-principles based approach for the calculation of phonon spectra in substitutional disordered alloys to treat mass, force constant and environmental disorder on equal footing. We demonstrate in case of $Ni_{0.5}Pt_{0.5}$ alloy, the importance of an accurate structural model of disorder taking into account the role of fluctuations in the local environment through atomic relaxations in interpreting the microscopic features of the lattice dynamics for these class of complex systems. The accurate modeling of the environmental disorder made possible by the SQS paves the way for reliable description of phonon spectra in alloys with short-range order where the force-constants between a pair of specie is dominated by a particular configuration of the nearest neighbor environment around an atom. Since the SQS produces numerous possible environments around an atom, simulating the effect of short-range order on the bond stiffnesses can be done by picking up the results of the desired configuration and discarding others, an option not viable by fitting the results of experiments or even first-principles calculations to an empirical model as was done in Ref. [91]. Thus, a combination of reliable force constants obtained from ab-initio and ICPA as a self-consistent analytic method for configuration-averaging enables us to solve the longstanding problem of theoretical computation of lattice dynamics in disordered alloys.

# Chapter 6

# Conclusions

In this thesis, we have worked on the development of new first-principles based formalism to compute lattice dynamics in substitutionally disordered alloys. Such a formalism is essential in state-of-the-art materials science research so as to get a proper microscopic understanding of the underlying physics in these systems. Here, we have employed our methodologies to provide a microscopic description of the lattice dynamics for a wide variety of alloys.

In the introductory chapter, the role of lattice vibrations in various areas of interest has been discussed in detail. This is necessary to establish the importance of lattice dynamical study. Thereafter, we have discussed very briefly the available experimental techniques and the necessary theoretical approximations and models which are essential to study lattice vibrations in solids. Finally, the concept of alloys has been introduced. We have provided a brief illustration of some of the relevant issues which are of due significance in the calculation of vibrational properties of alloys.

In the next chapter, we have discussed various methods to perform the all important configuration averaging in substitutionally disordered systems with main focus on the ICPA formalism which is a Green's function based multiple scattering theory with the ability to treat mass, force constant and environmental disorder for lattice vibrations on equal footing. The 'Augmented space formalism' and its use in constructing the self-consistent ICPA formalism has also been discussed in great detail.

Inspite of being an ideal tool to study lattice vibrations in disordered systems, a missing key component in establishing the ICPA as an accurate and reliable formalism, is its integration with a tractable structural model for positional disorder which can closely mimic the fluctuations in the inter-atomic force constants in a random alloy. Since state-of-the-art first-principles methods for disordered systems are computationally very demanding, hence, we have adopted different modelling strategy, employing results obtained from *ab initio* calculations, so that the inter-atomic force constants in random alloys can be computed with a moderate computational cost. In chapter 3, we have discussed the details of density functional theory (DFT) and density functional perturbation theory (DFPT) which form the basis of our first-principles calculations. Based on the observations of Ceder and co-workers that force constants between a pair of species depend on bond length alone, we have devised a modelling strategy for the random alloys with $Fe_xPd_{1-x}$ ($x$ is concentration of Fe in the alloy) chosen as example systems. Such a modelling strategy although improves upon previous theoretical results available for these systems, however, the crude approximations involved in it has reduced its applicability for random alloys for arbitrary concentrations. An improved modeling strategy has been realized by adopting the transferable force constant (TFC) model of Ceder and co-workers, which has been combined with the ICPA to formulate DFPT-TFC-ICPA method, a new first-principles based methodology to compute lattice dynamics in random alloys.

Chapter 4 has been devoted to the application of DFPT-TFC-ICPA method for a wide variety of binary alloys. Our motivations have been different for different alloys. For $Fe_xPd_{1-x}$ ($x$ is concentration of Fe in the alloy) which are magnetic type-II alloys, the calculated phonon dispersion curves and elastic constants show excellent agreement with the experimental results at low temperatures. However for $Fe_{0.50}Pd_{0.50}$, a quantitative disagreement between the both has been observed which could be due to non-incorporation of any temperature effect in our calculations. In case of $Cu_{0.715}Pd_{0.285}$ and $Cu_{0.75}Au_{0.25}$ systems, the role of size-mismatch of end point components on the lattice dynamics has been investigated in detail. In addition to mass and force constant disorders, local lattice relaxation has been found to play a crucial role in these systems. On incorporation of bond length fluctuations, the phonon dispersion curves agree very well with the experimental results for the alloy $Cu_{0.715}Pd_{0.285}$, whereas, some discrepancies have been observed for $Cu_{0.75}Au_{0.25}$. A thorough investigation of the role of different disorders present in $Cu_{0.75}Au_{0.25}$ system and the available experimental results for $Cu_{0.97}Au_{0.03}$ and $Cu_{0.91}Au_{0.09}$ alloys have revealed that our calculated results produce the

correct qualitative trends and that the reliability of the experimental results are questionable for this system. We have also calculated the phonon dispersion curves for $Ni_xPt_{1-x}$ alloys ($x$ is concentration of Ni in the alloy) over the entire range of concentration. Good agreement has been achieved between the theoretically calculated and the experimentally observed results for all concentrations except $x = 0.25$. It has been found that the limitations in both theoretical calculations and experimental measurements could be possible reasons for the discrepancy observed in $Ni_{0.25}Pt_{0.75}$ alloy specimen.

In chapter 5, in our quest for a model of positional disorder so that effects of random environments can be incorporated in a better fashion, we have developed an improved first-principles based methodology for the calculation of phonon spectra in substitutionally disordered systems. Our formalism, which is a combination of special quasi-random structure (SQS) and the ICPA, treats the environmental disorder in a much better way as compared to our previous schemes. We have demonstrated our formalism in case of $Ni_{0.5}Pt_{0.5}$ alloy, an ideal candidate in which the effects of disorders are most prominent. The better agreement of our results with the experiments than the previous models of disorder suggests that the proposed formalism represents a better structural model of positional disorder which determines the inter-atomic interactions among various pairs of chemical species in a disordered alloy environment much more realistically.

The extensions of the work presented in this thesis can be in various directions. These include the applications of the DFPT-TFC-ICPA and the SQS-ICPA method to a variety of problems. One immediate application of the SQS-ICPA method could be to investigate the effects of short-range order in the alloy systems *CuAu* and *NiPt* in order to gain more insight into the observed discrepancies between the theory and the experiments. This, then, can be extended to more such alloys where size-mismatch plays an important role.

Another possible extension could be in generalizing the ICPA for multi-component alloys with partial disorders. In the present thesis, we have used the version of the ICPA suitable for disordered binary alloys only. However, many state-of-the-art materials are multi-component and are partially disordered. The phonon dispersions in these alloys have not yet been explored in details although microscopic understanding of materials properties can be achieved from their lattice dynamics. One such example is the shape-memory alloys. Intensive investigations are going on in these systems in their disordered phases in order to obtain target properties suitable for industrial applications [178–180]. For the stoichiometric counterparts

of these systems, phonon spectra have been quite useful in understanding the phase stabilities in these systems [181, 182]. A generalization of the ICPA method could, thus, become a significant tool in investigating the relation between the phonon excitations and materials properties in these systems. Construction of an SQS for the multi-component systems and subsequent calculations of the force-constants could be prohibitively demanding. Therefore, the DFPT-TFC-ICPA formalism may be quite tractable in these cases.

Another possible extension could be the study of lattice dynamics in systems with magnetic disorder. The interrelations between magnetism and the phonon excitations can shed some light in understanding the properties of magnetic systems. The role of magnetic disorder in understanding materials behaviour has been exemplified by the INVAR alloys, for example [183–186]. Computation of phonon spectra in other materials with such disorders, thus, may enable us to gain useful information regarding relations between magnetism and the lattice dynamics. Generalization of the SQS for magnetic disorder and subsequent application of the SQS-ICPA technique as laid out in the thesis would be ideal for this problem.

# Bibliography


[1] A. A. Maradudin, E. W. Montroll and G. H. Weiss, *Theory of lattice dynamics in the harmonic approximation* Academic Press, New York and London (1963).

[2] Martin T. Dove, *Introduction to lattice dynamics* Cambridge University Press, New York (1993).

[3] Neil W. Ashcroft and N. David Mermin, *Soild state physics* Harcourt Brace College Publisher, New York (1976).

[4] P. Bruesch, *Phonon, Theory and Experiment* Springer-Verlag, New York (1982).

[5] D. C. Wallace, *Thermodynamics of Crystals* Wiley, New York (1972).

[6] A. A. Quong and A. Y. Liu, Phys. Rev. B **56**, 7767 (1997).

[7] J. Xie, S. de Gironcoli, S. Baroni and M. Scheffler, Phys. Rev. B **59**, 965 (1999).

[8] A. Y. Liu, A. A. Quong, J. K. Freericks, E. J. Nicol and E. C. Jones, Phys. Rev. B **59**, 4028 (1999).

[9] K. Persson, M. Ekman and V. Ozolins, Phys. Rev. B **61**, 11221 (2000).

[10] V. Ozolins, C. Wolverton and A. Zunger, Phys. Rev. B **58**, R5897 (1998).

[11] K. Einarsdotter, B. Sadigh, G. Grimvall and V. Ozolins, Phys. Rev. Lett. **79**, 2073 (1997).

[12] S. Klotz, J. M. Besson, M. Braden, K. Karch, P. Pavone, D. Strauch and W. G. Marshall, Phys. Rev. Lett. **79**, 1313 (1997).

[13] L. N. Cooper, Phys. Rev. **104**, 1189 (1956).

[14] J. Bardeen, L. N. Cooper and J. R. Schrieffer, Phys. Rev. **106**, 162 (1957).

[15] J. Bardeen, L. N. Cooper and J. R. Schrieffer, Phys. Rev. **108**, 1175 (1957).

[16] L. Brillouin, Ann. Phys. (Paris) **17**, 88 (1922).

[17] H. C. Teh and B. N. Brockhouse, Phys. Rev. B **8**, 3928 (1973).

[18] G. Shirane, Rev. Mod. Phys. **46**, 437 (1974).

[19] C. Stassis, D. Arch, B. N. Harmon, and N. Wakabayashi, Phys. Rev. B **19**, 181 (1979).

[20] R. Mittal, S. L. Chaplot, H. Schober, A. I. Kolesnikov, C.-K. Loong, C. Lind, and A. P. Wilkinson, Phys. Rev. B **70**, 214303 (2004).

[21] M. Kresch, O. Delaire, R. Stevens, J. Y. Y. Lin, and B. Fultz, Phys. Rev. B **75**, 104301 (2007).

[22] I. Tomeno, Y. Tsunoda, K. Oka, M. Matsuura, and M. Nishi, Phys. Rev. B **80**, 104101 (2009).

[23] G. Squires, *Introduction to the theory of thermal neutron scattering* Cambridge Univ. Press, Cambridge (1978).

[24] S. Lovesey, *Theory of neutron scattering from condensed matter* Clarendon Press, Oxford (1984).

[25] V. L. Hove, Phys. Rev. **95**, 249 (1954).

[26] M. Born and J. R. Oppenheimer, Ann. Phys. (Leipzig) **84**, 457 (1927).

[27] A. Einstein, Ann. Phys. **22**, 180 (1907).

[28] P. Debye, Ann. Phys. **39**, 789 (1912).

[29] M. Born and Th. von Karman, Phys. Z. **13**, 297 (1912).

[30] M. Born and K. Huang, *Dynamical Theory of Crystal Lattices* Oxford University Press, London (1956).

[31] R. M. Pick, M. H. Cohen and R. M. Martin, Phys. Rev. B **1**, 910 (1970).

[32] C. M. Bertoni, V. Bortolani, C. Calandra and E. Tosatti, Phys. Rev. Lett. **28**, 1578 (1972).

[33] R. Resta and A. Baldereschi, Phys. Rev. B **24**, 4839 (1981).

[34] H. Wendel and R. M. Martin, Phys. Rev. Lett. **40**, 950 (1978).

[35] K. Kunc and R. M. Martin, Phys. Rev. Lett. **48**, 406 (1982).

[36] S. Wei and M. Y. Chou, Phys. Rev. Lett. **69**, 2799 (1992).

[37] X. Gonze, D. C. Allan and M. P. Teter, Phys. Rev. Lett. **68**, 3603 (1992).

[38] S. de Gironcoli, Phys. Rev. B **51**, 6773 (1995).

[39] H. Bjerrum Moller and A. R. Mackintosh, Phys. Rev. Lett. **15**, 623 (1965).

[40] R. M. Cunningham, L. D. Muhlestein, W. M. Shaw and C. W. Tompson, Phys. Rev. B **2**, 4864 (1970).

[41] W. A. Kamitakahara and B. N. Brockhouse, Phys. Rev. B **10**, 1200 (1974).

[42] M. Mostoller, T. Kaplan, N. Wakabayashi and R. M. Nicklow, Phys. Rev. B **10**, 3144 (1974).

[43] H. J. Smith, N. Wakabayashi and M. Mostoller, *Superconductivity in d- and f-band Metals*

[44] R. M. Nicklow, P. R. Vijayaraghavan, H. G. Smith and M. K. Wilkinson, Phys. Rev. Lett. **20**, 1245 (1968).

[45] N. Wakabayashi, R. M. Nicklow and H. G. Smith, Phys. Rev. B **4**, 2558 (1971).

[46] W. A. Kamitakahara and J. R. D. Copley, ORNL 4952 (1973).

[47] N. Wakabayashi, Phys. Rev. B **8**, 6015 (1973).

[48] T. Kaplan and M. Mostoller, Phys. Rev. B **9**, 353 (1974).

[49] M. Mostoller and T. Kaplan, Phys. Rev. B **16**, 2350 (1977).

[50] M. S. Daw and M. I. Baskes, Phys. Rev. Lett. **50**, 1285 (1983).

[51] G. J. Ackland, *Alloy Modelling and Design*, edited by G. Stocks and P. Turchi (The Minerals, Metals and Materials Society, Pittsburgh, PA), p. 149 (1994).

[52] A. van de Walle, G. Ceder and U. V. Waghmare, Phys. Rev. Lett. **80**, 4911 (1998).

[53] A. van de Walle and G. Ceder, Phys. Rev. B **61**, 5972 (2000).

[54] C. Falter, M. Klenner and W. Ludwig, Phys. Rev. B **47**, 5390 (1993).

[55] C. Falter, M. Klenner and G. A. Hoffmann, Phys. Rev. B **52** 3702 (1995).

[56] C. Falter, G. A. Hoffmann and M. Klenner, Phys. Rev. B **53** 14917 (1996).

[57] J. Z. Liu, G. Ghosh, A. van de Walle and M. Asta, Phys. Rev. B **75**, 104117 (2007).

[58] D. K. Saha, K. Koga and K. Ohshima J. Phys.: Condens. Matter **4**, 10093 (1992).

[59] M. Rodewald, K. Rodewald, P. De Meulenaere and G. Van Tendeloo, Phys. Rev. B **55**, 14173 (1997).

[60] D. K. Saha and K. Ohshima, J. Phys.: Condens. Matter **5**, 4099 (1993).

[61] C. B. Walker and D. T. Keating, Phys. Rev. **130**, 1726 (1963).

[62] F. Klaiber, B. Schonfeld and G. Kostorz, Acta Crystallogr. A **43**, 525 (1987).

[63] B. Schnfeld, G. E. Ice, C. J. Sparks, H.-G. Haubold, W. Schweika and L. B. Shaffer, Phys. Status Solidi b **183**, 79 (1994).

[64] D. K. Saha and K. Ohshima, J. Phys.: Condens. Matter **7**, 3203 (1995).

[65] C. Wolverton, V. Ozolins and A. Zunger, Phys. Rev. B **57**, 4332 (1998).

[66] K. Tarafder, A. Chakrabarti, K. K. Saha and A. Mookerjee, Phys. Rev. B **74**, 144204 (2006).

[67] C. Wolverton and A. Zunger, Comp. Mat. Sci. **8**, 107 (1997).

[68] R. J. Elliott, J. A. Krumhansl and P. L. Leath, Rev. Mod. Phys. **46**, 465 (1974).

[69] L. Nordheim, Ann. Physik **9**, 607 (1931); **9**, 641 (1931).

[70] J. Korringa, J. Phys. Chem. Solids **7**, 252 (1958).

[71] P. Soven, Phys. Rev. **156**, 809 (1967).

[72] D. W. Taylor, Phys. Rev. **156**, 1017 (1967).

[73] N. Kunitomi, Y. Tsunoda and Y. Hirai, Solid State Comm. **13**, 495 (1973).

[74] T. Kaplan and M. Mostoller, Phys. Rev. B **9**, 353 (1974).

[75] W. A. Kamitakahara and D. W. Taylor, Phys. Rev. B **10**, 1190 (1974).

[76] W. A. Kamitakahara, Bull. Am. Phys. Soc. **19**, 321 (1974).

[77] H. G. Smith and N. Wakabayashi, Bull. Am. Phys. Soc. **21**, 410 (1976).

[78] T. Saha, I. Dasgupta and A. Mookerjee, J. Phys.: Condens. Matter **8**, 1979 (1996).

[79] A. Mookerjee and R. Prasad, Phys. Rev. B **48**, 17724 (1993).

[80] D. Paudyal, T. Saha-Dasgupta and A. Mookerjee, J. Phys.: Condens. Matter **16**, 2317 (2004).

[81] J. A. Blackman, D. M. Esterling and N. F. Berk, Phys. Rev. B **4**, 2412 (1971).

[82] H. Shiba, Prog. theor. Phys. **46**, 77 (1971).

[83] T. Kaplan and M. Mostoller, Phys. Rev. B **9**, 1783 (1974).

[84] S.Takeno, Prog. Theor. Phys. **40**, 942 (1968).

[85] B. G. Nickel and W. Butler, Phys. Rev. Lett. **30**, 373 (1973).

[86] F. Ducastelle, J. Phys. C. **7**, 1795 (1974).

[87] A. Gonis and J. W. Garland, Phys. Rev. B **18**, 3999 (1978).

[88] A. Gonis and J. W. Garland, Phys. Rev. B **16**, 2424 (1977).

[89] M. Tsukada, J. Phys. Soc. Japan **32**, 1475 (1972).

[90] A. Mookerjee, J. Phys. C **6**, L205 (1973).

[91] S. Ghosh, P. L. Leath and M. H. Cohen, Phys. Rev. B **66**, 214206 (2002).

[92] T. Saha, I. Dasgupta and A. Mookerjee, Phys. Rev. B **50**, 13267 (1994).

[93] A. Alam and A. Mookerjee, Phys. Rev. B **69**, 024205 (2004).

[94] R. Mills and P. Ratanavararaksha, Phys. Rev. B **18**, 5291 (1978).

[95] T. Kaplan and L. J. Gray, Phys. Rev. B **14**, 3462 (1976).

[96] T. Kaplan and L. J. Gray, Phys. Rev. B **15**, 3260 (1977).

[97] R. Haydock, V. Heine and M. J. Kelly, J. Phys. C **5**, 2845 (1972).

[98] D. A. Rowlands, J. B. Staunton, B. L. Gyorffy, E. Bruno and B. Ginatempo, Phys. Rev. B **72**, 045101 (2005).

[99] D. A. Baiva, S. Ghosh, D. D. Johnson, W. A. Shelton and A. V. Smimov, Phys. Rev. B **72**, 113105 (2005).

[100] M. Jarrell and H. R. Krishnamurthy, Phys. Rev. B **63**, 125102 (2001).

[101] M. Yussouf and A. Mookerjee, J. Phys. C **17**, 1009 (1984).

[102] H. W. Diehl and P. L. Leath, Phys. Rev. B **19**, 587 (1979).

[103] H. W. Diehl and P. L. Leath, Phys. Rev. B **19**, 596 (1979).

[104] T. Kaplan, P. L. Leath, L. J. Gray and H. W. Diehl, Phys. Rev. B **21**, 4230 (1980).

[105] A. Gonis, *Green functions for ordered and disordered systems* North-Holland, Amsterdam (1992).

[106] S. Ghosh, J. B. Neaton, A. H. Antons, M. H. Cohen and P. L. Leath, Phys. Rev. B **70**, 024206 (2004).

[107] A. Alam, S. Ghosh and A. Mookerjee, Phys. Rev. B **75**, 134202 (2007).

[108] J. M. Sanchez, F. Ducastelle and D. Gratias, Physica A **128**, 334 (1984).

[109] B. Dutta and S. Ghosh, J.Phys.: Condens. Matter **21**, 095411 (2009).

[110] P. Hohenberg and W. Kohn, Phys. Rev. **136**, B864 (1964).

[111] W. Kohn and L. J. Sham, Phys. Rev. **140**, A1133 (1965).

[112] S. Baroni, S. De Gironcoli, A. Dal Corso and P. Giannozzi, Rev. Mod. Phys. **73**, 515 (2001).

[113] H. Hellmann, *Einfuhrung in die Quantenchemie* Deuticke, Leipzig (1937).

[114] R.P. Feynman, Phys. Rev. **56**, 340 (1939).

[115] A. Messiah, *Quantum Mechanics* North-Holland, Amsterdam (1962).

[116] A. Van De Walle, *Ph.D. thesis*, MIT, Cambridge (2000).

[117] A. Van De Walle and G. Ceder, Rev. Mod. Phys. **74**, 11 (2002).

[118] E. J. Wu, G. Ceder and A.Van De Walle, Phys. Rev. B **67**, 134103 (2003).

[119] N. Singh, Phys. Rev. B **42**, 8882 (1990).

[120] I. Akgun and G. Ugur, Phys. Rev. B **51**, 3458 (1995).

[121] S. C. Upadhyay, D. Prakash, D. K. Sharma, R. Shyam and J. C. Upadhyay, Phys. Stat. Solidi B **179**, 357 (1993).

[122] J. Zarestky and C. Stassis, Phys. Rev. B **35**, 4500 (1987).

[123] E. Maliszewski, J. Sosnowski, S. Bednarski, A. Czachor and A. Holas, J. Phys. F: Met. Phys. **5**, 1455 (1975).

[124] P. Giannozzi et al., J. Phys.: Condens. Matter **21**, 395502 (2009).

[125] D. Vanderbilt, Phys. Rev. B **41**, 7892 (1990).

[126] S. G. Louie, S. Froyen and M. L. Cohen, Phys. Rev. B **26**, 1738 (1982).

[127] J. P. Perdew and A. Zunger, Phys. Rev. B **23**, 5048 (1981).

[128] J. P. Perdew, K. Burke and M. Ernzerhof, Phys. Rev. Lett. **77**, 3865 (1996).

[129] M. Methfessel and A. T. Paxton, Phys. Rev. B **40**, 3616 (1989).

[130] E. G. Moroni, G. Kresse, J. Hafner and J. Furthmller, Phys. Rev. B **56**, 15629 (1997).

[131] C. S. Wang, B. M. Klein and H. Krakauer, Phys. Rev. Lett. **54**, 1852 (1985).

[132] U. Gonser, K. Krischel and S. Nasu, J. Magn. Magn. Mater. **15-18**, 1145 (1980).

[133] M. H. F. Sluiter and Y. Kawazoe, Philos. Mag. A **78**, 1353 (1998).

[134] M. H. F. Sluiter, M. Weinert and Y. Kawazoe, Phys. Rev. B **59**, 4100 (1999).

[135] P. Ghosez, E. Cockayne, U. V. Waghmare and K. M. Rabe, Phys. Rev. B **60**, 836 (1999).

[136] P. Giannozzi, S. de Gironcoli, P. Pavone and S. Baroni, Phys. Rev. B **43**, 7231 (1991).

[137] B. Dutta and S. Ghosh, J.Phys.: Condens. Matter **21**, 395401 (2009).

[138] Y. Noda and Y. Endoh, J. Phys. Soc. Japan **57**, 4225 (1988).

[139] M. Sato, B. H. Grier, S. M. Shapiro and H. Miyajima, J. Phys. F: Met. Phys. **12**, 2117 (1982).

[140] B. Dutta, K. Bisht and S. Ghosh, Phys. Rev. B **82**, 134207 (2010).

[141] D. H. Dutton, B. N. Brockhouse and A. P. Miller, Can. J. Phys. **50**, 2915 (1972).

[142] J. W. Lynn, H. G. Smith and R. M. Nicklow, Phys. Rev. B **8**, 3493 (1973).

[143] Y. Noda, D. K. Saha and K. Ohshima, J. Phys. F: Met. Phys. **18**, 2195 (1998).

[144] Y. Noda, K. Ohshima and Y. Endoh, Physica B **219** and **220**, 490 (1996).

[145] E. D. Hallman, Can. J. Phys. **52**, 2235 (1974).

[146] S. Katano, M. Iizumi and Y. Noda, J. Phys. F: Met. Phys. **18**, 2195 (1998).

[147] B. Dutta and S. Ghosh, J. Appl. Phys. **109**, 053714 (2011).

[148] V. Pierron-Bohnes, M. C. Cadeville and G. Parette, J. Phys. F: Met. Phys. **15**, 1441 (1985).

[149] I. Mirebeau, M. Hennion and G. Parette, Phys. Rev. Lett. **53**, 687 (1985).

[150] R.E. Parra and J.W. Cable, Phys. Rev. B **21**, 5494 (1980).

[151] U. Kumar, P. K. Mukhopadhyay, B. Sanyal, O. Eriksson and P. Nordblad, Phys. Rev. B **74**, 064401 (2006).

[152] J. Staunton, P. Weinberger and B. L. Gyorffy, J. Phys. F: Met. Phys. **13**, 779 (1983).

[153] F. J. Pinski, B. Ginatempo, D. D. Johnson, J. B. Staunton, G. M. Stocks and B. L. Gyorffy, Phys. Rev. Lett. **66**, 766 (1991).

[154] M. Hansen, *Constitution of Binary Alloys* McGraw-Hill, New York (1958).

[155] G. A. DeWit and B. N. Brockhouse, J. Appl. Phys. **39**, 451 (1968).

[156] Y. Tsunoda, N. Kunitomi, N. Wakabayashi, R.M. Nicklow and H. G. Smith, Phys. Rev. B **19**, 2876 (1979).

[157] T. Mehaddene, E. Kentzinger, B. Hennion, K. Tanaka, H. Numakura, A. Marty, V. Parasote, M. C. Cadeville, M. Zemirli, and V. Pierron-Bohnes, Phys. Rev. B **69**, 024304 (2004).

[158] A. Dal Carso and S. De Gironcoli, Phys. Rev. B **62**, 273 (2000).

[159] N. Mousseau and M. F. Thorpe, Phys. Rev. B **45**, 2015 (1992).

[160] E. C. Svensson, B. N. Brockhouse and J. M. Rowe, Solid State Comm. **3**, 245 (1965).

[161] E. C. Svensson and B. N. Brockhouse, Phys. Rev. Lett. **18**, 858 (1967).

[162] E. C. Svensson and W. A. Kamitakahara, Can. J. Phys. **49**, 2291 (1971).

[163] O. Grånäs, B. Dutta, S. Ghosh and B. Sanyal, J. Phys.: Condens. Matter **24**, 015402 (2012).

[164] A. Zunger, S.-H. Wei, L. G. Ferreira and J. E. Bernard, Phys. Rev. Lett. **65**, 353 (1990).

[165] S.-H. Wei, L. G. Ferreira, J. E. Bernard and A. Zunger, Phys. Rev. B **42**, 9622 (1990).

[166] K. C. Hass, L. C. Davis and A. Zunger, Phys. Rev. B **42**, 3757 (1990).

[167] B. Velick, S. Kirkpatrick and H. Ehrenreich, Phys. Rev. **175**, 747 (1968).

[168] J. Kudrnovsk and J. Maek, Phys. Rev. B **31**, 6424 (1985).

[169] D. A. Papaconstantopoulos, A. Gonis and P. M. Laufer, Phys. Rev. B **40**, 12196 (1989).

[170] Z. W. Lu, S.-H. Wei and A. Zunger, Phys. Rev. B **44**, 10470 (1991).

[171] Z. W. Lu, S.-H. Wei and A. Zunger, Phys. Rev. B **45**, 10314 (1992).

[172] V. Ozolins, C. Wolverton and A. Zunger, Phys. Rev. B **57**, 6427 (1998).

[173] A. V. Ruban, S. I. Simak, S. Shallcross and H. L. Skriver, Phys. Rev. B **67**, 214302 (2003).

[174] C. Wolverton, Acta Mater **49**, 3129 (2001).

[175] G. Kresse and J. Hafner, Phys. Rev. B **47**, RC558 (1993).

[176] G. Kresse and J. Furthmüller, Phys. Rev. B **54**, 11169 (1996).

[177] D. Alfé, Comp. Phys. Comm. **180**, 2622 (2009).

[178] K. Ullakko, J. K. Huang, C. Kantner, R. C. O'Handley and V. V. Kokorin, Appl. Phys. Lett. **69**, 1966 (1996).

[179] S. J. Murray, M. Marioni, S. M. Allen, R. C. O'Handley and T. A. Lagrosso, Appl. Phys. Lett. **77**, 886 (2000).

[180] A. Planes, L. Manosa and A. Saxena, *Magnetism and Structure in Functional Materials (Materials Science Series)* Spinger, Berlin (2005).

[181] C. Bungaro, K. M. Rabe and A. Dal Corso, Phys. Rev. B **68**, 134104 (2003).

[182] L. Isaeva, D. Bazhanov, E. Isaev and O. Eriksson, Jpn. J. Appl. Phys. **50**, 05FE07 (2011).

[183] P. Entel, E. Hoffman, P. Mohn, K. Schwarz and V. L. Moruzzi, Phys. Rev. B **47**, 8706 (1993).

[184] E. Hoffmann, H. Herper, P. Entel, S. G. Mishra, P. Mohn and K. Schwarz, Phys. Rev. B **47**, 5589 (1993).

[185] E. F. Wassermann, M. Acet, P. Entel and J. Pepperhoff, J. Magn. Soc. Jpn. **23**, 385 (1999).

[186] B. Dutta and S. Ghosh, Intermetallics **18**, 1143 (2010).

# *Publications*

## Journal

1. Biswanath Dutta and Subhradip Ghosh, *The phonon spectra and elastic constants of $Pd_xFe_{1-x}$: an understanding from inter-atomic interactions*, J. Phys.: Condens. Matter **21**, 095411 (2009).
2. Biswanath Dutta and Subhradip Ghosh, *Phonon spectra of $Pd_xFe_{1-x}$ alloys with transferable force constants*, J. Phys.: Condens. Matter **21**, 395401 (2009).
3. Biswanath Dutta and Subhradip Ghosh, *First-principles based investigation on effects of magnetism on lattice dynamics in $Fe_{72}Pd_{28}$ alloy*, Intermetallics **18**, 1143 (2010).
4. Biswanath Dutta, Konark Bisht and Subhradip Ghosh, *Ab initio calculation of phonon dispersions in size-mismatched disordered alloys*, Phys. Rev. B **82**, 134207 (2010).
5. Biswanath Dutta and Subhradip Ghosh, *Vibrational properties of $Ni_xPt_{1-x}$ alloys: an understanding from ab initio calculations*, J. Appl. Phys. **109**, 053714 (2011).
6. O. Grånäs, B. Dutta, S. Ghosh and B. Sanyal, *A new first principles approach to calculate phonon spectra of disordered alloys*, J. Phys.: Condens. Matter **24**, 015402 (2012).

## Conferences

1. Biswanath Dutta and Subhradip Ghosh, *Self-consistent Cluster Theory for Disordered Alloys* in 'International Workshop and Conference on Statistical Physics Approaches to Multi-disciplinary Problems' at IIT Guwahati, Guwahati, India (2008).
2. Biswanath Dutta and Subhradip Ghosh, *An ab-initio based approach to calculate phonon spectra in random alloys: applications to $Fe_xPd_{1-x}$* Proceedings, $53^{rd}$ DAE Solid State Physics Symposium (2008).
3. Biswanath Dutta and Subhradip Ghosh, *Ab-initio based calculation of lattice dynamics in disordered alloys* in 'Discussion meeting on Statistical and Condensed Matter Physics' at IIT Guwahati, Guwahati, India (2009).
4. Biswanath Dutta and Subhradip Ghosh, *Role of magnetism in the lattice dynamics of $Fe_{72}Pd_{28}$* Proceedings, $54^{th}$ DAE Solid State Physics Symposium (2009).

5. Biswanath Dutta and Subhradip Ghosh, *Ab-initio calculation of in-band modes of vibration in $Cu_xAu_{1-x}$ alloy* in 'Condensed Matter Days 2010' at University of Kalyani, Westbengal, India (2010).
6. Biswanath Dutta, Souvik Paul and Subhradip Ghosh, *First-principles based investigation of the lattice dynamics in $Ni_{0.50}Pt_{0.50}$* in 'Condensed Matter Days 2011' at Gauhati University, Guwahati, India (2011).
7. Souvik Paul, Biswanath Dutta and Subhradip Ghosh, *A density-functional theory based prediction of shape-memory effect and magnetic structure in $Mn_2NiSn$* in 'Condensed Matter Days 2011' at Gauhati University, Guwahati, India (2011).

## Schools/ Workshops/ Conferences attended

1. *$52^{nd}$ DAE Solid State Physics Symposium* at University of Mysore, Mysore, India (2007).
2. *SERC school on Computational Statistical Physics* at IIT Guwahati, Guwahati, India (2008).
3. *ICTS Condensed Matter Programme 2009 (ICMP09)* at Mahabaleshwar, Maharashtra, India (2009).
4. *International workshop on Frontiers in Electronic structure calculations : Techniques and Applications* at University of Pune, Maharashtra, India (2010).
5. *International School and Conference on Functional Materials* at Harish-Chandra Research Institute, Allahabad, India (2011).

## Communicated/Unpublished

1. Biswanath Dutta, Sumanta Bhandary, Subhradip Ghosh and Biplab Sanyal, *First-principles study of magnetism in $Pd_3Fe$ under pressure*.

# *Vita*

Mr. Biswanath Dutta was born on 14th June 1982 in Assam, India. He did his B.Sc. with Physics Honours in 2003 from Birjhora Mahavidyalaya, Bongaigaon and M.Sc. in Physics in 2005 from Gauhati University, Guwahati. He enrolled into Ph.D. in 2006 in Indian Institute of technology Guwahati. He qualified Graduate Aptitude Test in Engineering (GATE) in 2005 and was awarded Junior Research Fellowship in 2006 and Senior Research Fellowship in 2008 by CSIR, India.